

Finite Element Analysis of the ACL-deficient Knee

David Jorge Carvalho Fernandes

Thesis to obtain the Master of Science Degree in

Biomedical Engineering

Supervisors: Professor Paulo Rui Alves Fernandes
Professor João Orlando Marques Gameiro Folgado

Examination Committee

Chairperson: Professor Mónica Duarte Correia de Oliveira
Supervisors: Professor João Orlando Marques Gameiro Folgado
Members of the Committee: Professor Fernando Manuel Fernandes Simões

December 2014

Agradecimentos

Aos meus orientadores, Professor João Folgado e Professor Paulo Fernandes, por terem aceitado a minha proposta de tese e por todo o acompanhamento ao longo da realização da mesma. Em especial ao Professor João Folgado, pela disponibilidade e incentivo constantes ao longo destes meses.

Ao Professor João Gamelas, pela pronta ajuda no esclarecimento de dúvidas de contexto clínico.

Aos meus pais, que por diferentes razões, me proporcionaram as condições necessárias para realizar o meu percurso académico.

À Susana, pela paciência e compreensão incondicionais, pelo apoio constante e pela disponibilidade para me ajudar, independentemente da situação.

Ao João Ramalinho, pelo companheirismo dentro e fora do IST.

Ao João Abreu e ao Vasco Conceição, parceiros de inúmeros trabalhos, que tanto me ensinaram e cuja ajuda em muito contribuiu para o meu sucesso académico.

A todos os meus restantes colegas de curso, que de alguma forma me ajudaram durante estes últimos 5 anos.

Resumo

A rotura do ligamento cruzado anterior (LCA) é uma lesão grave e cuja frequência tem vindo a aumentar nos últimos anos. Para compreender as causas e as consequências desta lesão é fundamental perceber qual o papel do LCA no joelho.

Este trabalho tem como objetivo analisar o comportamento do joelho humano após lesão do LCA, através do método dos elementos finitos. Para tal, é utilizado um modelo tridimensional da componente tibiofemoral do joelho, com e sem LCA, ao qual são aplicadas cargas que evidenciam a função do ligamento.

Os ligamentos foram modelados através de dois modelos constitutivos hiperelásticos distintos: o modelo isotrópico de Marlow e o modelo anisotrópico de Holzapfel-Gasser-Ogden (HGO). Ambos foram ajustados às mesmas curvas de tensão-deformação. Os parâmetros do modelo HGO foram obtidos através duma rotina de otimização, implementada num processo iterativo entre o MATLAB e o Abaqus.

A comparação dos resultados obtidos com os dois modelos constitutivos permitem concluir que o modelo HGO reproduz melhor o comportamento mecânico dos ligamentos.

Apesar de verificadas algumas diferenças em termos quantitativos, o modelo de elementos finitos é capaz de produzir resultados cinemáticos e de força que verificam o papel do LCA como principal opositor ao movimento de translação anterior da tibia (ou posterior do fémur). Para além disto, na ausência do ligamento é evidente a maior laxidão do joelho noutros graus de liberdade, em especial na rotação interna-externa da tibia.

Palavras-chave

Ligamento Cruzado Anterior, Joelho, Método dos Elementos Finitos, Biomecânica.

Abstract

Anterior cruciate ligament (ACL) rupture is a serious injury whose frequency has been increasing in the last few years. To understand the causes and consequences of this injury it is fundamental to know the role of the ACL in the knee.

This work aims to analyze the knee behavior after an ACL rupture, through the finite element method. For this purpose, it is used a fully tridimensional model of the tibiofemoral joint, with and without ACL, where loads that evidence the ligament function are applied.

The knee ligaments were modeled with two hyperelastic constitutive models: The isotropic Marlow and the anisotropic Holzapfel-Gasser-Ogden (HGO) models. Both material models were fitted using the same uniaxial stress-strain curves. The parameters of the HGO were estimated with the help of an optimization routine, connecting MATLAB to Abaqus.

The comparison between the results obtained through both the constitutive models allows to conclude that HGO model can better reproduce the mechanical behavior of the ligaments.

Despite some differences in quantitative terms were verified, the finite element model is able to produce kinematic and force results that confirm the ACL as the main restrainer to anterior tibial (or posterior femoral) translation. Furthermore, in ACL absence, there is a clear increase in knee laxity in more than other degrees of freedom, particularly in internal-external tibial rotation.

Keywords

Anterior Cruciate Ligament, Knee, Finite Element Method, Biomechanics.

Contents

| | |
|---|-------------|
| Agradecimentos | iii |
| Resumo | v |
| Abstract | vii |
| Contents | ix |
| List of Figures | xi |
| List of Tables | xv |
| List of Acronyms | xvii |
| List of Symbols | xix |
| 1. Introduction | 1 |
| 1.1. Motivation | 1 |
| 1.2. Literature Review..... | 2 |
| 1.3. Objectives | 5 |
| 1.4. Thesis Outline..... | 5 |
| 2. Knee Joint | 7 |
| 2.1. Anatomy..... | 7 |
| 2.1.1. Bones..... | 9 |
| 2.1.2. Articular Cartilage | 10 |
| 2.1.3. Menisci..... | 11 |
| 2.1.4. Ligaments | 13 |
| 2.2. Biomechanics and Kinematics | 18 |
| 2.3. ACL Injuries | 20 |
| 3. Methods | 25 |
| 3.1. Geometrical Model | 25 |
| 3.1.1. Known Limitations..... | 26 |
| 3.2. Mesh Definition..... | 26 |
| 3.3. Material Properties | 29 |
| 3.3.1. The Marlow Constitutive Model | 31 |
| 3.3.2. The Holzapfel-Gasser-Ogden Constitutive Model..... | 31 |
| 3.4. Contact Interactions and Constraints | 41 |
| 3.5. Loads and Boundary Conditions | 41 |
| 3.6. Output Variables | 43 |
| 4. Results and Discussion | 45 |
| 4.1. ACL-Intact Knee | 45 |

| | | |
|---------------------------------------|--------------------------------|-----------|
| 4.1.1. | Full Extension (0° of Flexion) | 46 |
| 4.1.2. | 15° of Flexion | 50 |
| 4.1.3. | 30° of Flexion | 52 |
| 4.2. | ACL-Deficient Knee | 55 |
| 4.2.1. | Full Extension (0° of Flexion) | 55 |
| 4.2.2. | 15° of Flexion | 60 |
| 4.2.3. | 30° of Flexion | 62 |
| 5. | Conclusion | 67 |
| 5.1. | Future Work | 68 |
| 6. | References | 71 |
| Appendix A – Optimization Code | | 77 |

List of Figures

Figure 1.1 – Schematic representation of the four-bar linkage model in the sagittal plane [19]. The cruciate ligaments are represented by rigid bars that are connected to the femur and tibia by hinges. . 3

Figure 2.1 - The reference planes of the human body in the standard anatomical position [75]...... 8

Figure 2.2 – Knee joint degrees of freedom: three translations and three rotations [48]. 8

Figure 2.3 - Anatomic structure of the right knee – anterior view. a) Schematic representation. b) An opened knee joint [1]. 9

Figure 2.4 - Bony structure of the knee [2]...... 10

Figure 2.5 - Superior view of the right tibia in the knee joint, highlighting the menisci and cruciate ligaments [1].11

Figure 2.6 - The menisci role in increasing tibiofemoral congruence. The menisci wedge-shaped cross-section area helps to increase the contact area between the femur and the tibia, leading to a wider distribution of compressive loads [47]. 12

Figure 2.7 - Internal hierarchical structure of ligaments and tendons [52]...... 13

Figure 2.8 - Typical load-elongation curve of ligaments with the three regions and the changes in collagen fiber structure. Adapted from [53]...... 14

Figure 2.9 - Left side) Load-elongation curve and structural properties. Right side) Stress-strain curve and mechanical properties [53]. 14

Figure 2.10 – Cadaveric right-knee specimen showing the anteromedial (AM) and posterolateral (PL) bundles of the ACL [12]. 16

Figure 2.11 - The rolling-sliding mechanism. A) In full extension there is central contact between the femur and the tibia (F1-T1). B) As flexion starts, the femur rolls on the tibia and the contact is made on a more posterior position (F2-T2). C) At greater flexion angles, the ACL is tensioned and the femur slides anteriorly [47]. 19

Figure 2.12 - The Lachman test. With the knee in 20 to 30 degrees of flexion, the examiner applies an anteriorly directed force on the tibia while holding the femur to assess the integrity of the ACL [56]. 22

Figure 3.1 - Partitions created on lateral tibial cartilage to define regular section for meshing. 27

Figure 3.2 – Mesh of the fully assembled knee. Different colors represent different tissues: grey for bones, blue for articular cartilages, yellow for menisci and green for ligaments. (Top left) Anterior view. (Top right) Posterior view. (Bottom left) Medial view. (Bottom right) Lateral view. 28

Figure 3.3 - Three-dimensional graphical representation of the orientation of the fibres based on the transversely isotropic density function [62]. The surface defined by the apex of the vector ρMM is plotted with respect to the Eulerian angles θ and ϕ 34

Figure 3.4 - Main PCL fiber direction. 35

Figure 3.5 - Main ACL fiber direction..... 35

Figure 3.6 - Schematic representation of the local coordinate system used in each element of the ACL to define the direction of the two fiber families. Considering the planes 567, 145 and 236 as the

anterior, medial and lateral planes, the AM and PL bundles of the ACL can be defined in the local coordinate system represented. The smaller lines around the AM and PL directions represent the dispersion of the collagen fibers direction, controlled by the κ parameter. 36

Figure 3.7 - Anterior view of the ACL showing the implementation of the fiber directions on a representative element. In each integration point, the implemented local coordinate system and the direction of the anteromedial (Localdir1) and posterolateral (Localdir2) fiber bundles are shown. 37

Figure 3.8 - Diagram of the optimization process. Adapted from [76]..... 38

Figure 3.9 - Results of the curve fitting procedure for each ligament and respective R^2 value. (Top Center) ACL Body. (Bottom Left) MCL. (Bottom Right) PCL. 39

Figure 3.10 - ACL division in head and body element sets. 40

Figure 3.11 - Mesh of the fully assembled knee with the new coordinate system and the femoral RP highlighted. (Left) Anterior view. (Right) Posterior view. 42

Figure 4.1 - ACL-intact knee joint after the application of a 134 N posteriorly directed force on the femur using the Marlow material model in the ligaments. (Left side) Anterior view. (Right side) Medial view. 46

Figure 4.2 - ACL-intact knee joint after the application of a 134 N posteriorly directed force on the femur using the HGO material model in the ligaments. (Left side) Anterior view. (Right side) Medial view. 47

Figure 4.3 - Kinematic results of relative tibial movement under a 134 N posterior femoral load at full extension. The results of the simulation are compared to the experimental data of Gabriel et al [70]. 48

Figure 4.4 - ACL-intact knee joint at 15° of flexion after the application of a 134 N posteriorly directed force on the femur using the HGO material model in the ligaments. (Left side) Anterior view. (Right side) Medial view. 50

Figure 4.5 - Kinematic results of relative tibial movement under a 134 N posterior femoral load at 15° of flexion. The results of the simulation are compared to the experimental data of Gabriel et al [70]. . 51

Figure 4.6 - ACL-intact knee joint at 30° of flexion after the application of a 134 N posteriorly directed force on the femur using the HGO material model in the ligaments. (Left side) Anterior view. (Right side) Medial view. 52

Figure 4.7 - Kinematic results of relative tibial movement under a 134 N posterior femoral load at 30° of flexion using the HGO model in the ligaments. The results of the simulation are compared to the experimental data of Gabriel et al [70]. 53

Figure 4.8 - ACL-deficient knee joint at full extension after the application of a 67 N posteriorly directed force on the femur using the HGO material model in the ligaments. (Left side) Lateral view. (Right side) Medial view. 55

Figure 4.9 - Kinematic results of relative tibial movement under a 67 N posterior femoral force at full extension using the Marlow model in the ligaments - comparison between the ACL-intact and ACL-deficient knees. 56

Figure 4.10 - Ligaments reaction force (magnitude) under a 67 N posterior femoral force at full extension using the Marlow model in the ligaments - comparison between ACL-intact and ACL-deficient knees. 56

| | |
|---|----|
| Figure 4.11 - Ligaments average maximum principal stress under a 67 N posterior femoral force at full extension using the Marlow model in the ligaments - comparison between ACL-intact and ACL-deficient knees..... | 57 |
| Figure 4.12 - ACL-deficient knee joint at full extension after the application of a 67 N posteriorly directed force on the femur using the HGO material model in the ligaments. (Left side) Lateral view. (Right side) Medial view..... | 57 |
| Figure 4.13 - Kinematic results of relative tibial movement under a 67 N posterior femoral load at full extension – comparison between the ACL-intact and ACL-deficient knees..... | 58 |
| Figure 4.14 - Ligaments reaction force (magnitude) under a 67 N posterior femoral force at full extension using the HGO model in the ligaments - comparison between the ACL-intact and ACL-deficient knees..... | 58 |
| Figure 4.15 - Ligaments average maximum principal stress under a 67 N posterior femoral force at full extension - comparison between ACL-intact and ACL-deficient knees..... | 59 |
| Figure 4.16 - ACL-deficient knee joint at 15° of flexion after the application of a 67 N posteriorly directed force on the femur using the HGO material model in the ligaments. (Left side) Lateral view. (Right side) Medial view..... | 60 |
| Figure 4.17 - Kinematic results of relative tibial movement under a 67 N posterior femoral load at 15° of flexion using the HGO model in the ligaments - comparison between the ACL-intact and ACL-deficient knees..... | 60 |
| Figure 4.18 - Ligaments reaction force (magnitude) under a 67 N posterior femoral force at 15° of flexion using the HGO model in the ligaments - comparison between ACL-intact and ACL-deficient knees..... | 61 |
| Figure 4.19 - Ligaments average maximum principal stress under a 67 N posterior femoral force at 15° of flexion using the HGO model in the ligaments - comparison between ACL-intact and ACL-deficient knees..... | 61 |
| Figure 4.20 - ACL-deficient knee joint at 30° of flexion after the application of a 67 N posteriorly directed force on the femur using the HGO material model in the ligaments. (Left side) Lateral view. (Right side) Medial view..... | 62 |
| Figure 4.21 - Kinematic results of relative tibial movement under a 67 N posterior femoral load at 30° of flexion using the HGO model in the ligaments - comparison between the ACL-intact and ACL-deficient knees..... | 63 |
| Figure 4.22 - Ligaments reaction force (magnitude) under a 67 N posterior femoral force at 30° of flexion using the HGO model in the ligaments - comparison between ACL-intact and ACL-deficient knees..... | 63 |
| Figure 4.23 - Ligaments average maximum principal stress under a 67 N posterior femoral force at 30° of flexion using the HGO model in the ligaments - comparison between ACL-intact and ACL-deficient knees..... | 64 |

List of Tables

| | |
|--|----|
| Table 3.1 - Specimen Information [58]. | 25 |
| Table 3.2- Number of elements of each 3D part of the FE model. | 27 |
| Table 3.3 - Material Properties | 40 |
| Table 4.1 - Ligaments reaction force in the ACL-intact knee at full extension under a 134 N posterior femoral force. | 47 |
| Table 4.2 - Ligaments average maximum principal stress in the ACL-intact knee at full extension under a 134 N posterior femoral force. | 48 |
| Table 4.3 - Experimental data from cadaveric studies applying a 134 N anterior tibial load in the fully extended knee. | 49 |
| Table 4.4 - Ligaments reaction force in the ACL-intact knee at 15° of flexion under a 134 N posterior femoral force. | 50 |
| Table 4.5 - Ligaments average maximum principal stress in the ACL-intact knee at 15° of flexion under a 134 N posterior femoral force. | 50 |
| Table 4.6 - Ligaments reaction force in the ACL-intact knee at 30° of flexion under a 134 N posterior femoral force. | 52 |
| Table 4.7 - Ligaments average maximum principal stress in the ACL-intact knee at 30° of flexion under a 134 N posterior femoral force. | 53 |
| Table 4.8 - Experimental data from cadaveric studies applying a 134 N anterior tibial load in the knee at 30° of flexion. | 54 |

List of Acronyms

| | |
|-------------|--------------------------------|
| 1D | One-Dimensional |
| 2D | Two-Dimensional |
| 3D | Three-Dimensional |
| ACL | Anterior Cruciate Ligament |
| AL | Anterolateral |
| AM | Anteromedial |
| CAE | Complete Abaqus Environment |
| CS | Coordinate System |
| DOF | Degree of Freedom |
| ECM | Extracellular Matrix |
| FE | Finite Element |
| LCL | Lateral Collateral Ligament |
| MCL | Medial Collateral Ligament |
| PCL | Posterior Cruciate Ligament |
| PF | Patellofemoral |
| PL | Posterolateral |
| PM | Posteromedial |
| RP | Reference Point |
| SEDF | Strain Energy Density Function |
| TF | Tibiofemoral |
| VM | Von-Mises |

List of Symbols

| | |
|----------------------|---|
| E | Young's Modulus (or Elastic Modulus) |
| ν | Poisson's Ratio |
| Ω | Current (Deformed) Configuration |
| Ω_0 | Reference Configuration |
| Ψ | Strain Energy Density Function |
| κ | Dispersion Parameter |
| \mathbf{F} | Deformation Gradient |
| I_1 | First Strain Invariant |
| I_2 | Second Strain Invariant |
| I_3 | Third Strain Invariant |
| \bar{I}_1 | Isochoric Component of the First Strain Invariant |
| \bar{I}_4 | Isochoric Component of the Fourth Invariant |
| \bar{I}_6 | Isochoric Component of the Sixth Invariant |
| $\mathbf{a}_{04,06}$ | Unit vectors that define the preferred direction of one family of fibers in the reference configuration |
| $\bar{\mathbf{C}}$ | Isochoric Right Cauchy-Green Deformation Tensor |
| \mathbf{C} | Right Cauchy-Green Deformation Tensor |
| C_{10} | Neo-Hookean Parameter |
| k_1, k_2 | Parameters of the HGO Model Anisotropic Component |
| ε | Uniaxial Strain |
| λ | Stretch Ratio |
| \mathbf{M} | Arbitrary unit vector located in three dimensional Eulerian space |
| ρ | Statistical distribution function |
| ϕ, θ | Eulerian angles |

1. Introduction

1.1. Motivation

The knee joint is the largest and most complex joint in the human body consisting of both femoropatellar and tibiofemoral joints [1]. The structure of the knee permits the bearing of very high loads, as well as the mobility required for locomotor activities [2].

A fully functional knee relies on a good balance of two mutually exclusive requirements: stability and mobility [3]. This problem is solved by a complex geometry constituted by different types of tissues, such as bones, articular cartilages, menisci and ligaments, and their mechanical interactions.

The knee ligaments act as joint stabilizers and movement restrainers [4]. The directions in which each ligament contributes to these processes is determined by its location and geometry [2].

The anterior cruciate ligament (ACL) plays a critical role in the physiological kinematics of the knee joint, acting as a stabilizing mechanism, being the primary restraint against anterior tibial translation and also limiting knee hyperextension [1,5,6]. ACL rupture is a serious and the most common ligament injury, with an increasing number of 100 000 to 200 000 incidences per year in the United States [7]. This injury results in many immediate effects such as pain, local instability of the knee, a change in the location of the center of rotation at the knee, changes in the tibiofemoral contact area during gait, and altered joint kinetics [2], inducing secondary lesions of other knee structures like the articular cartilage and the menisci [8]. In the long term, an ACL injured knee experiences an early development of tissue degeneration and the onset of osteoarthritis [2,8,9]. All of these complications can severely affect a person's mobility, making ACL rupture an especially threatening injury for athletes since it can compromise their performance or even dictate an early ending to their careers [7].

Due to the lack of regeneration capability of the ligaments [10,11], a torn ACL usually requires surgical intervention to restore proper knee function, with a recovery period normally not under six months to regain the ability to perform physically demanding sport activities [7].

The high frequency of this type of injury, associated with its disabling consequences, makes this topic a major focus of interest in the realm of orthopedics and biomechanics. Several aspects of ACL injuries have been studied, namely: the biomechanics of the intact and ACL replacement graft, different types of grafts, mechanism of failure, treatment, surgical techniques, and postoperative rehabilitation protocols [12].

A sound knowledge of both biomechanics and kinematics of the knee and the ACL role in it are indispensable to understand the causes of ACL injuries, its consequences, how to prevent them and even to improve surgical procedures.

Two ways of gaining insight about how the knee works is to perform *in vivo* or *in vitro* studies. However, these approaches have many limitations such as their high cost, low capability to reproduce some natural, pathological or degenerative conditions and also the difficulties in measuring forces and strains on specific structures [4,8,13].

Computational models are a good alternative to study several biomechanical quantities with reduced costs and high time and machinery efficiency. In particular, finite element (FE) method analysis can provide accurate and medical relevant results [4,14–16]. The FE simulation technique permits a precise calculation of both spatial and temporal variations of stresses, strains and contact areas/forces in different situations that can be easily reproduced [15–17].

The reliability and accuracy of FE models depend on three critical factors: geometrical complexity, the interaction between different parts of the model and the definition of material properties that correctly represent the mechanical behavior of the structure to be modeled [14,15]. Therefore, the application of the FE method on a complex structure like the knee joint represents a challenging problem due to all of its distinctive features. However, in FE modeling, the model complexity has to maintain a strict balance with computational efficiency. When this balance is achieved with success the FE method has proven to be a powerful tool in providing biomechanical information that can be extremely useful in a clinical context.

1.2. Literature Review

In order to comprehend the knee joint biomechanics and kinematics and the complex role of the cruciate ligaments in it, several models have been developed in the last years.

One of the first conceptual models that started by explaining the role of the cruciate ligaments was the “four-bar linkage” model (Figure 1.1). This model defines the cruciate ligaments as rigid bars in the sagittal plane, having variable attachments to the femur and tibia. The intersection point between these bars would be the instant center of rotation of the knee [18,19]. Its virtues covered the explanation of questions such as: the shape of the articular surfaces, the movement of the rotational axis and the resistance supplied by the cruciate ligaments in anterior and posterior drawer motion. However, it does not clarify the phenomenon of knee laxity, the role of the collateral ligaments, or internal-external rotation of the knee in the transverse plane [18].

Regarding computational FE models of the knee, they vary in diverse parameters, such as the degree of complexity, the study variables, material models definitions and loading cases. The choice of the parameters to study defines the nature of the analysis, which can be static or quasi-static [4,8,13,14,20–32] or dynamic, [14,33–37].

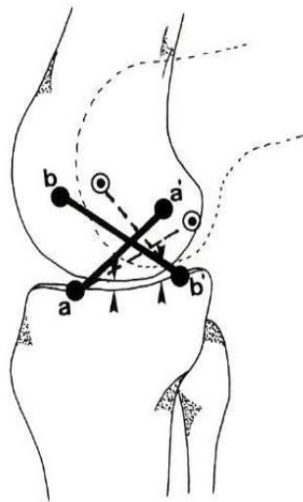


Figure 1.1 – Schematic representation of the four-bar linkage model in the sagittal plane [19]. The cruciate ligaments are represented by rigid bars that are connected to the femur and tibia by hinges.

Due to the intricate anatomy and structure diversity of the knee joint, many of the FE studies simplify the analysis by focusing only on the tibiofemoral joint [8,13,16,23,25,28,30,32,38,39] and by not including parts such as the menisci and the articular cartilage [8,13,16,25,32] or other ligaments [8,13,16,23,32].

Some simplifications were also applied to the FE modeling of the ligaments, with many studies using one-dimensional (1D) truss/beam [20,21,33] or spring [23,24,30,31,37] elements with simplified material properties. This approach can furnish some data regarding the kinematics of the knee and makes the calculation of ligament forces easier. However, it has the inherent limitation of not allowing to determine the stress distribution in the ligaments [8,14,40]. So, as stated in [18], the ACL (and, by extension, all the ligaments) role in the knee joint must be approached as a three-dimensional (3D) problem.

Having this premise into account, 3D representations of the knee ligaments have become the state of the art in this field.

With the 3D requirement fulfilled, the challenge was (and still is) to develop a material model that can characterize completely the nonlinear behavior of ligaments. To this matter, isotropic [8,13,26,27,40], transversely isotropic [4,16,22,32,39,41] and anisotropic hyperelastic material models [14,38] have been used.

A recent study, developed by Wan et al. [28], compares the application of three constitutive models to the ACL. The authors report that no constitutive model describes successfully all the different ligament material behaviors under longitudinal tension, transverse tension, and finite simple shear. The models considered (isotropic hyperelastic, transversely isotropic hyperelastic with neo-Hookean ground substance and transversely isotropic model with nonlinear ground substance) produced similar force results, but showed significant changes in kinematic response of the joint and in the stress distribution of the ACL.

Another challenge that has been issued in FE modeling of the knee is the inclusion of *in vivo* residual stresses that are present in the ligaments. This has been accomplished by the application of initial strains

in knee models with both 1D [20,21,30,33,37,42] and 3D [4,13,38,39] element representations of ligaments and in models that studied the behavior of the ACL by itself, just taking into account the bony insertions of the ligament [40,41].

So, it is clear that despite being a widely studied topic on the FE modeling context, the development of a trustworthy model of such a complex structure as the knee joint is a very challenging process. The difficulties increase even more when a good description of the ligaments behavior is required.

Despite these obstacles, ACL injuries have been a topic of much interest in the FE modeling of the knee.

Li et al. [31] studied the effects of ACL deficiency on joint function under simulated quadriceps force. A partially injured ACL was modeled by reducing its stiffness. The results showed that even when the stiffness was reduced by 75%, the ACL still supported more than 58% of the load taken up by the original non-injured ACL and that tibial translation and rotation were affected by no more than 20%.

Moglo and A. Shirazi-Adl [30] examined the response of the joint when submitted to a posterior femoral load in ACL-intact and -deficient knees. They have verified that the ACL acts as a primary restraint to drawer loads and that its absence increases knee laxity.

The effect of ACL-deficiency on the medial collateral ligament MCL insertion site and contact forces was also studied. Ellis et al. [32] verified that under anterior tibial loading, there was a significant increase in MCL insertion site and contact forces. However, these effects were not found under valgus tibial loading, indicating that the ACL does not provide valgus restraint in MCL-intact knees.

Yao et al. [29] measured the stress and strain in the medial compartment of an ACL-deficient knee when submitted to anterior loading. Although the general agreement of the model with digitized images, it was not able to capture the anterior and posterior areas of the meniscus behavior correctly, showing large shear stresses.

Westerman et al. [38] performed a simulated Lachman test in a knee model with an ACL graft varying in size as well as in an ACL-deficient knee to study the effect of graft diameter in joint laxity. The results indicate that increasing graft size reduces relative anterior translation and meniscal contact pressure and stresses.

Peña et al. [39] investigated the effect of graft stiffness and tensioning, with different stiffness corresponding to different types of tissues commonly used for ACL grafts. They have concluded that the most beneficial situation would be to use a patella tendon graft with a pretension of 40 N. The same problem had already been addressed by Suggs et al [42] with a knee model similar to the one used by Li et al [31].

In a posterior work, Peña et al. [4] studied the biomechanics of a full healthy human knee joint model, focusing on the load transmission and stabilizing roles of ligaments and menisci.

Another study focusing on the function of the healthy human ACL is the work of Song et al. [13]. In this case, the purpose was to calculate the force and stress distribution within the anteromedial (AM) and posterolateral (PL) bundles of the ACL in response to an anterior tibial load with the knee in full extension.

For a more detailed and extensive literature review in computational models of the human knee joint the reader is referred to the review work of Kazemi et al. [43].

1.3. Objectives

The overall goal of this work is to develop a 3D FE model that enables a biomechanical analysis of the knee behavior after an ACL rupture. In detail, this work aims to provide clinical relevant information regarding the force, stress and displacement changes that occur in an ACL deficient knee.

Another objective is to verify the biomechanical changes induced by isotropic and anisotropic hyperelastic constitutive models in the modeling of the knee ligaments.

It is expected that the model is able to reproduce qualitatively and, if possible, quantitatively the behavior found in the literature in order to form a reliable foundation for future FE studies regarding the knee joint.

1.4. Thesis Outline

This thesis is divided into five distinct chapters. This first introductory chapter presents the motivation and objectives of the work as well as a background review on the existing computational models of the human knee joint.

Chapter two describes the anatomical and functional aspects of the main structures present in the knee, with a special focus on the ligaments. The fundamental topics of knee biomechanics are also covered and the chapter ends with an overview of the causes and consequences of an ACL injury.

Chapter three explains in detail all the procedures that lead to the definition of the final FE model used in the simulations. The theory needed to understand the constitutive models used in the ligaments is also presented in this chapter.

The results of the conducted simulations are presented and discussed in chapter four. These include the kinematic outputs of both ACL-intact and ACL-deficient knee in response to a posterior femoral load, as well as the force supported and the stresses developed in each of the four ligaments considered.

Chapter five presents the conclusions of the conducted work and gives suggestions of future developments in the matter of finite element simulations of the knee behavior.

At last, the references are made available and the appendices that were found convenient are also listed.

2. Knee Joint

The knee is the largest and most complex joint in the human body [1]. It is classified as a synovial¹ joint [2] and like any joint, the knee is composed of bones, cartilage, ligaments, tendons and muscles [44].

A distinctive feature of the knee is the fact that its joint cavity is only partially enclosed by a capsule. Despite this single joint cavity, the knee consists of three joints in one: the patellofemoral joint, between the patella and the lower end of the femur, and the two condylar articulations between the medial and the lateral condyles of the tibia and the femur, forming the weight-bearing tibiofemoral joint [1]. The proximal tibiofibular joint also contributes slightly for the motion of the knee, due to its soft tissue connection, even though not being part of the knee joint [2] .

The tibiofemoral joint acts essentially as a modified hinge in the sagittal plane (see Section 2.2), due to the restricting behavior of the ligaments, permitting flexion and extension. Some lateral and rotational motions are also allowed, representing secondary degrees of freedom [1,2].

The patellofemoral joint is a plane joint that articulates the patella and the femur where the patella glides superiorly and inferiorly across the distal end of the femur during knee flexion [1,2,45]. This articulation allows the pull of the quadriceps femoris muscle to be directed anteriorly over the knee to the tibia without tendon wear [46].

In the following subsections, a brief description of the anatomy, biomechanics, and kinematics of the knee is done, with a particular focus on the ACL role. To end the chapter, the fundamental aspects of ACL injuries are discussed.

2.1. Anatomy

In order to explain the relative positions and movements of the knee joint it is necessary to introduce some concepts. The three anatomical reference planes are represented in Figure 2.1. The sagittal plane divides the body vertically in its right and left halves; the frontal (or coronal) plane divides the body vertically in its anterior and posterior halves; the transverse (or axial) plane divides the body in its, inferior and superior halves.

With this concepts in mind, the six degrees of freedom of the knee (Figure 2.2) can be defined: three translations: anterior-posterior, medial-lateral and proximal-distal; and three rotations: flexion-extension, internal-external (medial-lateral) and varus-valgus (adduction-abduction) [6,19,47,48].

¹ Synovial joints are those in which the articulating bones are separated by a fluid-containing joint cavity [1].

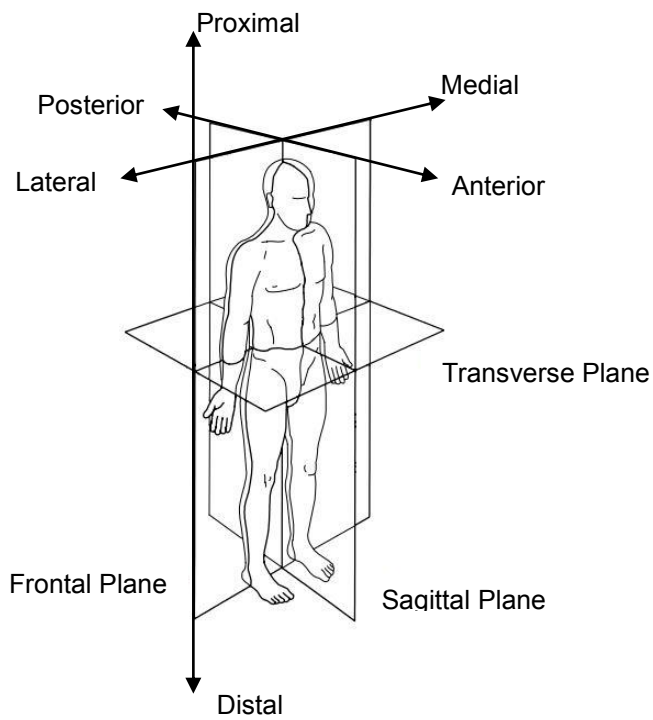


Figure 2.1 - The reference planes of the human body in the standard anatomical position [75].

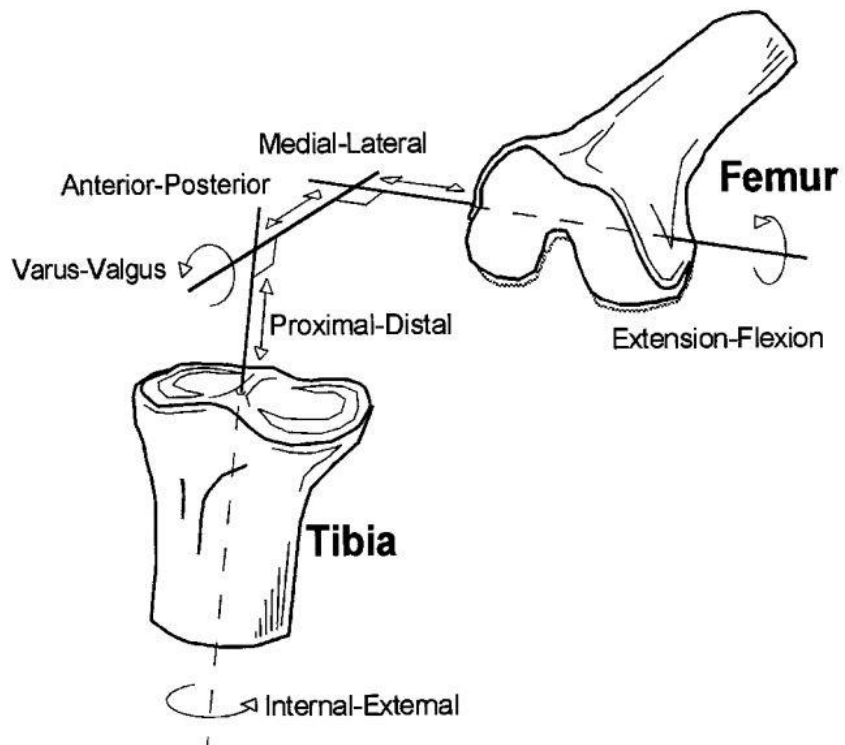


Figure 2.2 – Knee joint degrees of freedom: three translations and three rotations [48].

Very briefly, the knee joint is composed of three bones: the femur, the tibia and the patella, which are covered by articular cartilage in their distal, proximal and anterior ends, respectively. On the top of the tibial plateau, lie the medial and lateral menisci. The femur and the tibia are connected by four major ligaments, the anterior cruciate ligament (ACL), the posterior cruciate ligament (PCL), the medial collateral ligament (MCL), and the lateral collateral ligament (LCL). Covering the anterior part of the knee is the patella, which is encased in the patellar tendon. All of these structures are represented in Figure 2.3.

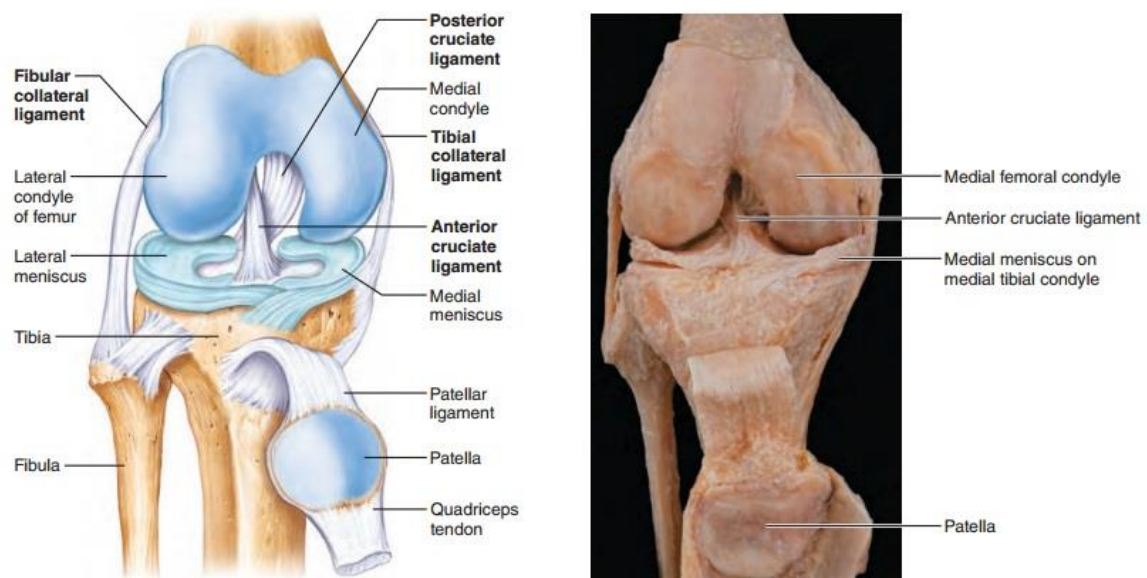


Figure 2.3 - Anatomic structure of the right knee – anterior view. a) Schematic representation. b) An opened knee joint [1].

2.1.1. Bones

The bony part of the knee joint is composed of three bones: the femur, the tibia and the patella (Figure 2.4).

The femur is the largest, longest, heaviest [45] and strongest bone in the human body [2]. Its durable structure permits to sustain stresses up to 280 kg/cm² (28 MPa) during vigorous activities like jumping [1].

Proximally, the femur articulates with the hip bone and then courses medially as it descends toward the knee [1], bringing this joint nearer to the middle line of the body [45]. This arrangement of the femur allows the knee joints to be closer to the body's center of gravity and provides for better balance [1].

The distal end of the femur expands into the large medial and lateral condyles that constitute the proximal articular surface of the knee joint [45,49].

The medial and lateral condyles are separated inferiorly by the intercondylar notch through most of their length but are joined anteriorly by an asymmetrical, shallow groove called the patellar groove or surface that engages the patella during early flexion [49].

The medial and lateral epicondyles (sites of muscle attachment) flank the condyles superiorly. On the superior part of the medial epicondyle is a bump, the adductor tubercle [1].

The tibia is second to the femur both in size and strength. It receives the weight of the body from the femur and transmits it to the foot.

At the proximal end of the tibia are the asymmetrical and concave [1] medial and lateral condyles (or tibial plateaus) that constitute the distal end of the knee joint [49]. The tibial condyles articulate with the corresponding condyles of the femur [1] and are separated by a roughened area, and two bony spines called the intercondylar tubercles. These tubercles become lodged in the intercondylar notch of the femur during knee extension [49].

Distally, the tibia has a concave shape and articulates with the talus bone of the foot [1,2].

The patella (knee cap) is a triangular shaped sesamoid bone (a bone formed with the tendon of a muscle [46]) located anteriorly to the knee joint, between the femur and the tibia. It is inserted in the tendon of the quadriceps femoris muscle that secures the anterior thigh muscles to the tibia [1]. During normal flexion and extension of the knee, the patella slides up and down in the patellar groove when the leg moves [44,45]. It protects the knee joint anteriorly and improves the leverage of the thigh muscles acting across the knee [1,50].

The fibula, even though its connection to the tibia, with which it forms the tibiofibular joint, does not form part of the knee joint. It also does not bear any weight but it serves as an insertion site for several muscles [1].

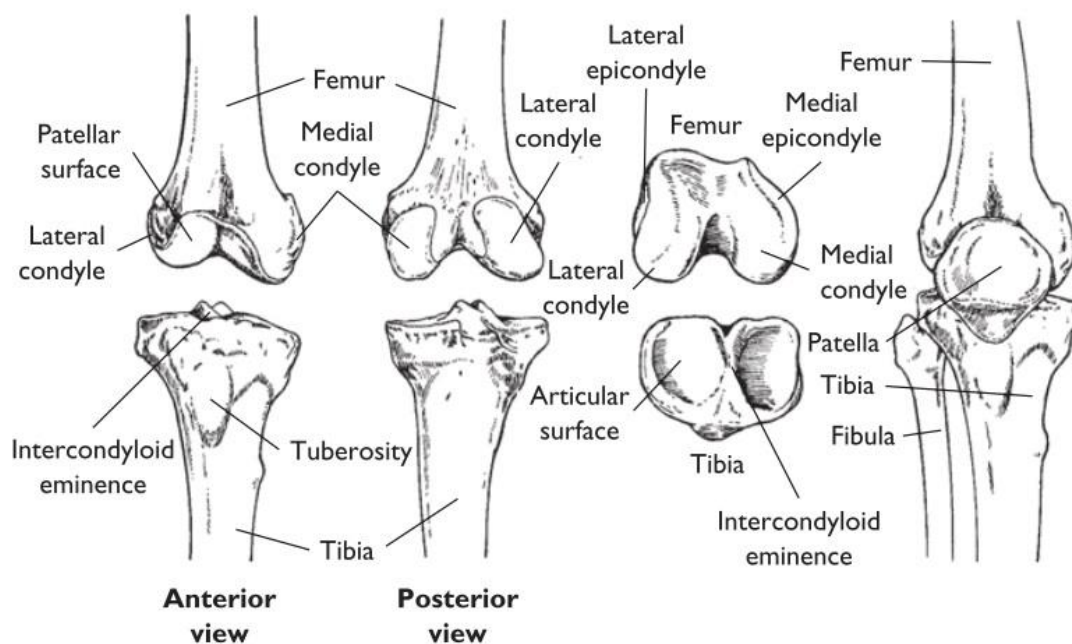


Figure 2.4 - Bony structure of the knee [2].

2.1.2. Articular Cartilage

The bones at a synovial joint, like the knee joint, are covered by articular cartilage, which is hyaline cartilage [45]. In the knee, articular cartilage is present at the end of the femur, the top of the tibia and at the posterior side of the patella [51].

The two main functions of articular cartilage are: spreading the load over a wide area so that the amount of stress at any contact point between the bones is reduced; and allowing movement of the articulating bones at the joint with minimal friction and wear [2].

Articular cartilage is a soft, porous, and permeable tissue that is hydrated. It consists of specialized cells called chondrocytes embedded in an extracellular matrix (ECM) of collagen fibers, proteoglycans, and noncollagenous proteins [2,49].

Articular cartilage can be divided in three different layers or zones with different collagen fiber orientations and, consequently, with different roles in shock absorbing and friction reducing functions. There is an extra fourth layer, the calcified layer of cartilage, that lies adjacent to subchondral bone and anchors the cartilage securely to the bone [49].

Unfortunately, once injured, hyaline articular cartilage has limited and imperfect mechanisms for self-repair [2,49]. Therefore, injuries to this tissue tend to progress, deteriorating more and more the protective coating of the bone ends, leading to the development of osteoarthritis [2].

2.1.3. Menisci

Since the bony architecture of the tibial plateaus does not match up well with the convexity of the femoral condyles, there is a need to improve the congruency of the knee joint so that it becomes more stable. This role belongs to the menisci, which are two semicircular discs of fibrocartilage, lying within the tibiofemoral joint, covering one half to two thirds of the articular surface of the tibial plateau [49] (see Figure 2.5).

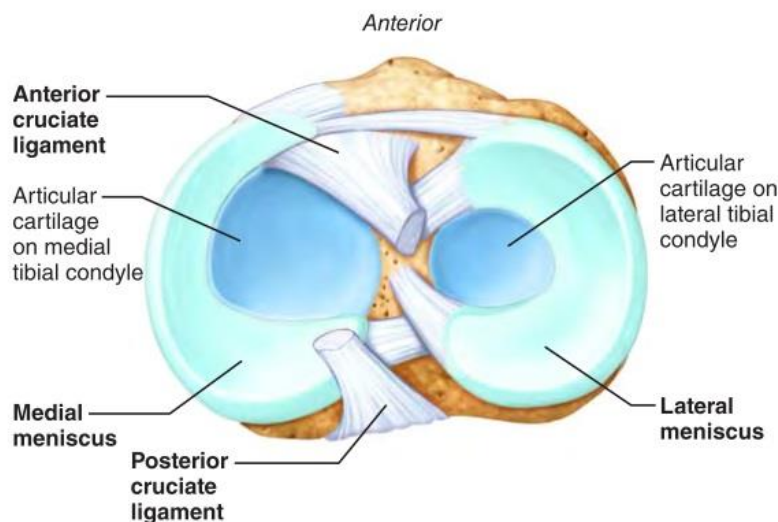


Figure 2.5 - Superior view of the right tibia in the knee joint, highlighting the menisci and cruciate ligaments [1].

The strong attachment of the menisci to the superior plateaus of the tibia is made by the coronary ligaments, the joint capsule and by the anterior and posterior ends of the menisci, the meniscal horns [2]. In addition, both menisci are also attached to the patella by the patellomeniscal ligaments and are connected anteriorly to each other via the transverse ligament.

The medial meniscus has less relative motion than the lateral meniscus, and it is more firmly attached to the joint capsule through medial thickening of the joint capsule that extends distally from the femur to the tibia [49]. The medial meniscus is also directly attached to the MCL [2].

The menisci help prevent side-to-side rocking of the femur on the tibia [1], enhance joint congruence [49], assist with load transmission [2] and also act as shock absorbers [1,49,51]. The shape of the menisci increases the contact area between the femur and the tibia, contributing to the reduction of the joint stress on the articular cartilage of the knee [2,49]. This function is depicted in Figure 2.6.

It is estimated that the menisci take up 50% to 70% of the compressive forces that are applied to the knee in activities like gait, stair climbing (one to two times the body weight) and running (three to four times the body weight) [49]. In menisci-deficient knees, the stresses at the tibiofemoral joint can get three times higher than in a healthy knee [2]. So, as it happens with the articular cartilage, an injury to the menisci, increases the wear on the articulating surfaces, leading to a knee joint more susceptible to the development of degenerative conditions [2].

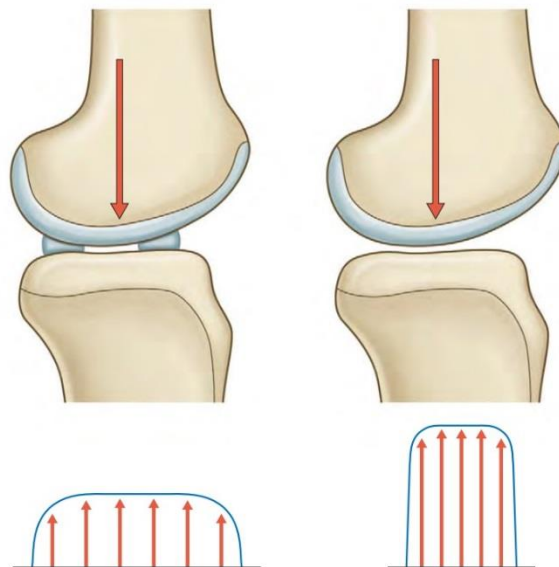


Figure 2.6 - The menisci role in increasing tibiofemoral congruence. The menisci wedge-shaped cross-section area helps to increase the contact area between the femur and the tibia, leading to a wider distribution of compressive loads [47].

2.1.4. Ligaments

Ligaments are defined as dense regular connective tissue that attaches bone to bone [45]. Histologically, the ligaments consists of mostly parallel oriented and closely packed collagen fiber bundles dispersed in a highly compliant ground substance matrix of proteoglycans, glycolipids and fibroblasts [10,41,48,52]. The internal hierarchical structure of ligaments is represented in Figure 2.7. About two-thirds of the dry weight of ligaments is composed of water, being the remaining weight due to the fibrillar protein collagen [10,52].

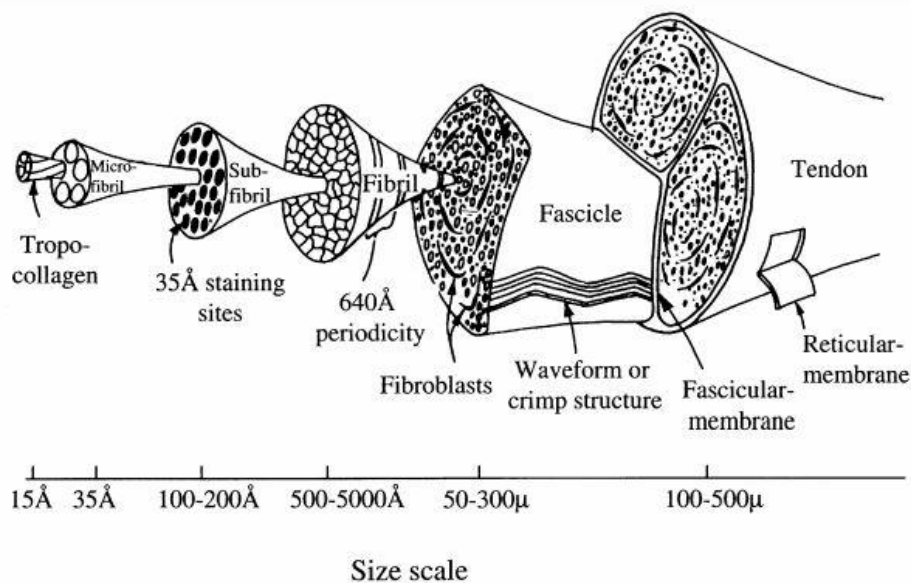


Figure 2.7 - Internal hierarchical structure of ligaments and tendons [52].

Collagen is the major responsible for the tensile strength of the ligament. Since the collagen fibers are mainly aligned along the longitudinal direction (in a waveform referred to as the crimp pattern), ligaments are best suited to transfer load from bone to bone along this direction. So, even though ligaments experience some shear and transverse loading *in vivo*, their mechanical properties are usually studied by performing uniaxial tensile tests on bone-ligament-bone units. These tests show that the ligaments have a nonlinear load-elongation response, with an upwardly concave curve that can be divided in three regions. The initial portion of the curve is the toe region, where the application of small loads produces a considerable stretching in the ligaments due to the “un-crimping process”, the recruitment of crimped collagen fibers which are easily stretched out. As the load increases, more fibers are involved and the curve gradually enters the linear region, with the load-elongation response being mainly dictated by the straightened collagen fibers. The ligament continues to stretch until the collagen fibers get to their rupture point, entering the failure region. The typical load-elongation curve of ligaments is presented in Figure 2.8 [10,48,52,53].

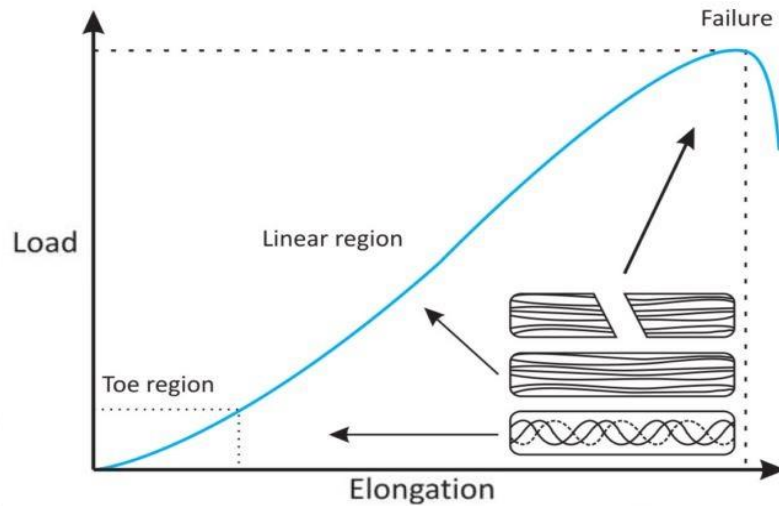


Figure 2.8 - Typical load-elongation curve of ligaments with the three regions and the changes in collagen fiber structure. Adapted from [53].

The load-elongation curve describes the structural properties of the bone-ligament-bone complex such as stiffness, ultimate load, ultimate elongation, and energy absorbed at failure. Given the initial cross-section and the length of the specimen, a stress-strain curve can be derived from the original load-elongation curve. This new curve provides information regarding the mechanical properties of the ligament such as tangent modulus, ultimate tensile strength, ultimate strain, and strain energy density. Both curves and respective properties are presented in Figure 2.9.

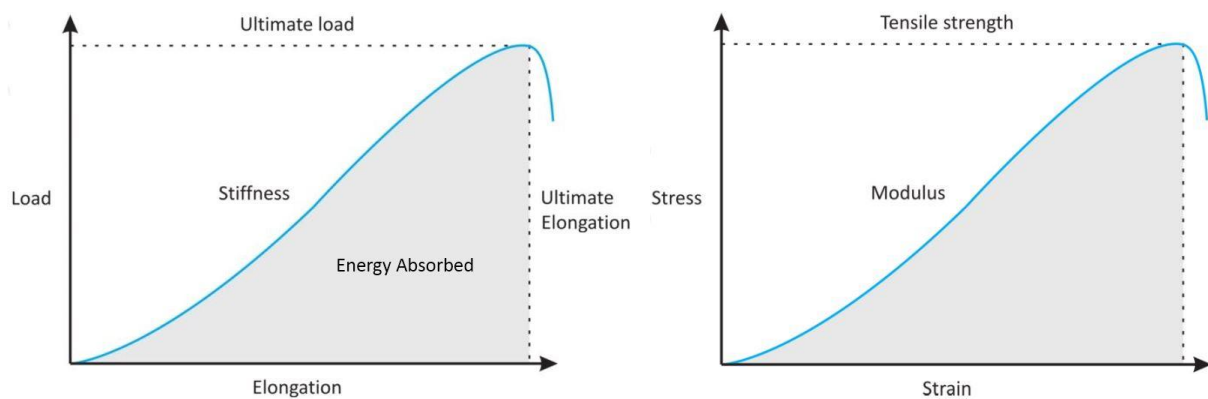


Figure 2.9 - Left side) Load-elongation curve and structural properties. Right side) Stress-strain curve and mechanical properties [53].

Due to their three-dimensional fibrous structure, the ligaments are considered to be highly anisotropic [10,52]. This fact has mechanical implications, with the ligaments showing low resistance and stiffness to compression, bending and transverse loading to the collagen fiber direction [52].

In addition to the non-linear elasticity, ligaments also display time- and history-dependent viscoelastic properties such as creep, stress-relaxation and hysteresis [10,19,48,52,53].

The main function of the ligaments is to provide for stability of joints in the musculoskeletal system [10].

In the knee joint, their role assumes a major importance due to the incongruence of the articulating surfaces of the tibia and the femur. The knee ligaments are responsible for controlling and/or resisting: knee hyperextension, varus and valgus stresses at the knee, anterior and posterior displacement of the tibia beneath the femur, medial or lateral rotation of the tibia beneath the femur and combinations of anteroposterior displacements and rotations of the tibia, together known as rotatory stabilization of the tibia [49]. Even when the knee is in neutral positions, the ligaments present some level of *in situ* stress, providing joint stability when no muscle or tendon forces are being exert [52].

The anatomical geometry and location of each ligament determines the direction in which it is capable of resisting the dislocation of the knee [2,52].

The knee has four major ligaments that can be separated in two groups: the cruciate ligaments, composed of the anterior cruciate ligament (ACL) and the posterior cruciate ligament (PCL), and the collateral ligaments, constituted by the medial (or tibial) collateral ligament (MCL) and the lateral (or fibular) collateral ligament (LCL).

The cruciate ligaments of the knee are intracapsular² and extrasynovial [6,10,50] ligaments that ensure the anteroposterior stability of the knee by limiting the forward and backward sliding of the femur on the tibial plateaus during knee flexion and extension as well as restraining hyperextension. They also allow hinge-like movements to occur while keeping the articular surfaces together [2,3]. The name *cruciate* is derived from the fact that these ligaments cross each other and the denominations *anterior* and *posterior* refer to their respective tibial attachments [2,10,47].

The collateral ligaments of the knee are extracapsular³ [50] ligaments that strengthen the articular capsule on its medial and lateral aspects. This group of ligaments is responsible for the transverse stability of the knee during extension [3].

In addition to these, there are other ligaments that also contribute to maintain the integrity and stability of the knee. Namely, the oblique and arcuate popliteal ligaments that cross the knee posteriorly, the transverse ligament that connects the two menisci and the Humphrey and Wrisberg ligaments that are sometimes found anteriorly and posteriorly to the PCL, respectively [2,10].

The anatomical and functional aspects of the four major ligaments are described in greater detail in the following sections.

2.1.4.1. Anterior Cruciate Ligament

The ACL runs posteriorly, laterally, and superiorly from tibia to femur [3,49]. It extends from a broad area anterior to and between the intercondylar eminences of the tibia to a semicircular area on the posteromedial aspect of the lateral femoral condyle [2,6,49]. In addition, the ACL twists inwardly

² Ligaments that occur within the articular capsule but are excluded from the synovial cavity by folds of the synovial membrane [50].

³ Ligaments that lie outside the articular capsule [50].

(medially) as it goes in the proximal direction [49]. The ACLs length and width ranges from 31 to 38 mm and 10 to 12 mm, respectively [6].

Although some authors [3] claim that the ACL can be divided into three different macroscopic bundles, the division in only two different bundles, the anteromedial (AM) and the posterolateral (PL), is widely more accepted [6,7,10,12,49,54]. These bundles are named based on their origins on the tibia [7,49] and represent a functional division of the ACL. Since these groups of fibers experience independent episodes of lengthening and slackening throughout the range of motion [5]: with the knee in full extension, the posterolateral bundle is taut and as the knee flexes, this bundle becomes more lax and the AM bundle becomes tight [6,49,54]. The location of each bundle is highlighted in Figure 2.10.

The primary function of the ACL is to prevent anterior tibial translation [1,5,6,11,49,52,54], bearing around 90% of and anteriorly directed load applied to the tibia, between the 30 and 90° of flexion [9,19]. The ACL is also responsible for restraining hyperextension of the knee [1,49] and it acts as a secondary stabilizer against internal rotation of the tibia and valgus angulation at the knee [6,11,49].

The contraction of the quadriceps is one of the mechanisms that loads the ACL, since it exerts an anterior tibial force through the patellar ligament [6,9]. The peak of the force in the ACL is at 30° of flexion and this effect is lost for higher degrees of flexion, since in this situation the patellar ligament pulls the tibia posteriorly [9].

ACL loading is also increased by the weight bearing conditions at the knee. A possible explanation for this is related to the posteroinferior slope of the proximal tibial surface which induces an anterior shift on tibiofemoral compression [9].

It is estimated that the ACL strains around 7% from full extension to 90° of flexion [19].

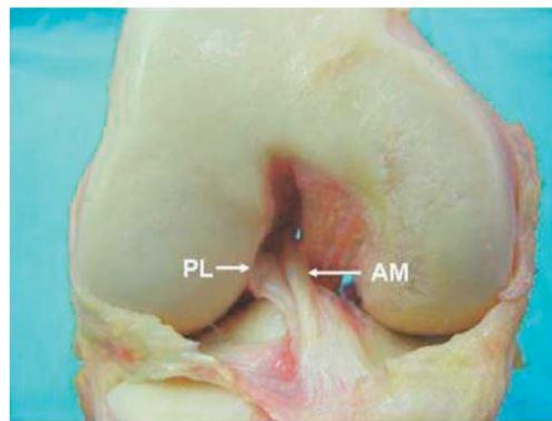


Figure 2.10 – Cadaveric right-knee specimen showing the anteromedial (AM) and posterolateral (PL) bundles of the ACL [12].

2.1.4.2. Posterior Cruciate Ligament

The PCL is attached distally to the posterior tibial spine and courses superiorly, medially and anteriorly to join the lateral aspect of the medial femoral condyle [2,3,49]. As it crosses to its tibial attachment, PCL blends with the posterior capsule and the tibial periosteum⁴ [49]. The PCL length and width are 38 and 13 mm in average, at its midportion [6].

The posterior cruciate ligament, like the ACL, is intra-articular with a much larger part existing extrasynovially [6,49].

In comparison to the ACL, the PCL is shorter, stronger, less oblique and has a cross-sectional area 20 to 50% larger [2,6,49]. The angle of inclination is also different, with the ACL more vertical in full extension as the PCL lies in a more horizontal position. A similar difference is also found in their femoral insertions, with the PCL having a horizontal insertion while that of the ACL is more vertical [3].

As it happens with the ACL, the PCL can also be divided in two distinct fiber bundles: a larger anterolateral (AL) bundle, which is tight in flexion, and a smaller posteromedial (PM) unit, which is tight in extension [6,54].

The main function of the PCL is to act as a primary restraint against the posterior displacement of the tibia or anterior sliding of the femur [1,6]. It is estimated that the PCL absorbs 93% of a posteriorly directed load applied to the tibia [49].

It is a secondary stabilizer against external rotation of the tibia and excessive varus or valgus angulation at the knee [6].

2.1.4.3. Medial Collateral Ligament

The MCL has an average length of 80 mm [10] and runs obliquely inferiorly and anteriorly, from the medial aspect of the femoral condyle to the upper end of the tibia [3]. Its femoral insertion lies on the postero-superior aspect of the medial femoral condyle, and its tibial attachment is just below the pes anserinus, the insertion site of three medial tibial muscles (semitendinosus, semimembranosus, and gracilis). The anterior fibers of the MCL are separated from those of the capsule but its posterior fibers merge with those of the capsule at the medial border of the medial meniscus [2,3].

The MCL is the primary restraint to excessive abduction (valgus) and lateral rotation stresses at the knee [2,49]. The MCL is taut when the knee is fully extended, position where this joint is best able to resist a valgus stress. As the knee starts to bend, the MCL becomes slacker and greater joint space opening is allowed (medially gapping). Despite the joint gapping, the MCL role on restraining valgus stresses is more pronounced when the knee is flexed. It is estimated that the MCL accounts for 78% of the restraining force against valgus opening at 25° of knee flexion and around 57% with the knee near full extension [49].

⁴ The fibrous layer covering all bones [49].

As secondary function, the MCL also plays a supportive role in resisting anterior translation of the tibia on the femur in the absence of the primary restraints against anterior tibial translation [49], like the ACL.

2.1.4.4. Lateral Collateral Ligament

The lateral collateral ligament runs obliquely inferiorly and posteriorly from the outer surface of the lateral condyle to the fibular head where it joins the tendon of the biceps femoris muscle to form the conjoined tendon [3,49].

The LCL is considered to be an extracapsular ligament, since it is free of the capsule along its entire course [3,49].

The LCL is primarily responsible for checking varus stresses, and like the MCL, limits varus motion most successfully at full extension. With the knee fully extended, the LCL is responsible for 55% of the restraining force against varus stress, value that raises to 69% when the knee is flexed at 25°.

Adding to this primary function, the LCL also limits excessive lateral rotation of the tibia due to its orientation [49].

2.2. Biomechanics and Kinematics

As previously stated in Section 2.1, the knee joint has six degrees of freedom: three translations: anterior-posterior, medial-lateral and proximal-distal; and three rotations: flexion-extension, internal-external (medial-lateral) and varus-valgus (adduction-abduction) [6,19,47,48].

Flexion-extension, permitted by the tibiofemoral joint in the sagittal plane, is the primary motion of the knee [2,6,9,47]. The normal passive range of motion in this plane goes from 0° to 130-140° [6,9,49] and can be increased in 5-10° in hyperextension [9,47]. The flexion-extension motion is characterized by complex movements of both rolling and sliding (or gliding) (Figure 2.11), which are controlled by the geometry of the articulating surfaces and by the cruciate ligaments. Due to morphological differences, the rolling and gliding movements are associated with the lateral and medial femoral condyles, respectively. In the sagittal plane, the medial femoral condyle is composed of two functional facets while the lateral femoral condyle is usually composed of a single circular facet, making the rolling movement more predominant on this condyle [5].

Starting from full extension, with the tibia fixed, the flexion of the knee is initiated by the unlocking mechanism of the popliteus muscle, which acts to laterally rotate the femur with respect to the tibia [2,47]. This effect is facilitated by the size differences between the lateral and medial sides [49].

Until about 20° of flexion, the femoral condyles (especially the lateral one) roll on the tibial surface. After this point, the rolling motion is accompanied by an anteriorly directed sliding motion [6,49]. This sliding mechanism is what keeps the femoral condyles on the tibial plateau as they roll to increase the flexion angle [49] with relative femoral movement on the tibia. The flexion of the knee can also be described in the reverse way, with tibia moving on a fixed femur as it happens, for instance, in the swing

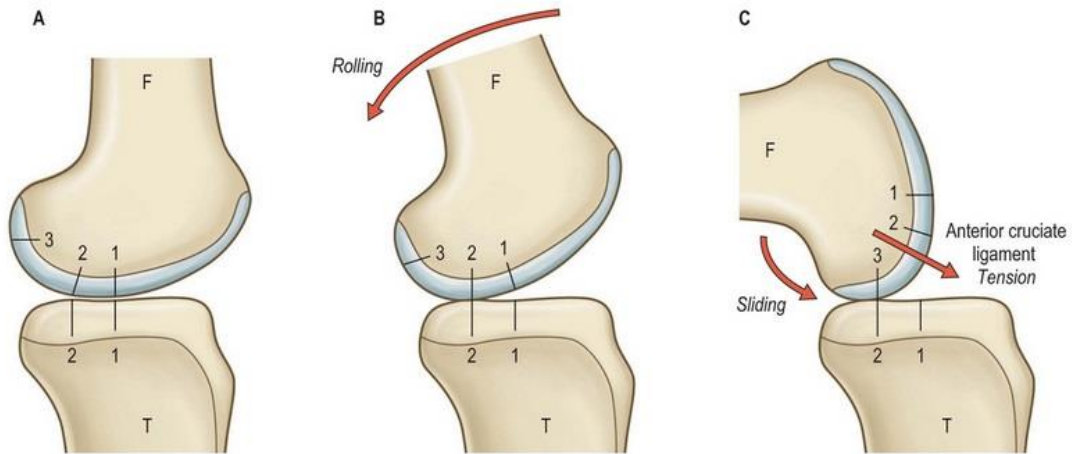


Figure 2.11 - The rolling-sliding mechanism. A) In full extension there is central contact between the femur and the tibia (F1-T1). B) As flexion starts, the femur rolls on the tibia and the contact is made on a more posterior position (F2-T2). C) At greater flexion angles, the ACL is tensioned and the femur slides anteriorly [47].

phase of gait. In this case, the tibia rolls and slides on the relatively fixed femoral condyles, posteriorly in flexion and anteriorly in extension [49].

The complex interplay between the cruciate ligaments helps maintain stability throughout the entire range of flexion. As mentioned before, in a fully extended knee, the ACL is taut, while the PCL is relatively slack. As flexion increases, the PCL tightens and the ACL becomes lax. From 20 to 50° of flexion the knee is more unstable, since neither of the ligaments is particularly tense. These slackening and tensioning episodes are accompanied by changes in the ligaments orientation: the ACL goes from vertical to a more horizontal position with increasing flexion; the opposite occurs in the PCL [6].

The location of the axis of rotation of the flexion-extension movement has been a topic of much discussion in last years, with four main theories describing differently both the nature and the location of this axis [9]. For simplification purposes, this axis can be defined as the horizontal line passing through the femoral epicondyles that despite being a fixed axis is considered to be an accurate estimate [49].

In the transverse plane, the knee can rotate internally or externally about a longitudinal axis that runs through or close to the medial intercondylar tubercle [5,9,49] and also very close to the ACLs tibial attachment [9]. This axis is located within the tibia and does not intersect with the axis of flexion-extension [9]. The internal and external rotations are denominations of movements of the tibia with respect to the femur [9,49]. The medial position of the axis, makes the medial condyle to act as pivot point, the lateral condyle moves in a wider range, regardless of the direction of rotation [49]. These axial rotations are possible due to the incongruence of the knee articulating surfaces and are influenced by the laxity of the ligaments and, therefore, depend upon the degree of knee flexion [5,9,49]. At full extension, the rotation is minimal because the tibial tubercles are lodged in the intercondylar notch, the ligaments are taut and the menisci are tightly held between the tibia and the femur [9,49]. The maximal rotation possible is near 90° of flexion [2,9,49] with values of total rotation around 35° [49].

Lastly, in the frontal plane a few degrees of rotation are also possible, constituting the valgus-varus motion. The knee joint is most restricted in this plane [9], explaining the small range of motion of only 8° at full extension and 13° with 20° of knee flexion [49].

The movements above described do not act separately. Instead, the knee motion is characterized by a complex combination of movements in all the three planes [18,49], with the degree of coupling being highly dependent on the external load [18]. Many studies have been undertaken in order to discover and understand these combinations of movements and the most reported findings indicate that:

- An internal tibial rotation occurs when a (small) axial load is applied on the knee in flexion [18]. An anterior directed force also generates an internal tibial rotation [9,18] that ceases if the ACL is cut [9], while a posterior force produces an external rotation [18];
- A coupling of internal and external rotations with applied valgus and varus torques, respectively [9];
- Another very important coupled motion is the “screw home” mechanism. This motion, also referred to as automatic or terminal rotation is an involuntary external rotation of the tibia that occurs near full extension [19,47,49].

Due to the anatomical differences between the medial and lateral articulating surfaces of the knee, in the last 30° of knee extension, the lateral side of the knee joint completes its rolling-gliding motion before the longer medial side. The motion of the medial side, which continues after the lateral one has stopped, induces a lateral tibial rotation on the femur. As the knee gets closer to extension, there is an increase in the knee ligaments tension which might also contribute to this rotational motion. In full extension, the joint congruence is maximal with the tibial tubercles lodged in the intercondylar notch, the ligaments taut and the menisci firmly positioned between the articulating surfaces of the tibiofemoral joint. In this position the knee is said to be “locked” [49].

As previously mentioned, the action of the popliteus muscle, facilitated by the joint incongruence, unlocks the knee, and the flexion movement can start again.

The tibiofemoral joint supports a compressive force of 2 to 3 times the body weight during normal gait. This force can increase up to 4 times the body weight during running or stair climbing [2,49].

2.3. ACL Injuries

Of all body joints, the knee is the most injury vulnerable joint because it is a mobile, weight-bearing joint. Furthermore, its stability is highly dependent on nonarticular structures like ligaments and muscles, due to the lack of congruence between the surfaces of the articulating bones [1,50].

There are two main types of knee problems: mechanical and inflammatory.

Mechanical problems may result from injury, such as a direct blow or abrupt movements that force the knee to exceed its normal range of movement. Other source of mechanical problems are the wear and tear of knee parts that can result in injuries like osteoarthritis.

Inflammatory problems occur due to certain rheumatic diseases, such as rheumatoid arthritis and systemic lupus erythematosus [44].

Ligament injuries, such as an ACL rupture, where the ligament is stretched beyond its normal range or torn, fit into the mechanical knee problems and are classified in a scale of one to four according to the severity of the lesion. Level one is for first-degree sprains when there is an acute mild trauma due to the tear of some fibers, resulting in mild pain but without loss of joint stability. The next levels increase as the number of torn fibers and joint instability go up, until the fourth-degree sprain when the rupture is complete and the joint becomes unstable, with high amounts of pain and swelling associated [51].

Amongst ligament injuries, the ACL is the most affected ligament [7,55], with an increasing number of 100 000 to 200 000 incidences of injury per year in the United States [7].

ACL injuries usually occur during sport activities where sudden stresses are applied to the knee joint while the tibia is in contact with the ground. These abrupt stresses are usually generated in non-contact acceleration, deceleration, jumping or cutting situations, involving a change in direction that creates valgus/valgus and internal rotation moments on the slightly flexed knee joint. A typical situation is when an athlete lands on one leg and tries to rotate in the opposite direction, an action present in many sports that involve pivoting movements, such as basketball or football [2,5,7,51,56]. Another sport highly associated with this injury is alpine skiing, where a common injury mechanism involves catching a ski tip in the snow, with the skier simultaneously twisting and falling [2,19]. Since the quadriceps are the main muscular restraint to anterior translation during vigorous activities such as running and jumping, there is a higher propensity of ACL rupture when these muscles (and the other surrounding the knee) are fatigued [2].

Although less commonly (around one third of the times), the cause of ACL injuries can also be a direct blow to the knee. Incidents of this type may happen in situations such as car accidents and in high-contact sports (e.g. football) where the knee can get directly hit [7,51,56].

The ACL rupture is also present in one of the most severe knee injuries, known as the O'Donoghue's (or unhappy) triad, where the medial meniscus and the medial collateral ligament are also torn [19,51].

Regardless of the injury mechanism, an ACL injury is almost always accompanied by secondary lesions to other structures such as the menisci and articular cartilage. These can be damaged due to the possible shock between the femur and tibia when the ACL rupture occurs [5,19].

The high rate of injury and the fact that in 20% of the times, the ACL rupture is bilateral, suggests that there might be some predisposing factors for this lesion to occur such as reduced notch width (leading to notch stenosis and associated with the size of the cruciate ligaments) and constitutional hyperlaxity [7,19,57]. It is also known that women are (around three to six times) more prone to ACL injuries than men [2,7,10,50,57], fact that has been explained with anatomical and neuromuscular factors, yet without definite conclusions.

There are several effects produced by injuries to the ACL, both immediate and in the long term.

When the ACL tears, a loud pop is usually heard and/or felt, meaning that the threshold of fibers resistance has been exceeded. The knee may start to swell right away and continue to do so until it reaches its maximum a few hours later, developing a painful hemarthrosis (accumulation of blood in the joint). The person affected is almost always forced to stop the activity that generated the injury [6,7,11,19,51,56].

Following an ACL rupture, individuals experience episodes of knee instability or “giving way” and difficulties performing movements that require lateral or rotational loads at the knee. This is caused by the deterioration of the physiologic roll-glide mechanism of the tibiofemoral joint that leads to an increase in both anterior tibial translation and internal tibial rotation [2,5,7,9,49]. On the other hand, the range of motion of flexion-extension decreases, which is attributed to the phenomenon of “quadriceps avoidance”, an adaptation mechanism to the absence of the ACL that minimizes the activation of the quadriceps muscle when the knee is close to full extension [2]. Since the ACL is the primary restraint against anterior tibial translation, its disruption will force secondary structures to perform this action to help stabilize the knee. The load increase in this secondary structures, such as articular cartilage and menisci, may negatively contribute to their degeneration process [2,5,8,9].

The diagnosis of an ACL injury usually starts with a physical examination of the knee using the Lachman, anterior drawer and pivot-shift tests to assess the anterior stability of the knee joint [19,48,56].

The Lachman test is performed with the knee at 20° to 30° of flexion with the muscles relaxed, while a manual anterior force is applied to the proximal tibia while holding the distal femur (Figure 2.12). The degree of anterior tibial translation of the injured leg is compared to the one from the other leg to evaluate the laxity of the knee [7,11,38,51,54,56]. In a healthy knee, anterior tibial translation of 3 to 5 mm is considered normal during an anterior drawer, or Lachman test [48]. A difference superior to 5 mm between the healthy and the injured knees is indicative of complete ACL dysfunction [11]. The Lachman test has been found to have a sensitivity of 85% and a specificity of 94% for ACL rupture [7] being the most sensitive of the three maneuvers [56]. The test can also be quantified using the KT 1000 arthrometer [7,8,38,54].



Figure 2.12 - The Lachman test. With the knee in 20 to 30 degrees of flexion, the examiner applies an anteriorly directed force on the tibia while holding the femur to assess the integrity of the ACL [56].

The anterior drawer test is similar to the Lachman’s test, the difference being the 90° flexion angle at which the knee is tested. With the foot fixed by the examiner’s thigh, an anterior load is applied to the tibia.

Lastly, the pivot-shift test is performed in a fully extended knee by applying an axial load and a valgus torque with gradual flexion. If the ACL is torn, the tibia will subluxate anteriorly and rotate internally [9,11,54,56].

The results from the physical tests might be complemented by magnetic resonance imaging [7,11,54,56], which has a specificity of 95% and a sensitivity of 86% for diagnosing ACL injuries [7]. Despite the very accurate results produced by these tests, in cases of a partial tear, an arthroscopy may be the only reliable means of detecting an injury [44].

There are two ways of treatment for ACL injuries: nonsurgical (conservative) and surgical [5,7,11,54,56]. The choice of the treatment option is conditioned by the patient's age, activity level, associated injuries, clinical history and expectations [11,54,56].

The nonsurgical, conservative way of treatment is usually applied to individuals with serious comorbid conditions or to people who will not participate in demanding physical activities. In these cases, the focus of the treatment is on strengthening the leg muscles, especially the hamstrings and the biceps femoris, through the practice of physical therapy [7,11,54,56]. However, without surgical repair, an ACL-deficient knee will continue to show altered biomechanics and kinematics with increased anterior translation and internal rotation of the tibia, changes in the center of rotation of the knee (medial shift) and altered tibiofemoral area during gait [2,7,9,19,48]. These joint behavior alterations have to be compensated by other components of the knee, making it prone to further injury in the long-term, such as additional subluxation episodes, cartilaginous and meniscal lesions and osteoarthritis [2,7,11,19,48,54,56]. Studies focusing on the long-term outcomes of non-surgical treatment of ACL injuries have reported the prevalence of radiographic osteoarthritis in 60-90% of subjects that went through conservative treatment 10-15 years after injury [5].

Surgical treatment is the choice for almost all athletes (and non-athletes) who want to maintain a high level of activity [7,54]. The injured ACL is usually replaced with an autograft (a piece of tissue harvested from the patient) from either the middle third of the patellar tendon or with one or more hamstring tendons (gracilis and semitendinosus) [2,5-7,9,11,51,54,56]. As an alternative, a graft transplanted from a deceased donor, an allograft, might also be used [5,7,11,51,56].

The outcome of the surgical procedure depends on several factors and decisions, namely: the choice of graft tissue, single-bundle versus double-bundle reconstruction, the graft placement, whether to leave the ruptured ACL remnant in the knee, the timing of the surgery, the graft (pre-) tension and the choice of the femoral tunnel drilling technique [5,7,9,56].

After a successful surgery, the patient still has a long road ahead before returning to preinjury functioning levels. In the early postsurgical period, the rehabilitation starts with simple exercises like straight leg raises, heel slides and continuous passive motion to regain mobility on the joint.

For the first six weeks, the patient should use crutches and perform quadriceps isometric and range-of-motion exercises. After this period, when the inflammation has decreased and the range of motion from full extension to, at least, 90° is restored, the patient can walk without crutches and proceed to more demanding exercises such as stationary bike and hamstring strengthening. More difficult exercises are progressively included in the rehabilitation program increasing strength, flexibility in the affected limb

over the course of six months. Functional sport-specific activities are usually initiated between six and nine months after surgery [7,56].

Even though the arthroscopic ACL reconstruction merits in restoring knee stability and function, the great number of variables underlying the surgical procedure may produce significant differences between the ACL-reconstructed and normal knees. It is reported that ACL reconstruction can restore anterior translation to intact levels at flexion angles greater than 30°, but fails to do so for smaller angles [9]. Other shortcomings are related to internal rotation motions which seem to be over constrained and produce a bigger anterior tibial displacement in comparison to intact knees. The *in situ* forces experienced by the grafts in this type of motion also present discrepancies [7,9,10].

In addition to the intrinsic issues of the surgery, rehabilitation also plays an important role in the long-term outcome of the surgery, so it is difficult to generalize the kinematic and biomechanical differences introduced by the ACL reconstruction.

Nevertheless, surgical treatment has positive results, restoring the level of performance in 65% of the patients [56].

It is expected that this number increases even further in the future, with innovations in surgical techniques and tissue engineering [7,56].

3. Methods

3.1. Geometrical Model

A FE simulation requires a geometrical model that depicts the reality as much as possible. The knee joint is a complex structure, composed by several different parts with very characteristic morphologies, making its 3D modeling a highly challenging task.

The tridimensional knee joint geometry here adopted was obtained from the Open Knee project. [58,59]. The Open Knee project intends to provide a freely available and open source finite element representation of the knee for predictive simulations of joint loading and its effects on the underlying tissue structures [58]. It is a work in progress, currently funded by the National Institute of General Medical Sciences, National Institutes of Health. Besides the studies made by the development team, the Open Knee enabled other studies, with a total of eleven publications that can be consulted in [59], contributing to the constant verification and development of the project.

This thesis used the Open Knee – Generation 1 (version 1-0-1) available for download in [59] which includes 3D solid representations of eleven parts of the tibiofemoral joint: distal femur, proximal tibia, articular cartilages (femoral, medial tibial, and lateral tibial), ligaments (ACL, PCL, MCL and LCL) and the medial and lateral menisci. All of these structures were in .IGS file format.

In addition to the individual solid parts, an Abaqus (Simulia, Providence, USA) input file (.inp) with the whole knee model assembled and fully meshed with 8-noded hexahedral elements was also available.

The geometries of the knee parts were generated from magnetic resonance images of the right knee of a donor subject whose information is itemized in Table 3.1.

Table 3.1 - Specimen Information [58].

| | |
|-----------------------|------------------|
| Side | Right |
| Donor Age | 70 Years |
| Body Weight | 77.1 kg |
| Height | 1.68 m |
| Gender | Female |
| Cause of Death | Pneumonia/Cancer |

3.1.1. Known Limitations

The process of modeling a complex structure such as the knee joint has inherent limitations. Some of these may lead to deficiencies in the model's predictive capacity. The Open Knee version used in this thesis has some documented limitations that have to be taken into account when analyzing and comparing the results with other studies, namely [58]:

- The model does not include representations of patella, patellar tendon, articular cartilage of the patella and other components such as the fibula, joint capsule, muscles, etc.;
- Attachment of MCL to medial meniscus is not modeled;
- Attachment of medial meniscus periphery to tibial cartilage is not modeled.
- Due to contrast/resolution issues, the geometry of the menisci, LCL, and MCL may have inaccuracies or approximations. The most evident case is the distal end of the LCL which is not directly connected to any part. This is because the LCL connects distally to the fibula, which is not modeled. However, this is just a visual limitation, since the fibula is attached to the tibia and does not contribute directly to the knee movement. So it is reasonable to admit that the LCL distal end follows the movements of the tibia (see Section 3.5).

Adding to these, the intrinsic errors associated with the process of manual segmentation in this type of 3D modeling may also affect the simulations outcome.

3.2. Mesh Definition

For all the parts except for the ligaments, the mesh was defined in the graphical interface of Abaqus, Abaqus/CAE (Complete Abaqus Environment).

Since the knee bones were defined as rigid bodies (see Section 3.3), the femur and tibia were meshed with R3D4 (4-node 3D bilinear rigid quadrilateral) and R3D3 (3-node 3D rigid triangular facet) elements. The remaining parts were meshed with C3D8 (8-node linear brick) elements.

To mesh the complex geometries of the soft tissue parts of the knee with C3D8 elements it was necessary to create partitions to define more regular sections so that Abaqus meshing algorithms could work. This was accomplished by defining several *Datum Planes* and *Datum Points* that served as geometrical references to create *Partition Faces* and *Partition Cells* where needed. As an illustrative example of this process, Figure 3.1 shows the partitions created on the lateral tibial cartilage.

As for the ligaments, despite the many attempts to define regular sections, their intricate 3D structure precluded Abaqus from creating a mesh of hexahedral elements without errors. The solution to get a full hexahedral mesh was to use the Abaqus input file provided in the Open Knee. In this input file the whole knee was defined as a unique part. With the help of a developed Python script, the input file was manipulated to extract the information relative to the nodes and elements that composed the ligaments, creating an independent part for each ligament. These parts were then imported to the knee model as

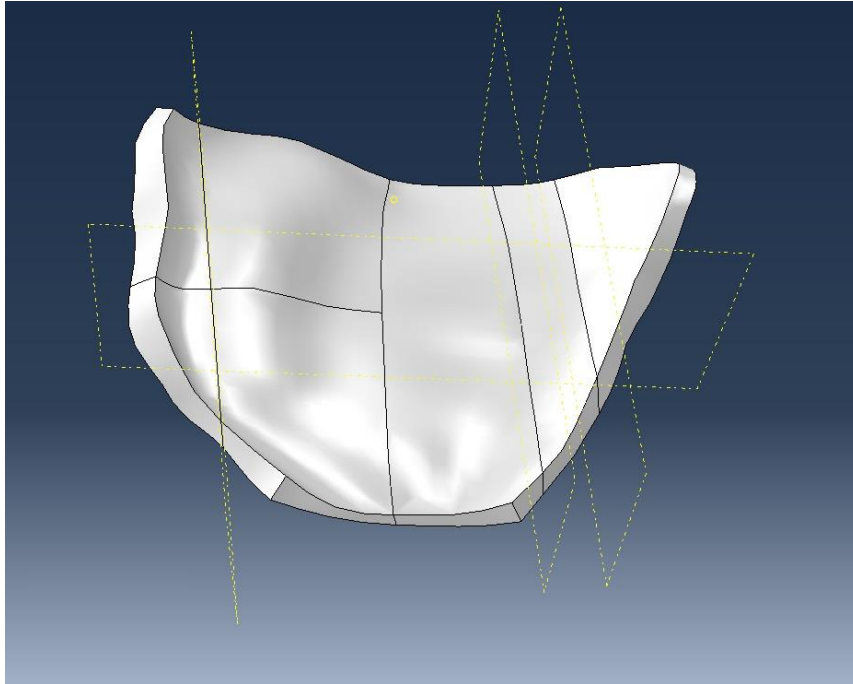


Figure 3.1 - Partitions created on lateral tibial cartilage to define regular section for meshing.

Orphan Mesh parts. Due to incompressibility condition discussed in the next section, hybrid formulation was defined for the elements of the ligaments (C3D8H elements).

The final mesh of the entire assembly was composed, 78759 elements divided by each part as described in Table 3.2 and is represented in Figure 3.2.

Table 3.2- Number of elements of each 3D part of the FE model.

| | Number of Elements |
|-------------------------------------|--------------------|
| ACL | 4096 |
| LCL | 6656 |
| MCL | 5120 |
| PCL | 5248 |
| Lateral Tibial Cartilage | 2146 |
| Medial Tibial Cartilage | 2768 |
| Lateral Meniscus | 1888 |
| Medial Meniscus | 1728 |
| Femoral Cartilage | 13684 |
| Total of Deformable Elements | 43334 |
| Femur | 22133 |
| Tibia | 13292 |
| Total of Rigid Elements | 35425 |

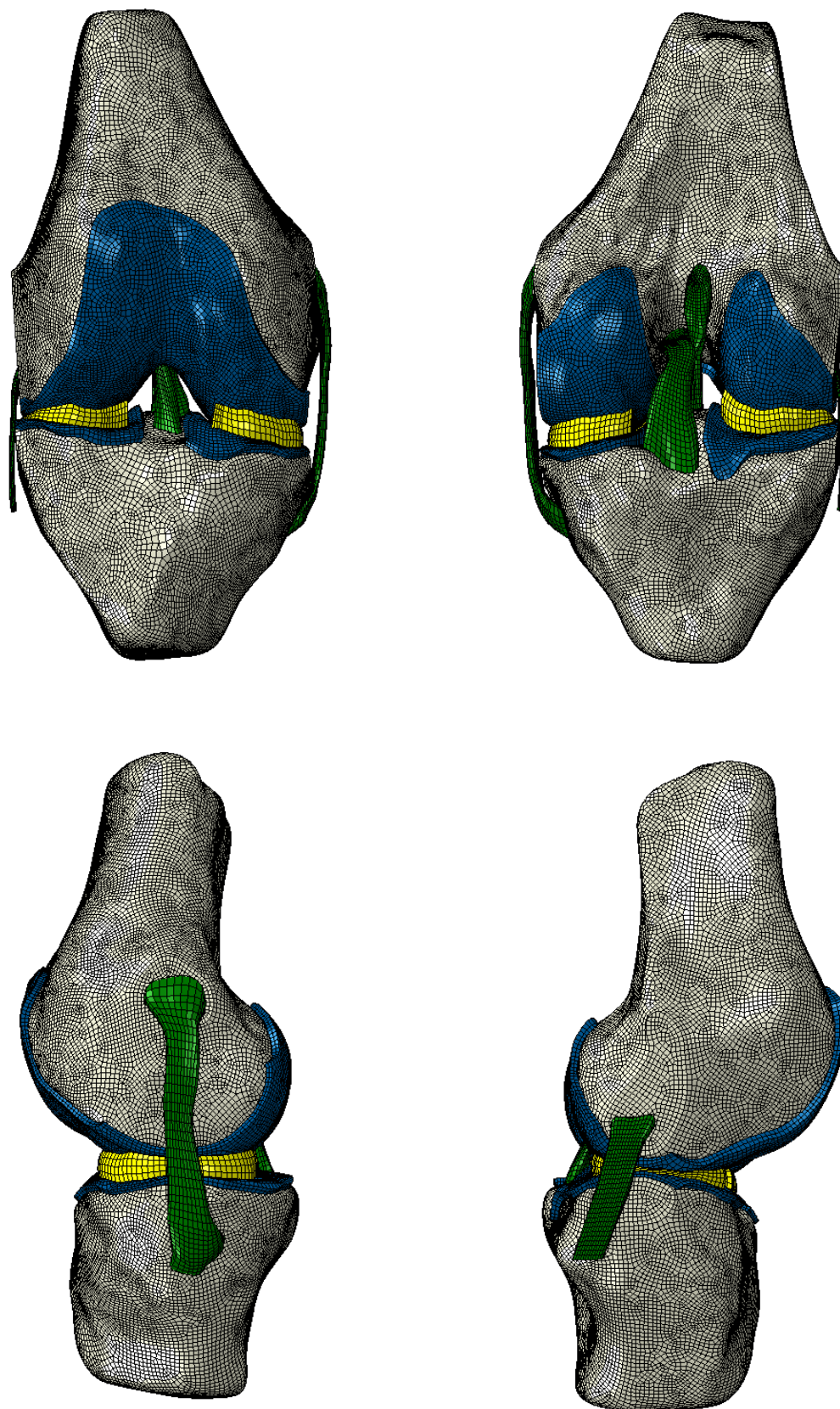


Figure 3.2 – Mesh of the fully assembled knee. Different colors represent different tissues: grey for bones, blue for articular cartilages, yellow for menisci and green for ligaments. (Top left) Anterior view. (Top right) Posterior view. (Bottom left) Medial view. (Bottom right) Lateral view.

3.3. Material Properties

The bones were modeled as rigid bodies due to their much greater stiffness in comparison to soft tissues. This approach has been extensively used in other FE studies [4,16,20,21,23,24,26–30,32–34,36–39] with no significant loss of accuracy in any contact variable [23] and with the advantage of greatly reducing the simulations computational cost.

Articular cartilage was modeled as linear elastic isotropic material. Despite being a hydrated tissue, the time of interest of the loading cases discussed in this thesis is too small compared to the viscoelastic time constant of cartilage (1 s versus 1500 s), making this is a reasonable approximation. The same approach has been adopted in many studies [4,14,21,23,24,26–29,33,37]. From the many values available in the literature, the Young's modulus (E) and Poisson's ratio (ν) of the articular cartilage were chosen to be 5 MPa [4,24,28,29] and 0.46 [4,28], respectively. The same explanation goes for the menisci, for which was assumed $E=59$ MPa and $\nu=0.49$ [4,28].

The viscoelastic behavior of the ligaments was also neglected due to the explanation given above. However, considering their highly non-linear stress-strain curve presented in Section 2.1.4 and the information found in the literature with respect to their material modeling, it would be too simplistic to describe the ligaments with linear elastic properties. Therefore, two hyperelastic constitutive models available in the material set library of Abaqus were tested: the Marlow and the Holzapfel-Gasser-Ogden (HGO) constitutive models. Both models were used to define the material properties of ligaments in previous studies, [28] and [14,38] for Marlow and HGO, respectively. Before proceeding to a more detailed explanation of each model, a very brief introduction to some concepts of continuum mechanics and constitutive hyperelastic modeling has to be made. The information here presented can be found in the work of Weiss and Gardiner [52] and in Abaqus Theory Manual [60] (chapter 1 and section 4.6.1) to which the reader is referenced for more detailed explanations.

Accordingly to the standard notational convention, \mathbf{X} defines the position of a material point in the reference configuration Ω_0 while \mathbf{x} represents the material point in the deformed (current) configuration Ω .

The deformation χ gives the position $\mathbf{x} = \chi(\mathbf{X}) \in \Omega$ of the material point $\mathbf{X} \in \Omega_0$. The kinematics of deformation are described locally in terms of the deformation gradient tensor, denoted as \mathbf{F} :

$$\mathbf{F}(\mathbf{X}) = \frac{\partial \mathbf{x}}{\partial \mathbf{X}} \quad (3.1)$$

The Jacobian of the transformation is the local volume ratio, which is the ratio of the undeformed volume over the deformed value for a homogeneous deformation at a given material point.

$$J = \det \mathbf{F} = \left(\frac{\rho_0}{\rho} \right) \quad (3.2)$$

Where ρ_0 and ρ are the reference and current material densities, respectively. If the material is incompressible $J = 1$.

Next, the right and left Cauchy-Green deformation tensors are defined. These tensors provide deformation measures that are independent of rigid body rotations and form the basis of constitutive hyperelastic models development for soft tissues.

$$\mathbf{C} = \mathbf{F}^T \mathbf{F} \text{ and } \mathbf{B} = \mathbf{F} \mathbf{F}^T \quad (3.3)$$

Hyperelastic materials are described in terms of a scalar function from which the stress can be derived at any point \mathbf{X} . This is the strain energy density function (SEDF) which defines the strain energy stored in the material per unit of reference volume (volume in the initial configuration) as a function of the deformation at that point in the material [60]. The SEDF can be exclusively defined in terms of \mathbf{F} :

$$\Psi = \Psi(\mathbf{F}) \quad (3.4)$$

The SEDF must respect the Principle of Material Frame indifference, which ensures that rigid body motions will not change its value. This means that Ψ can be expressed in terms of \mathbf{C} :

$$\Psi = \Psi(\mathbf{C}) \quad (3.5)$$

If the material considered is isotropic, Ψ can be defined only through the three principal strain invariants of \mathbf{C} :

$$\Psi = \Psi(I_1, I_2, I_3) \quad (3.6)$$

where

$$I_1 = \text{tr}(\mathbf{C}) = \lambda_1^2 + \lambda_2^2 + \lambda_3^2, \quad I_2 = \frac{1}{2}[(\text{tr}(\mathbf{C}))^2 - \text{tr}(\mathbf{C}^2)] \quad I_3 = \det \mathbf{C} \quad (3.7)$$

Lastly, the quantities needed to understand the curve-fitting procedure described later are also introduced. The nominal stress is defined in Eq. (3.8) as the force F applied over the initial cross section A_0 :

$$S = \frac{F}{A_0} \quad (3.8)$$

The stretch ratio λ is the ratio of the length of a deformed line element, l , to the length of the corresponding undeformed line element, l_0 :

$$\lambda = \frac{l}{l_0} \quad (3.9)$$

The nominal strain ϵ is the change in length per unit of the initial length as defined in Eq. (3.10).

$$\epsilon = \frac{l - l_0}{l_0} \quad (3.10)$$

With these concepts in mind, the previously mentioned constitutive models are succinctly characterized in the following subsections.

3.3.1. The Marlow Constitutive Model

The Marlow constitutive model is a general first-invariant hyperelastic constitutive model developed by R.S. Marlow [61]. In this model, it is assumed that the SEDF depends exclusively on the first-invariant, I . This means that the strain energy density can be expressed in terms of uniaxial test data, without having to assume any particular functional form.

The SEDF of the model for the incompressible case is presented in Eq. (3.12).

$$\Psi = \Psi(\bar{I}_1) \quad (3.11)$$

where

$$\Psi(\bar{I}_1) = \int_0^{\lambda_T(\bar{I}_1)-1} T(\varepsilon) d\varepsilon \quad (3.12)$$

Where $T(\varepsilon)$ is the nominal uniaxial traction, $\lambda_T(I)$ is the uniaxial stretch and ε is the uniaxial strain. The incompressibility constraint is introduced by \bar{I}_1 , which is the isochoric part of the first strain invariant, I_1 . (see next section).

Similar expressions can be derived based on equibiaxial or planar tension (see [61]).

To adjust this model to a given stress-strain curve in Abaqus, we need only to provide the experimental stress-strain data points, which will substitute the term T and, therefore there is no need of a curve-fitting procedure. By doing this, the curve created by the model will pass in each of the points given, reproducing exactly the stress-strain behavior used in its definition [61].

3.3.2. The Holzapfel-Gasser-Ogden Constitutive Model

The HGO constitutive model was developed by Gasser et al. [62] to describe the histology and mechanical properties of arterial tissue. By adding a scalar parameter to account for the dispersion of collagen fibers to a previous structural framework [63,64], they defined a model especially suited to describe the anisotropic hyperelastic behavior of collagen fiber reinforced materials.

Although originally created for modeling the arterial layers, this model has been applied to represent other soft tissues such as the hip capsule [65] and the knee ligaments [14,38]. In order to understand all the components of the HGO model SEDF, new theoretical concepts have to be added to the ones already presented.

The deformation gradient defined in Eq.(3.1) can be decomposed in two parts: a volumetric part, $(J^{1/3} \mathbf{I})$, that accounts for volume-changing deformations and an isochoric part, $\bar{\mathbf{F}}$.

$$\mathbf{F} = (J^{1/3} \mathbf{I})\bar{\mathbf{F}} \quad (3.13)$$

Where \mathbf{I} is the identity tensor. The volume preserving nature of $\bar{\mathbf{F}}$ has the obvious implication that $\det \bar{\mathbf{F}} = 1$ at all times.

Consequently, and following the definition given in Eq. (3.3), we get the isochoric right Cauchy-Green deformation tensor, given by:

$$\bar{\mathbf{C}} = \bar{\mathbf{F}}^T \bar{\mathbf{F}} = J^{-2/3} \mathbf{C} \quad (3.14)$$

Now consider a material that consists of two families of fibers. Each family is characterized by a mean referential (preferred) direction about which the fibers are distributed with rotational symmetry. The two distinct directions in the reference configuration are defined in terms of two unit vectors $\mathbf{a}_{0i}, i = 4,6$. This permits the definition of two additional invariants:

$$I_4 = \mathbf{a}_{04} \cdot (\mathbf{C}\mathbf{a}_{04}), \quad I_6 = \mathbf{a}_{06} \cdot (\mathbf{C}\mathbf{a}_{06}) \quad (3.15)$$

With these definitions, and the one given in Eq. (3.7) for I_1 , the isochoric counterparts of I_1, I_4 and I_6 are given as:

$$\bar{I}_1 = \text{tr}(\bar{\mathbf{C}}) = J^{-2/3} I_1, \quad \bar{I}_4 = J^{-2/3} I_4, \quad \bar{I}_6 = J^{-2/3} I_6 \quad (3.16)$$

We can now proceed to the definition of the SEDF of the HGO model, which is divided in three parts: volumetric, Ψ_{vol} , isotropic $\bar{\Psi}_{iso}$ and anisotropic $\bar{\Psi}_{aniso}$:

$$\Psi(\mathbf{C}, \mathbf{a}_{04}, \mathbf{a}_{06}) = \Psi_{vol}(J) + \bar{\Psi}_{iso}(\bar{\mathbf{C}}) + \bar{\Psi}_{aniso}(\bar{\mathbf{C}}, \mathbf{a}_{04}, \mathbf{a}_{06}) \quad (3.17)$$

The original HGO model was designed for incompressible materials, so it did not include a volumetric term. This is only introduced in the FE implementation of the model in Abaqus as a penalty function to account for a possible compressible behavior of the material.

$$\Psi_{vol}(J) = \frac{1}{D} \left(\frac{(J^{el})^2 - 1}{2} - \ln J^{el} \right) \quad (3.18)$$

Where J^{el} is the elastic volume ratio and the parameter D is related to the bulk modulus, K_0 , by $D = 2/K_0$. By setting $D = 0$ in Abaqus, this term disappears and the material is modeled as incompressible.

The isotropic component of the model serves to model the non-collagenous ground matrix by means of a neo-Hookean incompressible isotropic model.

$$\bar{\Psi}_{iso}(\bar{\mathbf{C}}) = C_{10}(\bar{I}_1 - 3) \quad (3.19)$$

Here, \bar{I}_1 is the first invariant of $\bar{\mathbf{C}}$, as defined in Eq. (3.16) and C_{10} is the neo-Hookean parameter.

Finally, the anisotropic component:

$$\Psi_{aniso}(\bar{\mathbf{C}}, \mathbf{a}_{04}, \mathbf{a}_{06}) = \frac{k_1}{2k_2} \sum_{i=4,6} \{\exp[k_2(\bar{E}_i)^2] - 1\} \quad (3.20)$$

with

$$\bar{E}_i \stackrel{\text{def}}{=} \kappa(\bar{I}_1 - 3) + (1 - 3\kappa)(\bar{I}_i - 1) \quad (3.21)$$

This component accounts for the previously mentioned two families of fibers with different directions embedded in the ground matrix.

The index $i = 4,6$ represents the two fiber families, so that the invariants defined in Eq. (3.15) appear in the exponential term of Eq. (3.20).

C_{10}, D, k_1, k_2 are the parameters of the model that change the stress-strain response to model different materials.

The spatial distribution of the fibers orientation is governed by a statistical distribution function, $\rho(\mathbf{M}(\theta, \phi))$ (defined in detail in the original article [60]) which characterizes the distribution of fibres in the reference configuration Ω_0 with respect to the referential orientation \mathbf{M} . The vector \mathbf{M} is an arbitrary unit vector located in three dimensional Eulerian space characterized in terms of two Eulerian angles $\theta \in [0, \pi]$ and $\phi \in [0, 2\pi]$.

κ is a parameter derived from the statistical distribution function, $\rho(\mathbf{M}(\theta, \phi))$ which controls the dispersion around the mean direction of each family of fibers. When $\kappa = 0$, the fibers are perfectly aligned in the preferential direction. As the value increases, the fiber dispersion also increases until κ reaches $1/3$, which represents randomly distributed fibers (isotropic situation). A graphical representation of the density function and the effect of κ in it is exhibited in Figure 3.3.

In Eq. (3.20) it is assumed that both fiber families have the same mechanical properties, meaning that the set of parameters (k_1, k_2) is equal in both cases. The same assumption is made for the dispersion parameter κ .

For more technical details on the model definition and FE implementation, the reader is referred to the original article and Abaqus Theory Guide, [62] and [60], respectively.

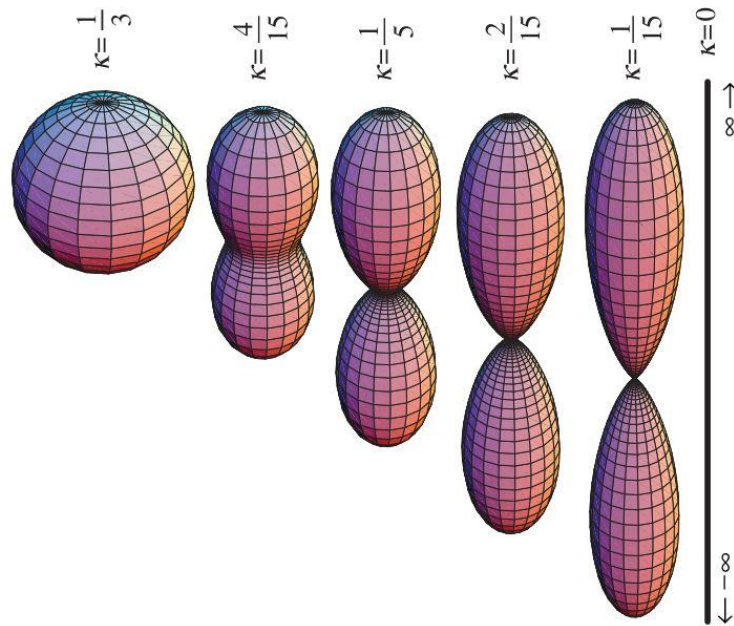


Figure 3.3 - Three-dimensional graphical representation of the orientation of the fibres based on the transversely isotropic density function [62]. The surface defined by the apex of the vector $\rho(\mathbf{M})\mathbf{M}$ is plotted with respect to the Eulerian angles θ and ϕ .

3.3.2.1. Orientation Definition

The application of the HGO model implies the definition of a preferential direction for the fibres. As mentioned in section 2.1.4, the collagen fibers of ligaments are mainly oriented along the longitudinal direction. To simulate this, a continuous element-by-element orientation was defined for each ligament as in [38], using the option **Orientation, Definition=Offset to Nodes* in Abaqus input file. This option creates a local coordinate system by giving local node numbers on the elements where the orientation is being used. The local node numbers refer to the order in which nodes are indicated in the element connectivity [66]. The first local node number to be specified dictates the position of the local X axis, the second node number must be on the XY plane and the last point is the origin. The implementation of this type of orientation was only possible due to the well-structured and regularly stacked hexahedral mesh provided the Open Knee project that was created in TrueGrid (XYZ Scientific Applications, Livermore, CA). Figure 3.5 and Figure 3.4 show the variation of the local X axis along the longitudinal axis of ACL and PCL, respectively.

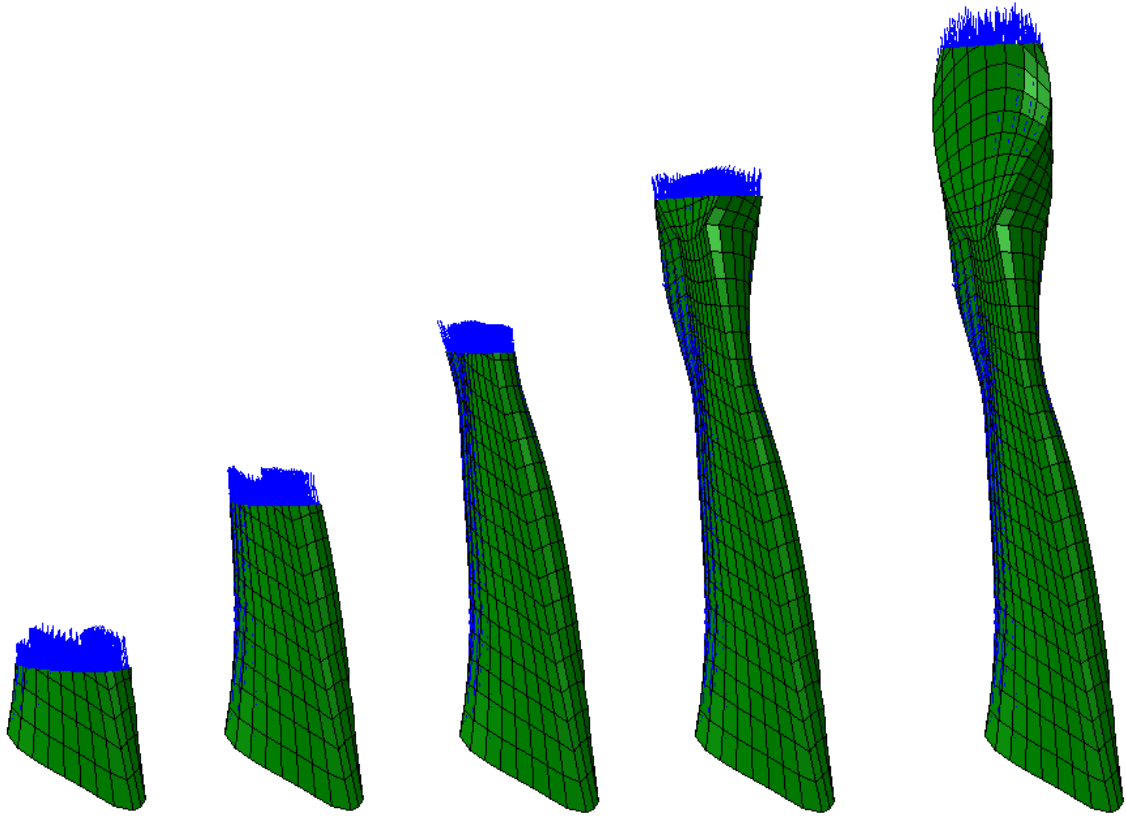


Figure 3.5 - Main ACL fiber direction.

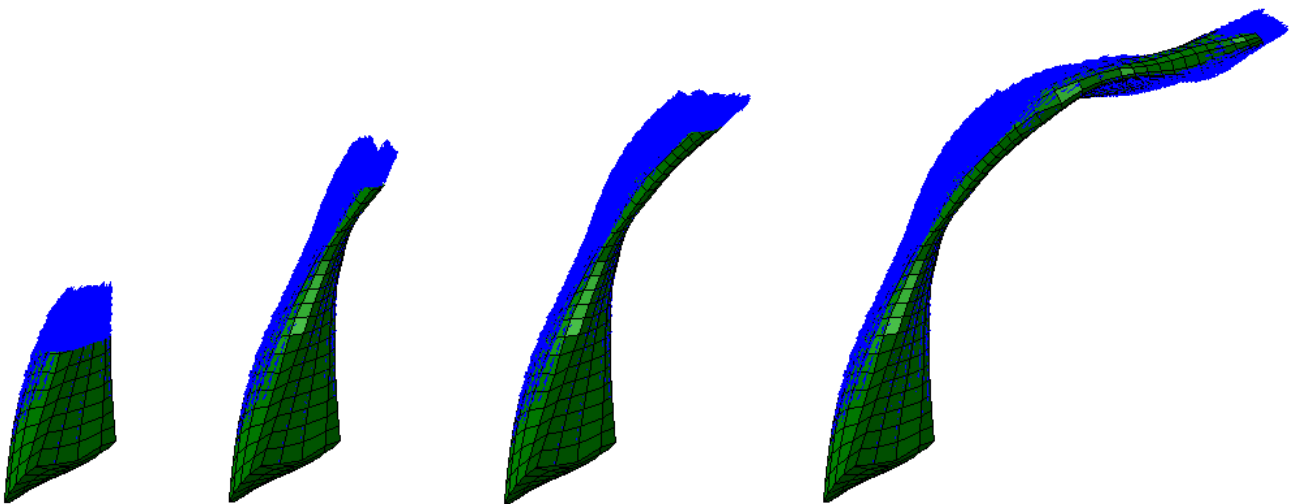


Figure 3.4 - Main PCL fiber direction.

The collateral ligaments were modeled with just one family of fibers along the longitudinal direction, using the procedure just described.

However, as mentioned in section 2.1.4, the cruciate ligaments are composed of two distinct fiber bundles. In an attempt to simulate these structures, two fiber families were defined by adding the option *Local Directions=2* to the orientation card previously indicated. To recreate the anteromedial (AM) and

posterolateral (PL) family fibers of the ACL, the two vectors ($\alpha_{0i}, i = 4,6$) governing the two different directions of each fiber family were defined resorting to a γ value that defined an angle with the local x-axis in the local xy plane. By setting the γ value equal to 10° , the x-component of the first local material direction with respect to the coordinate system (CS) defined at a given element is $\cos \gamma$, while the y-component is $\sin \gamma$. Similarly, the x and y components of the second local material direction are given by $\cos \gamma$ and $\sin -\gamma$, respectively. The local coordinate system and local directions in the xy plane are schematically represented in Figure 3.6.

To define the posteromedial (PM) and anterolateral (AL) directions of the PCL fiber bundles the local coordinate system had to be altered. Considering the element in Figure 3.6 as the representative element, the origin of the PCL local CS was set to node 4, node 1 defined the X-axis and node 7 defined the Y-axis. The implementation of the coordinate system and local directions in the FE model of the ACL are presented in Figure 3.7.

Since no information regarding a specific value defining the orientation change between bundles was found on the literature, the γ value was estimated such that it would create a sufficient separation between the bundles, but not deviating too much from the longitudinal direction of the ligament.

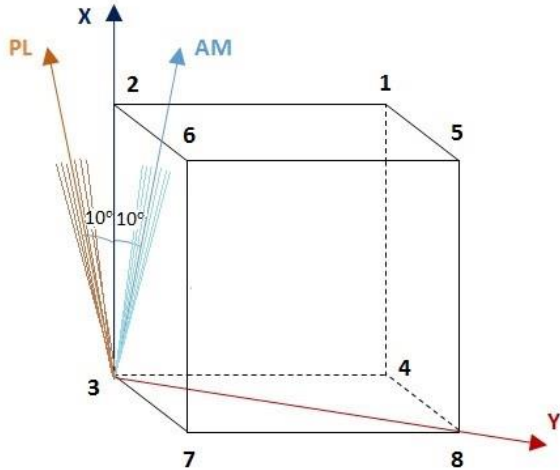


Figure 3.6 - Schematic representation of the local coordinate system used in each element of the ACL to define the direction of the two fiber families. Considering the planes 567, 145 and 236 as the anterior, medial and lateral planes, the AM and PL bundles of the ACL can be defined in the local coordinate system represented. The smaller lines around the AM and PL directions represent the dispersion of the collagen fibers direction, controlled by the κ parameter.

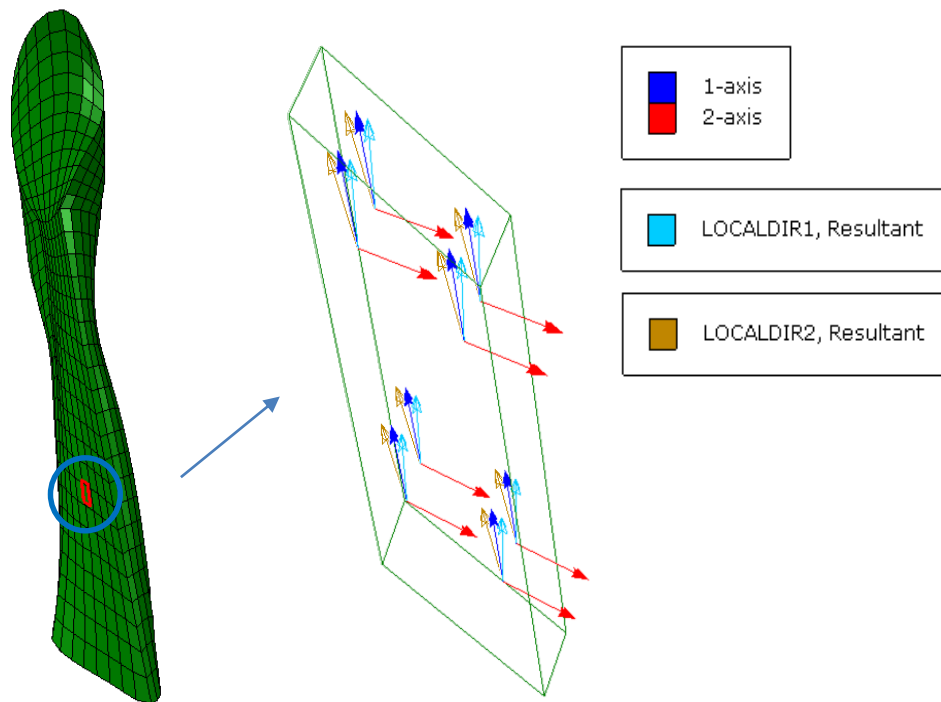


Figure 3.7 - Anterior view of the ACL showing the implementation of the fiber directions on a representative element. In each integration point, the implemented local coordinate system and the direction of the anteromedial (Localdir1) and posterolateral (Localdir2) fiber bundles are shown.

3.3.2.2. Parameter Estimation

The estimation of the model parameters was performed through an optimization routine (Appendix A) that used the Python scripting language to connect MATLAB (The MathWorks Inc., Natick, MA, USA) to Abaqus. The objective of this optimization routine was to reproduce the experimental nominal stress-strain curves of uniaxial tests presented in [28] for the ACL, [67] for the MCL, and [68] for the PCL. The stress-strain data points were obtained from the plots presented in the articles mentioned using the *WebPlotDigitizer* tool⁵. The initial set of parameters was defined in the routine *HGO_optim_routine.m* where the MATLAB optimization function *lsqcurvefit* was invoked. The *lsqcurvefit* function starts with the initial set of values, $c0$, and finds the set of coefficients c , that best fit the nonlinear function $fun(x, xdata)$ to the $ydata$, using a least-squares approach. In this case, the nonlinear function is *abqvalues.m* that receives $C_{10}, D, k_1, k_2, \kappa$ and an iteration number *iter* (for log purposes), write those values to *Var_iter.py*, gives the instruction to run Abaqus/CAE with the script *Main.py* and returns the stress-strain data calculated in Abaqus for that set of input values. *Main.py* was the file that had the Python commands to execute the Job in Abaqus and extract the respective results. The whole optimization process is presented schematically in Figure 3.8.

⁵ Available in <http://arohatgi.info/WebPlotDigitizer/>

The result of the curve fit procedure for the ACL, MCL and PCL is presented in Figure 3.9.

An initial set of parameters starts the optimization process.

Main.py reads the input variables, updates the .inp file and generates a .csv report with the stress-strain data.

Comparison of experimental and simulated stress-strain data points.

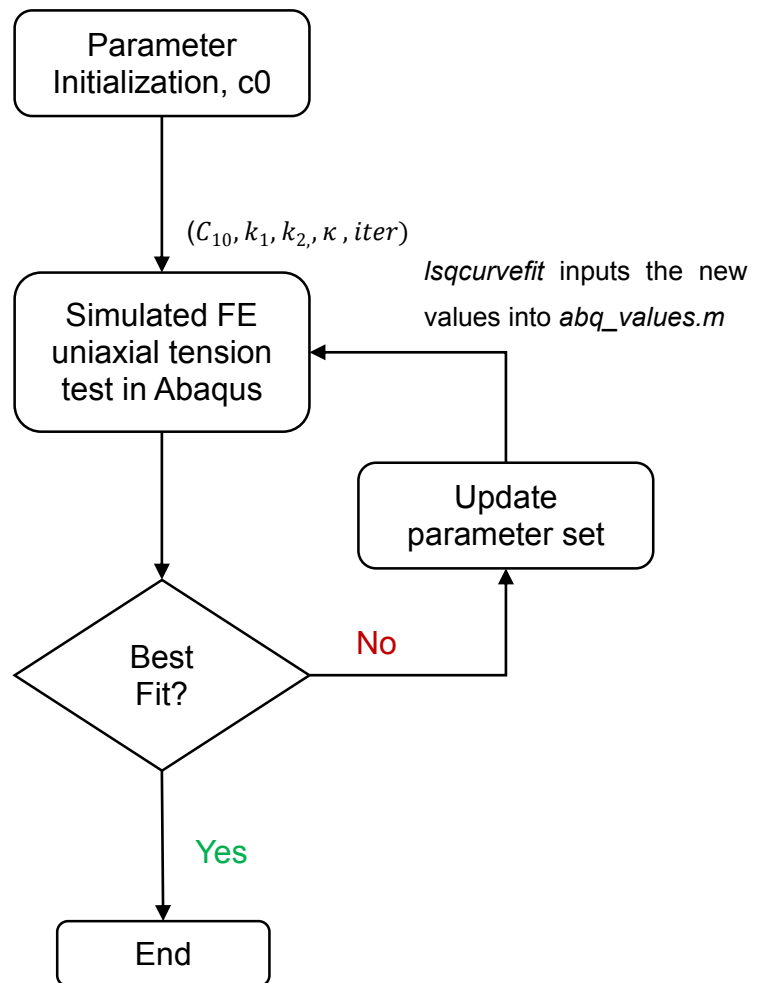


Figure 3.8 - Diagram of the optimization process. Adapted from [76].

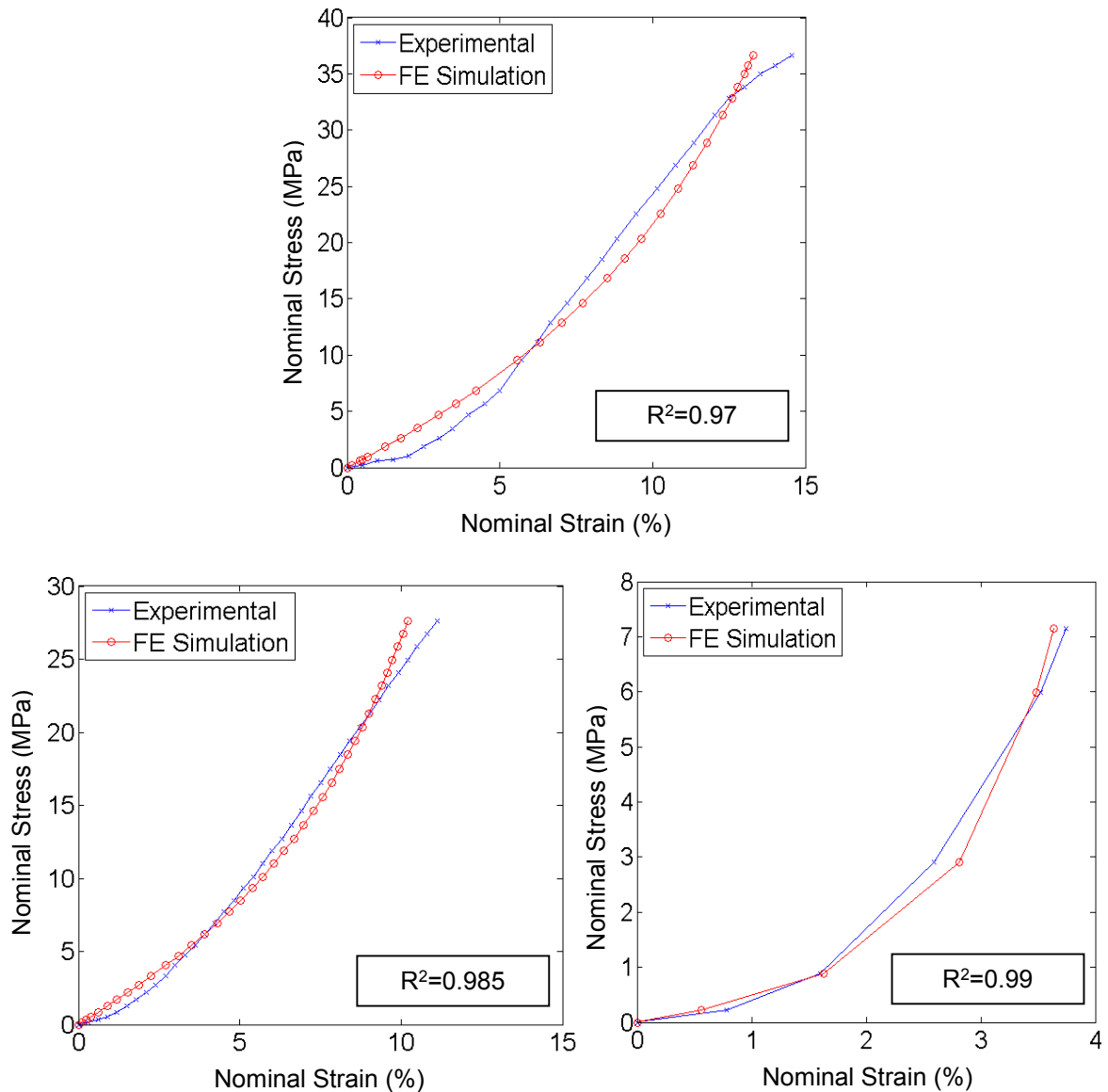


Figure 3.9 - Results of the curve fitting procedure for each ligament and respective R^2 value. (Top Center) ACL Body. (Bottom Left) MCL. (Bottom Right) PCL.

Preliminary analyses revealed discrepancies in stress distribution in the proximal portion of the ACL, referred from now on as “ACL head”. The main reason for this is related to the three dimensional modeling of the ligament. The high curvature presented in the ACL head region implies a significant distortion of elements in this zone which introduces incompatibilities when defining the orientations for the HGO model. To overcome this problem, the ACL was divided in two element sets, the ACL head and the ACL body, represented in Figure 3.10. The ACL head was then modeled as isotropic by setting $\kappa = 1/3$. The results of the material parameter optimization for the isotropic ACL head were similar to the ones show in Figure 3.9 for the ACL body.

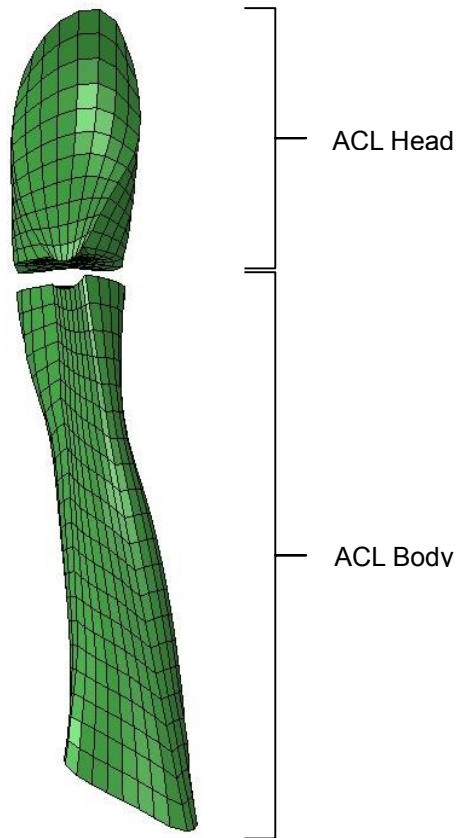


Figure 3.10 - ACL division in head and body element sets.

The final material properties used are summarized in Table 3.3.

Table 3.3 - Material properties

| Linear Elastic Isotropic Materials | | | | | |
|--|---------------------|------------|-----------------|----------|-----------------------|
| Structure | Young's Modulus/MPa | | Poisson's Ratio | | |
| Articular Cartilage | 5 | | 0.46 | | |
| Menisci | 59 | | 0.49 | | |
| Incompressible Anisotropic Hyperelastic Materials | | | | | |
| | C_{10} /MPa | k_1 /MPa | k_2 | κ | No. of Fiber Families |
| ACL (body) | 0.11652 | 30.77898 | 8.41086 | 0.06626 | 2 |
| ACL (head) | 19.997 | 2912.8339 | 0.1 | 1/3 | 2 |

| | | | | | |
|-----------|---------|----------|-----------|---------|---|
| PCL | 0.01088 | 7.82604 | 446.19805 | 0.05691 | 2 |
| MCL & LCL | 0.21287 | 61.34446 | 18.7062 | 0.08544 | 1 |

3.4. Contact Interactions and Constraints

Eleven locations of potential contact were identified, namely:

- Distal end of femoral cartilage with proximal medial meniscus;
- Distal end of femoral cartilage with proximal lateral meniscus;
- Distal end of femoral cartilage with proximal medial tibial cartilage;
- Distal end of femoral cartilage with proximal lateral tibial cartilage;
- Distal lateral meniscus with proximal lateral tibial cartilage;
- Distal medial meniscus with proximal medial tibial cartilage;
- MCL with the tibia;
- MCL with the femur;
- PCL with the tibia;
- PCL with the femur;
- ACL with PCL.

The contact was defined as *Surface-to-Surface Contact* with frictionless finite sliding between each contact pair as in [4,14,23,24,28,29].

Each of the distal ends of the four ligaments were constrained to a different reference point (RP) by a *Kinematic Coupling* constraint. These reference points were fixed in all degrees of freedom. In this way, the reaction force measured on each RP would represent the *in situ* force taken up by each ligament in response to tibial motion.

The proximal ends of the four ligaments and the femoral cartilage were rigidly tied to the femur by a *Rigid Body Constraint*. The same type of constraint was applied to the lateral and medial tibial cartilages to fix them to the tibia.

The medial end of the lateral meniscus and the lateral end of the medial meniscus were attached to the tibia using a *Tie* constraint to simulate the meniscal horns.

3.5. Loads and Boundary Conditions

The Open Knee 3D geometries were provided in a coordinate system (CS) aligned with the first sagittal MR image used for segmentation.

Following the instructions given in the Open Knee guide [58] and the files provided in the project repository, the model was aligned with a CS consistent with the CS developed by Grood and Suntay [69] to describe the tibiofemoral joint movements. The CS is defined as follows (Figure 3.11):

- Origin: mid-point of the femoral condyles;
- x-axis: flexion axis
- y-axis: anterior-posterior axis
- z-axis: mechanical axial axis.

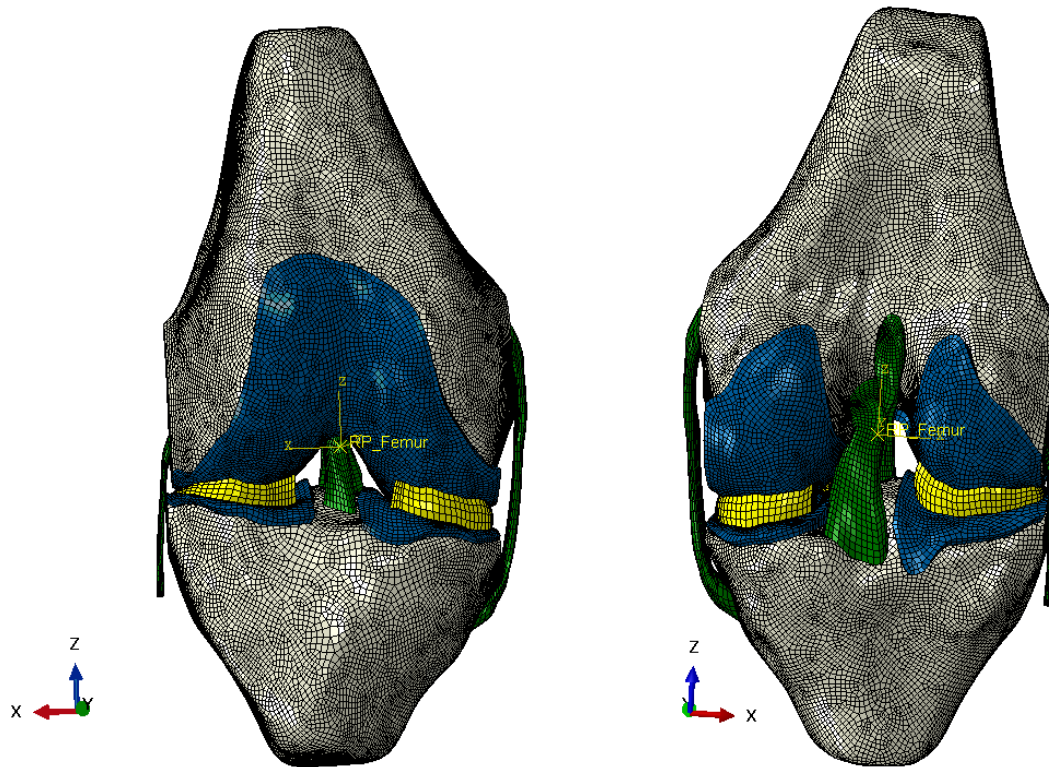


Figure 3.11 - Mesh of the fully assembled knee with the new coordinate system and the femoral RP highlighted. (Left) Anterior view. (Right) Posterior view.

To verify the role of the ACL as the main constraint to anterior tibial displacement, a typical loading case found in the literature, in both experimental [13,70–72] and FE studies [4,13,14,28,39] is the application of a 134 N anterior force on the tibia. However, to verify the ACL function at higher flexion angles, a first step of rotation is necessary. If the rotation was to be applied on the tibial RP, it would be difficult to define *a priori* the real anterior direction to the tibia after the rotation. To overcome this, it was decided to apply the rotation on the femoral RP (defined at the origin of the CS) in the first step and then a posteriorly directed force on the same point. In this way, the direction of the force applied in the second step would remain in the anterior-posterior axis, simulating the relative anterior displacement of the tibia. These loading conditions were designed to simulate clinical examinations used to diagnose ACL deficiency, such as the Lachman anterior drawer test [70]. The same approach was used by Moglo and Shirazi-Adl [30] and by Westerman et al. [38].

During the application of the force, the flexion-extension DOF (UR1) of the femur was fixed and the tibia was fixed in all degrees of freedom. Therefore, the posterior displacement of the femur relative to the tibia is equivalent to the anterior tibial translation relative to the femur that happens during clinical

evaluations of the ACL function. The 134 N posterior femoral force was applied at 0, 15 and 30° of flexion to compare the knee kinematics at different angles of flexion with the experimental data.

However, due to the large displacements of the femur in ACL absence, only half of the force value was applied in the ACL-deficient knee.

3.6. Output Variables

The kinematic behavior of the ACL-intact and ACL-deficient knee was studied by measuring the movements in all degrees of freedom except for the flexion-extension rotation, which is fixed in all the analysis.

In addition, an estimation of the *in situ* forces in all ligaments is also calculated by determining the reaction force of the rigid tibial insertion surfaces of the ligaments in response to the different loading cases. This approach has been used in other studies [13,38]. An average value of maximum principal stress is obtained in each ligament in order to enable the comparison with the literature.

4. Results and Discussion

4.1. ACL-Intact Knee

A posterior femoral load of 134 N was applied to the healthy and ACL-deficient knee at varying angles, 0, 15 and 30° of flexion.

For each of these flexion angles, the results presented are: both anterior and medial views of the tibiofemoral joint, showing the maximum principal stress of the soft tissues; the kinematic results in terms of tibial relative displacement; the magnitude of the reaction force at the tibial insertion of each ligament and the maximum principal stress at each ligament, calculated as an average of the nodal stresses of the corresponding ligament. To facilitate the visual comparison of the stress results, the maximum value of the scale was fixed to 30 MPa.

The comparison between the two materials models was made only for the knee in full extension. For higher flexion angles, only the HGO model was considered.

The kinematic results for all degrees of freedom of the FE simulations of the ACL-intact knee are compared to the experimental data presented in [70] for validation purposes. In this study, Gabriel et al. measured 5 DOF kinematics of 10 cadaveric ACL-intact knees in response to 134 N anterior tibial load at different flexion angles. The same study also provides data regarding the *in situ* forces of the two ACL bundles. To further validate the model, the simulation results were also compared with experimental data from other authors regarding the anterior-posterior and internal-external tibial movements, as well as ligament forces and stresses.

4.1.1. Full Extension (0° of Flexion)

4.1.1.1. Marlow Model

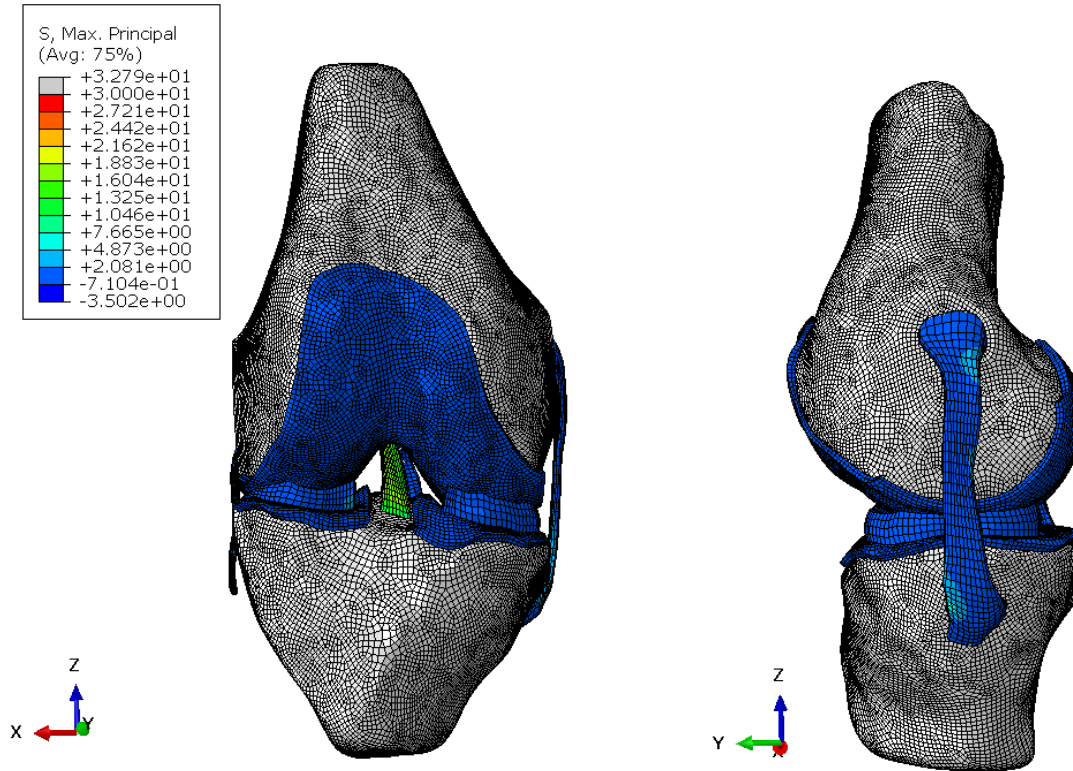


Figure 4.1 - ACL-intact knee joint after the application of a 134 N posteriorly directed force on the femur using the Marlow material model in the ligaments. (Left side) Anterior view. (Right side) Medial view.

4.1.1.2. HGO Model

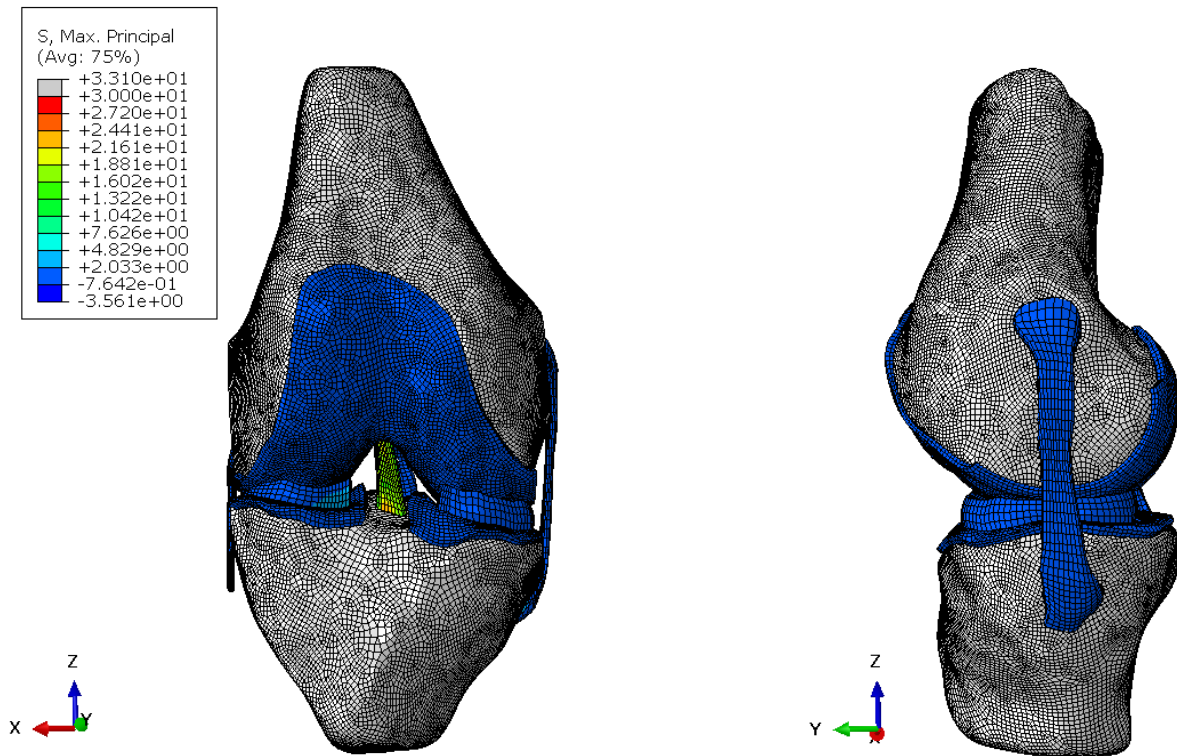


Figure 4.2 - ACL-intact knee joint after the application of a 134 N posteriorly directed force on the femur using the HGO material model in the ligaments. (Left side) Anterior view. (Right side) Medial view.

Figures 4.1 and 4.2 show the stress results of the soft tissues of the knee in extension under the 134 N posterior femoral force using the Marlow and HGO models, respectively. In both cases we can see that the ACL is undoubtedly the most stressed structure in the knee, which is restraining the posterior movement of the femur.

Table 4.1 - Ligaments reaction force in the ACL-intact knee at full extension under a 134 N posterior femoral force.

| | Ligaments Reaction Force (Magnitude)/N | | | |
|---------------|--|-------|---------|--------|
| | ACL | LCL | MCL | PCL |
| HGO | 133.200 | 0.757 | 7.906 | 0.007 |
| Marlow | 121.719 | 5.844 | 13.0366 | 3.2275 |

Table 4.2 - Ligaments average maximum principal stress in the ACL-intact knee at full extension under a 134 N posterior femoral force.

| | Ligaments Average Maximum Principal Stress/MPa | | | |
|--------|--|-------|-------|--------|
| | ACL | LCL | MCL | PCL |
| HGO | 11.350 | 0.130 | 0.578 | 0.0012 |
| Marlow | 10 | 1.368 | 0.967 | 0.29 |

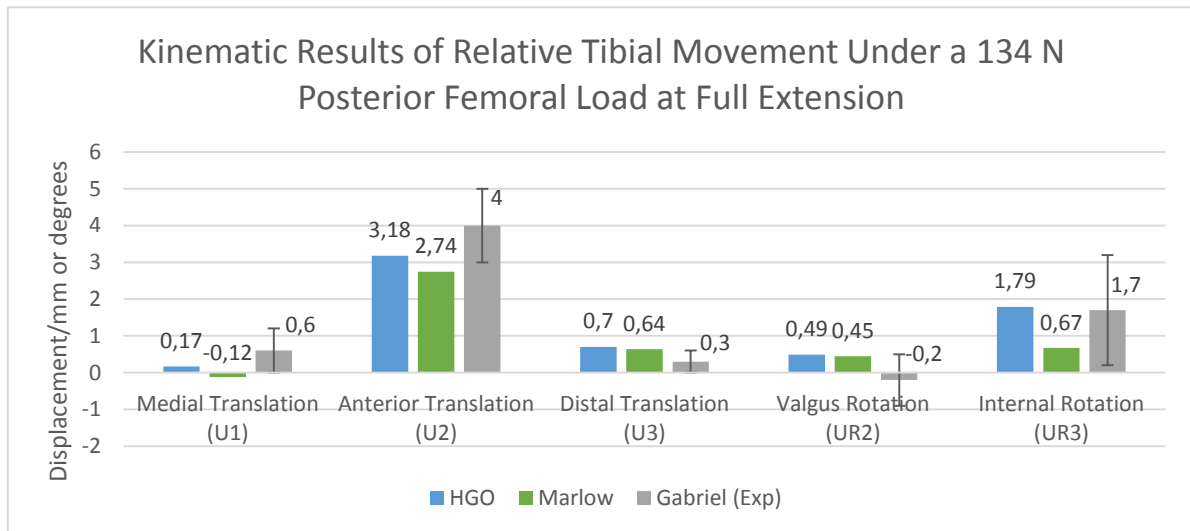


Figure 4.3 - Kinematic results of relative tibial movement under a 134 N posterior femoral load at full extension. The results of the simulation are compared to the experimental data of Gabriel et al [70].

The comparison between the two material models shows that with the Marlow model, there is less movement in all degrees of freedom. This was an expected result, since this model defines the ligaments as isotropic materials, and consequently, their resistance to longitudinal and transverse loads is the same, thus providing more restraint in each direction.

This behavior is also expressed by the forces taken up by each ligament. In the Marlow model, the ACL is less loaded than in the HGO model and the contrary happens to the other ligaments due to their ability to sustain loads in directions other than in the longitudinal one.

The simulations with the HGO model show a better agreement with the experimental data than the simulations with the Marlow model, with all the displacements falling in the region delimited by the standard deviation. The exception to this is the distal translation (U3), which is slightly above the superior limit of the standard deviation.

Table 4.3 shows experimental data from other cadaveric studies where the same 134 N anterior tibial load was applied in the fully extended knee.

Table 4.3 - Experimental data from cadaveric studies applying a 134 N anterior tibial load in the fully extended knee.

| Experimental Study | Anterior Tibial Translation/mm | Internal Rotation/degrees |
|----------------------|--------------------------------|---------------------------|
| Yagi et al. [72] | 4.1 ± 0.6 | |
| Song et al. [13] | 4.6 | 1.6 |
| Kanamori et al. [71] | 5.3 ± 1 | 2.1 ± 3.1 |

The anterior tibial translation obtained in the FE simulation was less than the experimental average values, which might suggest that the ACL was modeled a bit too stiffer than it should be. This topic is further discussed in the following sections.

Regarding the ACL *in situ* force, all the three experimental studies above mentioned report values between 115 and 140 N, validating the value of 133.2 N obtained in the simulations.

As for the ligament stresses, there was not much data available in the literature. In experimental tests using cadaveric knees it is difficult to accurately measure the stress. In the case of FE studies the lack of data is related to the fact that many of them use one dimensional (truss/beam or spring) elements to model the ligaments, which cannot give stress information. Nevertheless, the values obtained for the ACL seem to be within the range of values reported in two FE studies simulating similar loading conditions: Peña et al. [4] obtained an average maximal principal stress of 6.5 MPa for the ACL and a maximum value of 15 MPa, while Song et al. [13] obtained an average value of 6.9 MPa and a maximum value of 24 MPa.

As previously mentioned in Section 2.1.4, being soft tissues, the ligaments have low resistance to compressive loads. This type of loads are introduced as the knee flexes, making the isotropy of the Marlow model an invalid assumption [8]. Therefore, the following analysis of the knee behavior at higher degrees of flexion, presented in the next sections, were performed only using the HGO model.

4.1.2.15° of Flexion

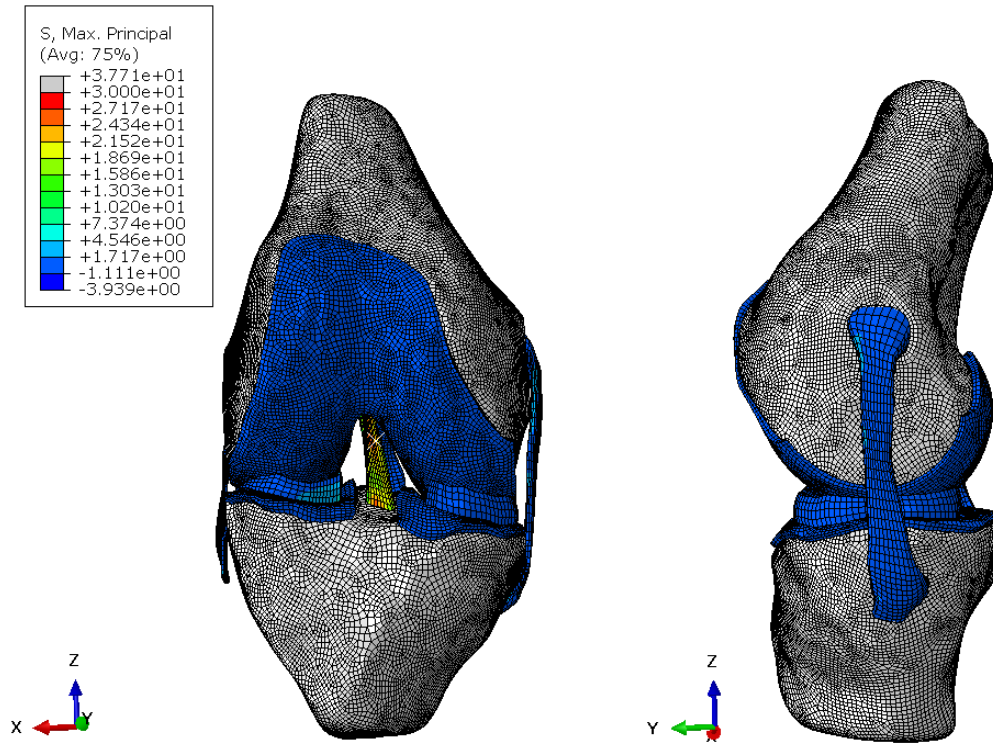


Figure 4.4 - ACL-intact knee joint at 15° of flexion after the application of a 134 N posteriorly directed force on the femur using the HGO material model in the ligaments. (Left side) Anterior view. (Right side) Medial view.

Table 4.4 - Ligaments reaction force in the ACL-intact knee at 15° of flexion under a 134 N posterior femoral force.

| | Ligaments Reaction Force (Magnitude)/N | | | |
|-----|--|-------|-------|-------|
| | ACL | LCL | MCL | PCL |
| HGO | 136.732 | 1.322 | 5.998 | 0.011 |

Table 4.5 - Ligaments average maximum principal stress in the ACL-intact knee at 15° of flexion under a 134 N posterior femoral force.

| | Ligaments Average Maximum Principal Stress/MPa | | | |
|-----|--|-------|-------|--------|
| | ACL | LCL | MCL | PCL |
| HGO | 11.724 | 0.198 | 0.436 | 0.0017 |

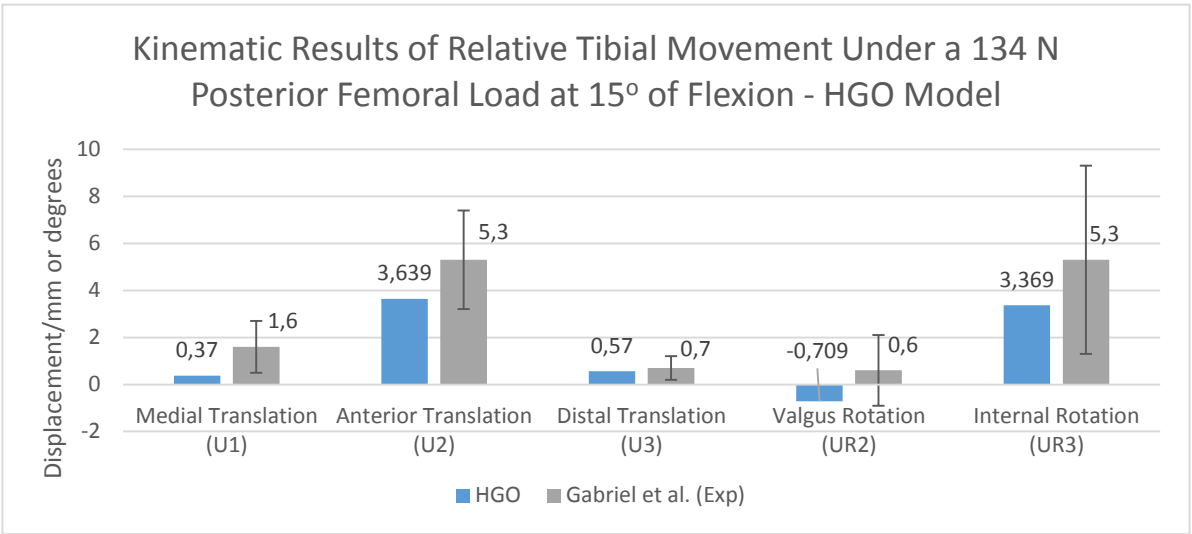


Figure 4.5 - Kinematic results of relative tibial movement under a 134 N posterior femoral load at 15° of flexion. The results of the simulation are compared to the experimental data of Gabriel et al [70].

4.1.3.30° of Flexion

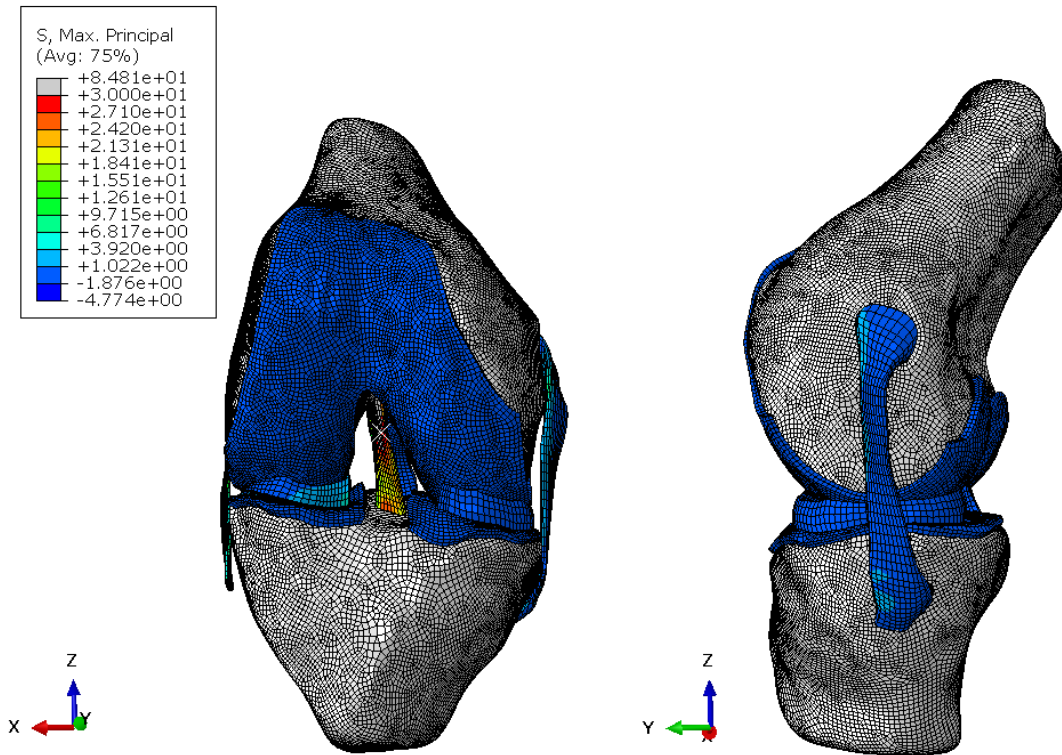


Figure 4.6 - ACL-intact knee joint at 30° of flexion after the application of a 134 N posteriorly directed force on the femur using the HGO material model in the ligaments. (Left side) Anterior view. (Right side) Medial view.

Figures 4.4 and 4.6 show the stress results of the soft tissues of the knee under the 134 N posterior femoral force at 15 and 30° of flexion, respectively. In comparison to the fully extended knee, it is visible that the ACL remains the most tensioned structure with even higher stresses. This means that with higher degrees of flexion, the ACL function gets more demanding and ACL has to deform more to stop the anterior-posterior movements.

Table 4.6 - Ligaments reaction force in the ACL-intact knee at 30° of flexion under a 134 N posterior femoral force.

| | Ligaments Reaction Force (Magnitude)/N | | | |
|-----|--|-------|-------|-------|
| | ACL | LCL | MCL | PCL |
| HGO | 138.634 | 9.783 | 5.876 | 0.018 |

Table 4.7 - Ligaments average maximum principal stress in the ACL-intact knee at 30° of flexion under a 134 N posterior femoral force.

| | Ligaments Average Maximum Principal Stress/MPa | | | |
|-----|--|-------|-------|-------|
| | ACL | LCL | MCL | PCL |
| HGO | 11.724 | 1.459 | 0.409 | 0.003 |

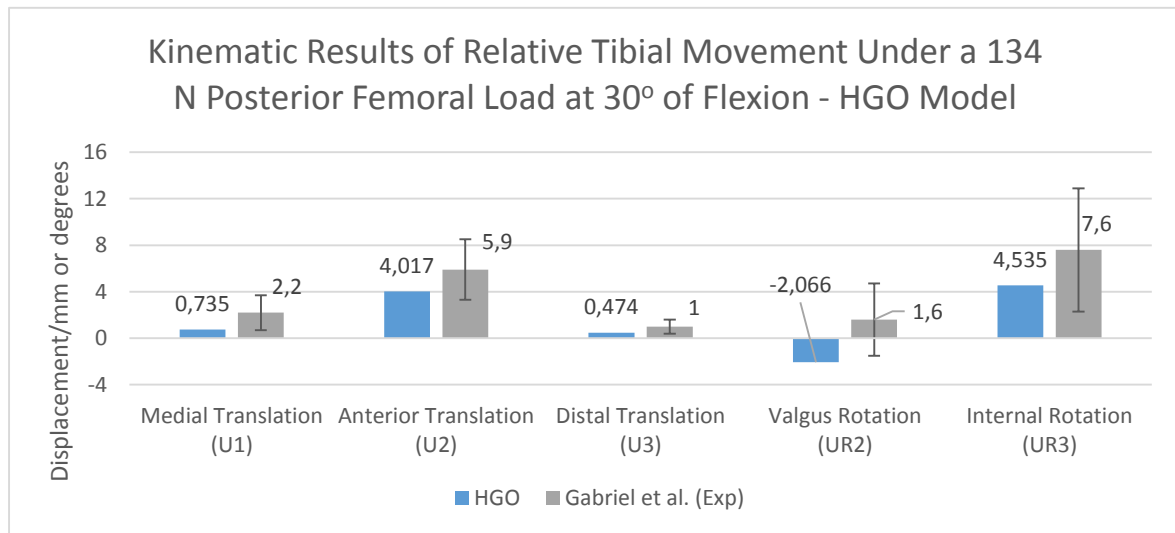


Figure 4.7 - Kinematic results of relative tibial movement under a 134 N posterior femoral load at 30° of flexion using the HGO model in the ligaments. The results of the simulation are compared to the experimental data of Gabriel et al [70].

At 15° of flexion, the results also present a good agreement with experimental data as can be seen in Figure 4.5, with the anterior tibial translation increasing, as expected. The internal rotation also rose considerably, again following the experimental data trend.

At 30°, the FE kinematic results (Figure 4.7) are again in accordance to the experimental data of Gabriel et al, except for the valgus rotation. Both anterior tibial translation and internal rotation continue to increase as the flexion angle goes from 15 to 30°. This is concomitant with the higher force magnitude of the ACL, which is more requested as the flexion angle increases (in the range of flexion considered). To complement the model validation, experimental data from other cadaveric studies, where the same 134 N anterior tibial load was applied in the knee at 30° of flexion, are show in Table 4.8.

Table 4.8 - Experimental data from cadaveric studies applying a 134 N anterior tibial load in the knee at 30° of flexion.

| Experimental Study | Anterior Tibial Translation/mm | Internal Rotation/degrees | ACL <i>in situ</i> Force/N |
|----------------------|--------------------------------|---------------------------|----------------------------|
| Yagi et al. [72] | 6.4 ± 2.4 | | 133±22 |
| Kanamori et al. [71] | 10.1 ± 3.8 | 7.8 ± 9.9 | 106±20 |

By comparing the simulation results with all sets of experimental data for this flexion angle, we can again verify that the model underpredicts anterior tibial translation, supporting the hypothesis of increased ACL stiffness posed in section 4.1.1.2.

Making a global analysis of the results obtained for the ACL-intact knee, it is reasonable to say that the model provides kinematic outputs that are qualitatively (and mostly quantitatively) consistent with the experimental data except for the valgus-varus rotation. The remaining DOFs, despite some verified differences in terms of absolute values (as it happens with the underprediction of the anterior tibial movement) are almost always within the range of values indicated and tend to follow the behavior reported in the literature.

The results of the ACL *in situ* forces are also in good agreement with the literature values. For the other ligaments, the only data found was again from Kanamori et al [71] which reports values between 14 and 15 N for the MCL *in situ* forces for all the range of flexion here considered. The obtained values were lower than this. While on one hand this could also point to some change to be made to the ligament properties, on the other hand, it would be interesting to have more experimental data on this matter to draw more solid conclusions.

The validity of the stress results is more difficult to evaluate due to the lack of experimental data, but when in comparison to similar FE simulations, the obtained average values seem to be in the correct interval of values, at least when the knee is in full extension.

4.2. ACL-Deficient Knee

As mentioned in section 3.5, the posterior load applied to the femur was reduced to half of the value (67 N) applied to the ACL-intact knee, due to the much larger displacements produced in the absence of the ACL. The results obtained are compared with the same value of load applied to the ACL-intact knee. In this section, since the ACL is not present, the anterior view of the full knee shown in the ACL-intact case is replaced by a lateral view to demonstrate the stresses developed in the LCL.

4.2.1. Full Extension (0° of Flexion)

4.2.1.1. Marlow Model

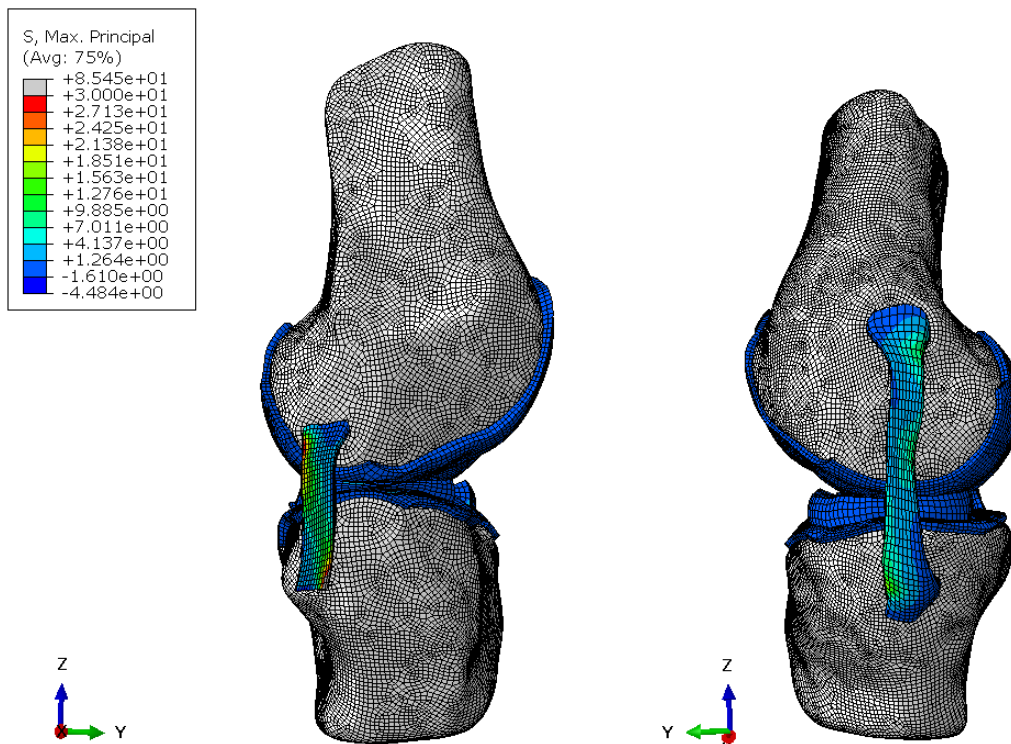


Figure 4.8 - ACL-deficient knee joint at full extension after the application of a 67 N posteriorly directed force on the femur using the HGO material model in the ligaments. (Left side) Lateral view. (Right side) Medial view.

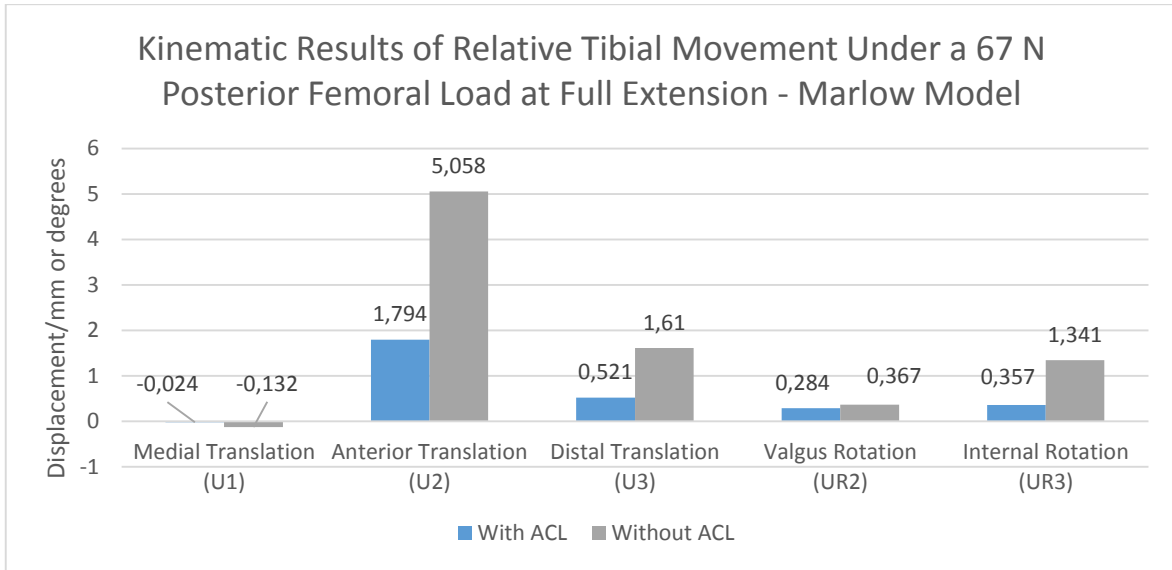


Figure 4.9 - Kinematic results of relative tibial movement under a 67 N posterior femoral force at full extension using the Marlow model in the ligaments - comparison between the ACL-intact and ACL-deficient knees.

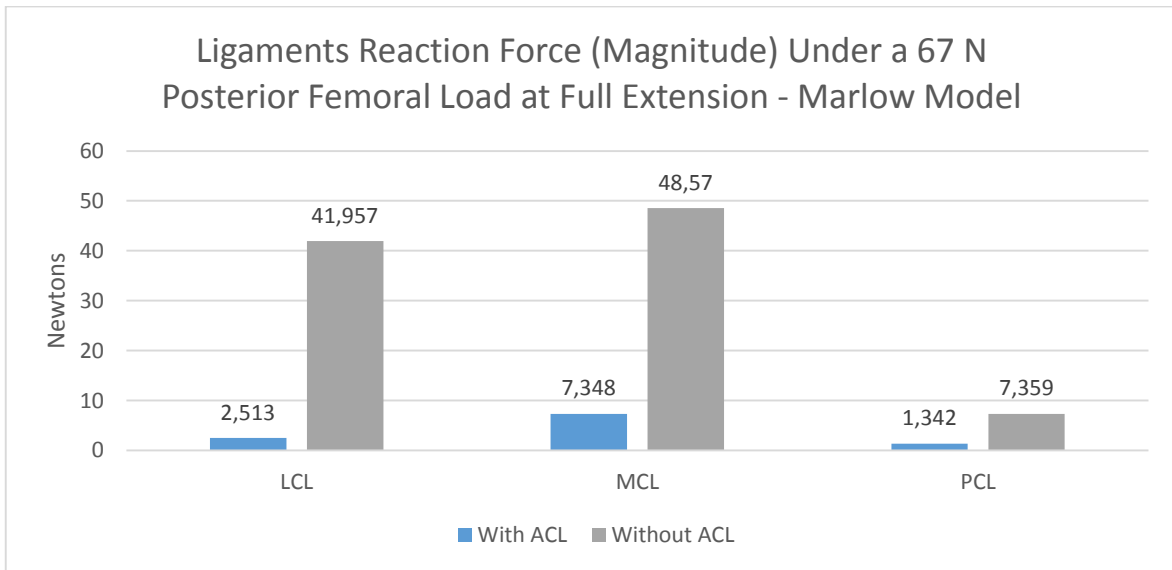


Figure 4.10 - Ligaments reaction force (magnitude) under a 67 N posterior femoral force at full extension using the Marlow model in the ligaments - comparison between ACL-intact and ACL-deficient knees.

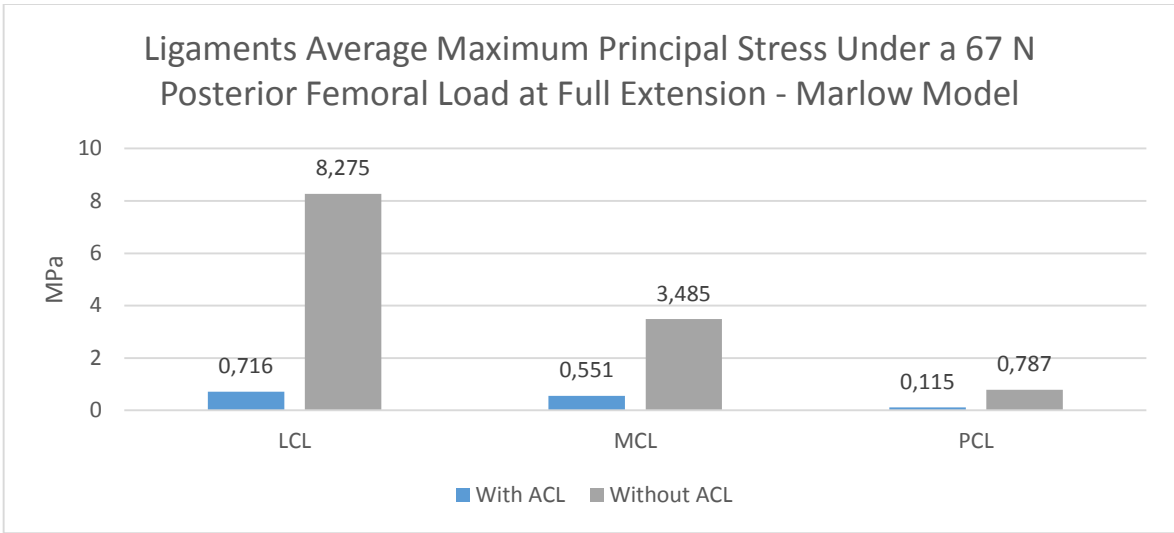


Figure 4.11 - Ligaments average maximum principal stress under a 67 N posterior femoral force at full extension using the Marlow model in the ligaments - comparison between ACL-intact and ACL-deficient knees.

4.2.1.2. HGO Model

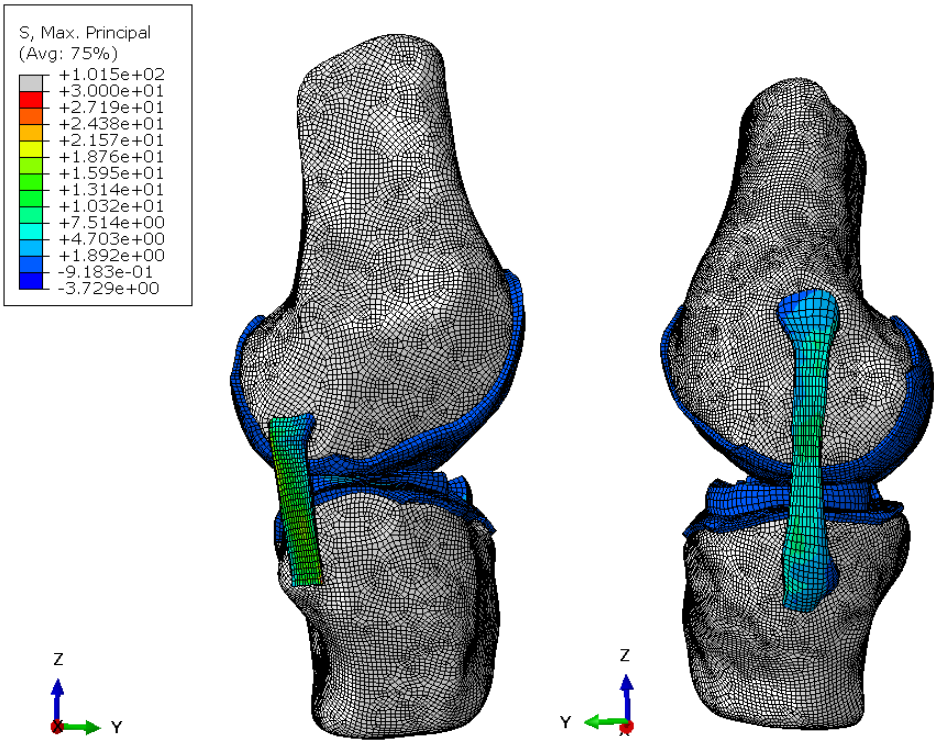


Figure 4.12 - ACL-deficient knee joint at full extension after the application of a 67 N posteriorly directed force on the femur using the HGO material model in the ligaments. (Left side) Lateral view. (Right side) Medial view.

By analyzing Figures 4.8 and 4.12, we can observe clear changes to ACL-intact knee case. After removing the ACL, only half of the force value initially applied was needed to develop much higher stress in the collateral ligaments, which became the primary restraints to the force applied. The region of higher stresses was the anterior portion in both MCL and LCL.

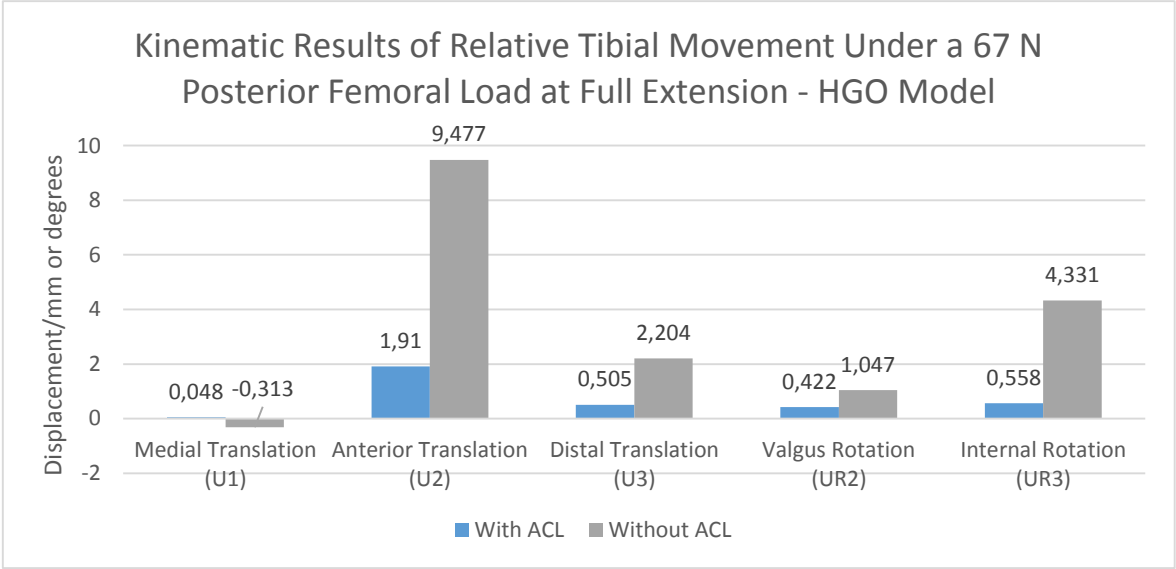


Figure 4.13 - Kinematic results of relative tibial movement under a 67 N posterior femoral load at full extension – comparison between the ACL-intact and ACL-deficient knees.

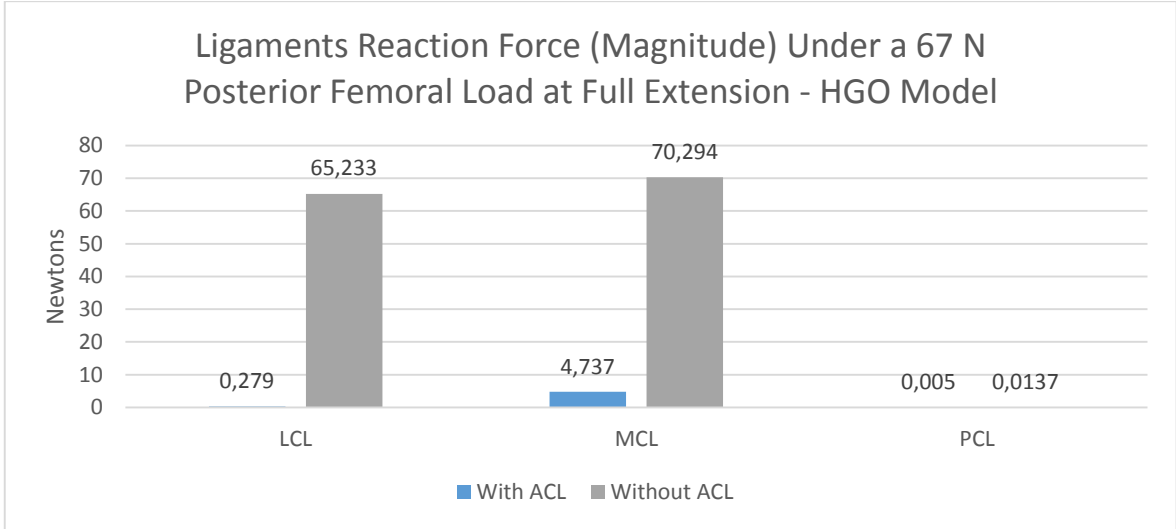


Figure 4.14 - Ligaments reaction force (magnitude) under a 67 N posterior femoral force at full extension using the HGO model in the ligaments - comparison between the ACL-intact and ACL-deficient knees.

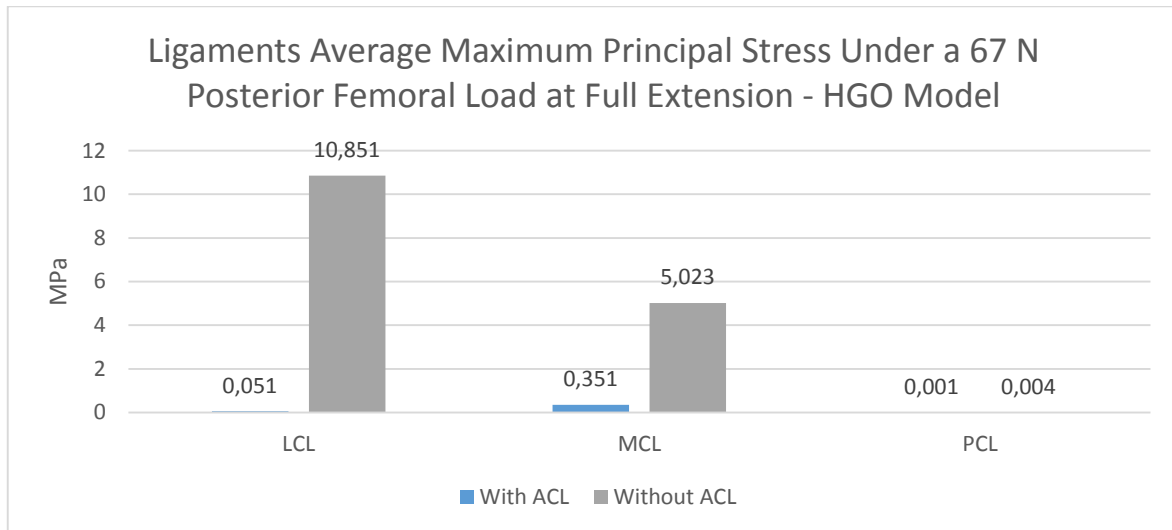


Figure 4.15 - Ligaments average maximum principal stress under a 67 N posterior femoral force at full extension - comparison between ACL-intact and ACL-deficient knees.

In both material models there was a clear increase in the anterior-posterior displacement in the ACL-deficient knee, confirming the ACL as the primary restraint to anterior tibial translation.

As observed in section 4.1.1.2, when comparing the two material models, we can verify that the application of the force in ACL-deficient knee, the Marlow model produces less movement in all DOFs due to the isotropic definition of the ligaments.

In the absence of the ACL, the collateral ligaments become much more important in restraining the anterior-posterior movement, with the MCL being slightly more loaded. This supports the role attributed to the MCL as the secondary restraint to anterior tibial displacements.

As for the PCL, being in compression, it does not contribute to restrain this type of movement, with no relevant changes in its stress or load when the ACL is removed.

In addition to the obvious increase in U2, the distal-proximal and internal external-rotations also suffered significant changes, showing that without the ACL, the knee laxity increases in multiple DOFs.

4.2.2.15° of Flexion

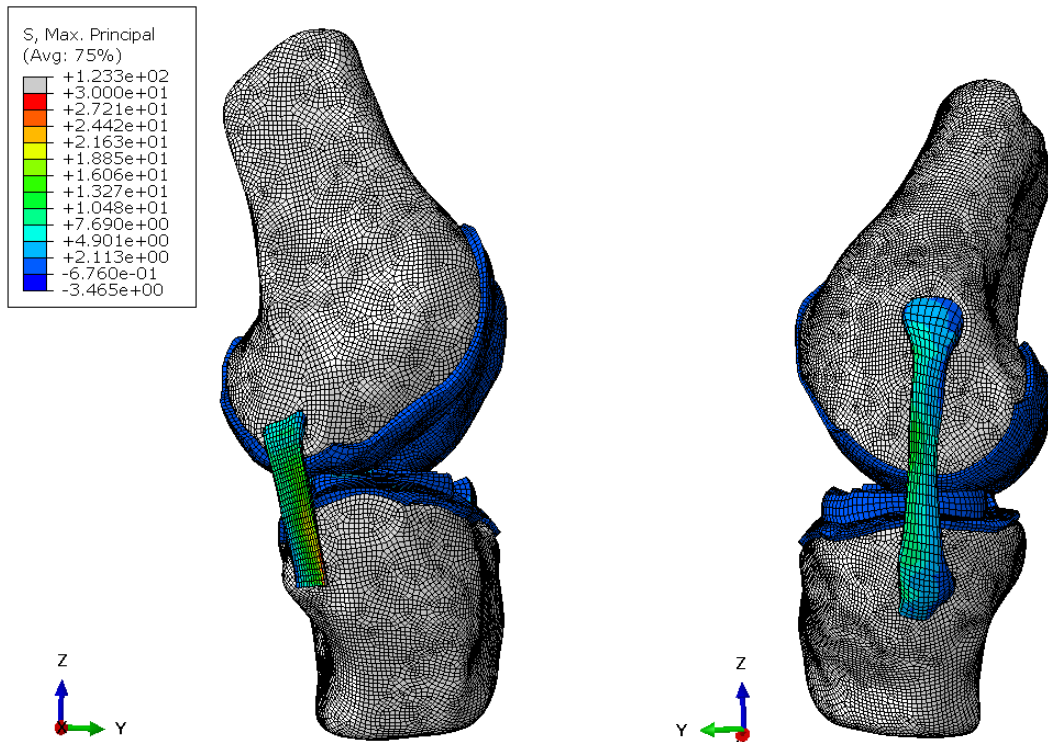


Figure 4.16 - ACL-deficient knee joint at 15° of flexion after the application of a 67 N posteriorly directed force on the femur using the HGO material model in the ligaments. (Left side) Lateral view. (Right side) Medial view.

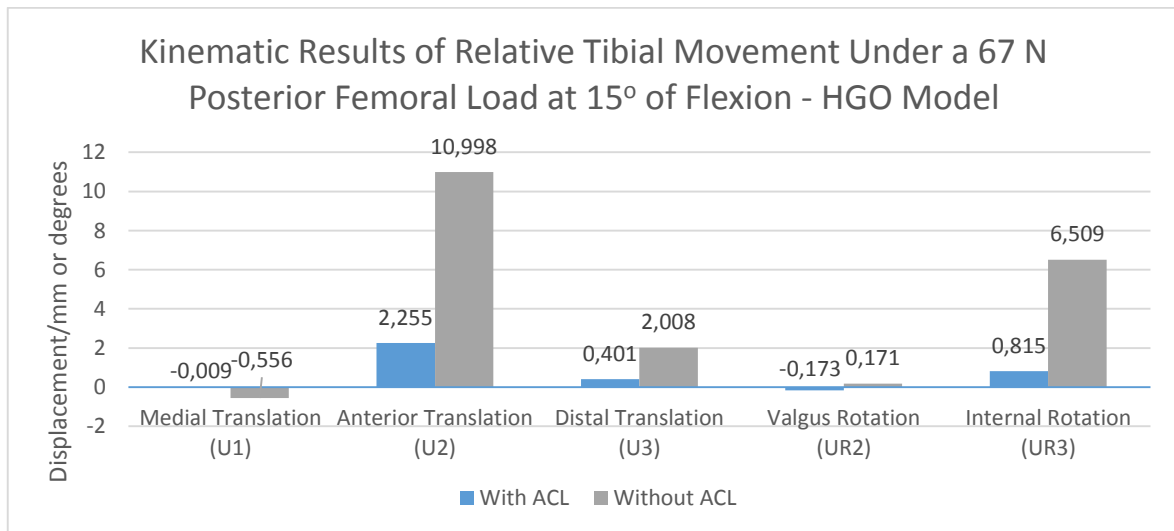


Figure 4.17 - Kinematic results of relative tibial movement under a 67 N posterior femoral load at 15° of flexion using the HGO model in the ligaments - comparison between the ACL-intact and ACL-deficient knees.

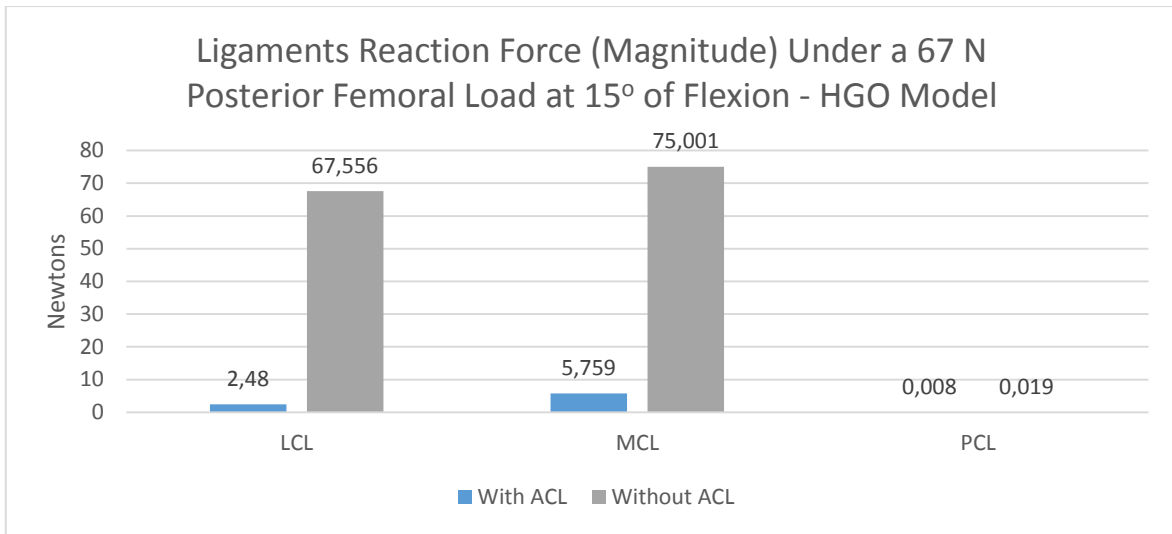


Figure 4.18 - Ligaments reaction force (magnitude) under a 67 N posterior femoral force at 15° of flexion using the HGO model in the ligaments - comparison between ACL-intact and ACL-deficient knees.

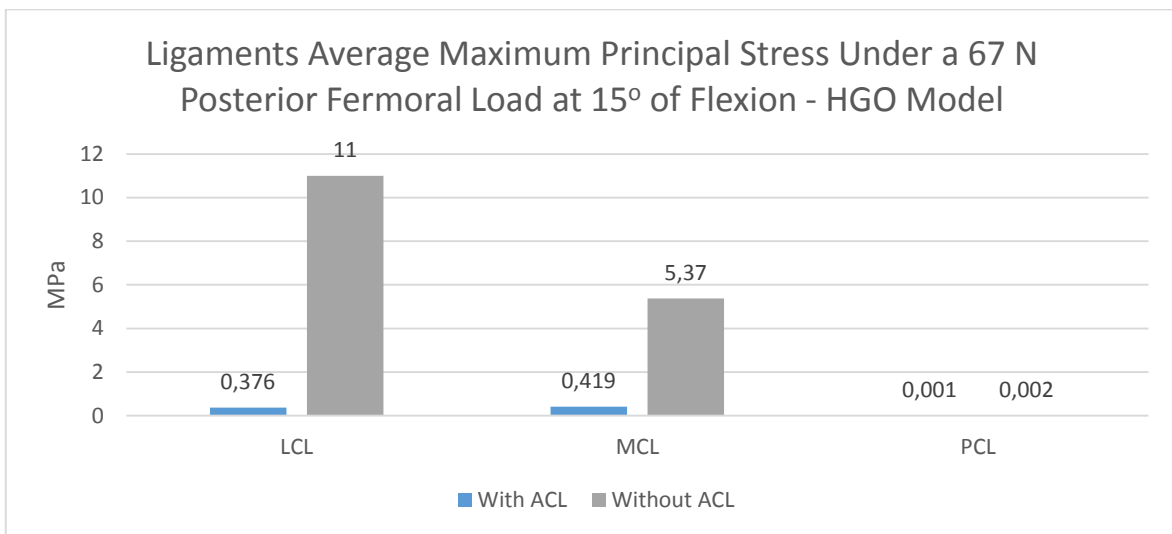


Figure 4.19 - Ligaments average maximum principal stress under a 67 N posterior femoral force at 15° of flexion using the HGO model in the ligaments - comparison between ACL-intact and ACL-deficient knees.

4.2.3.30° of Flexion

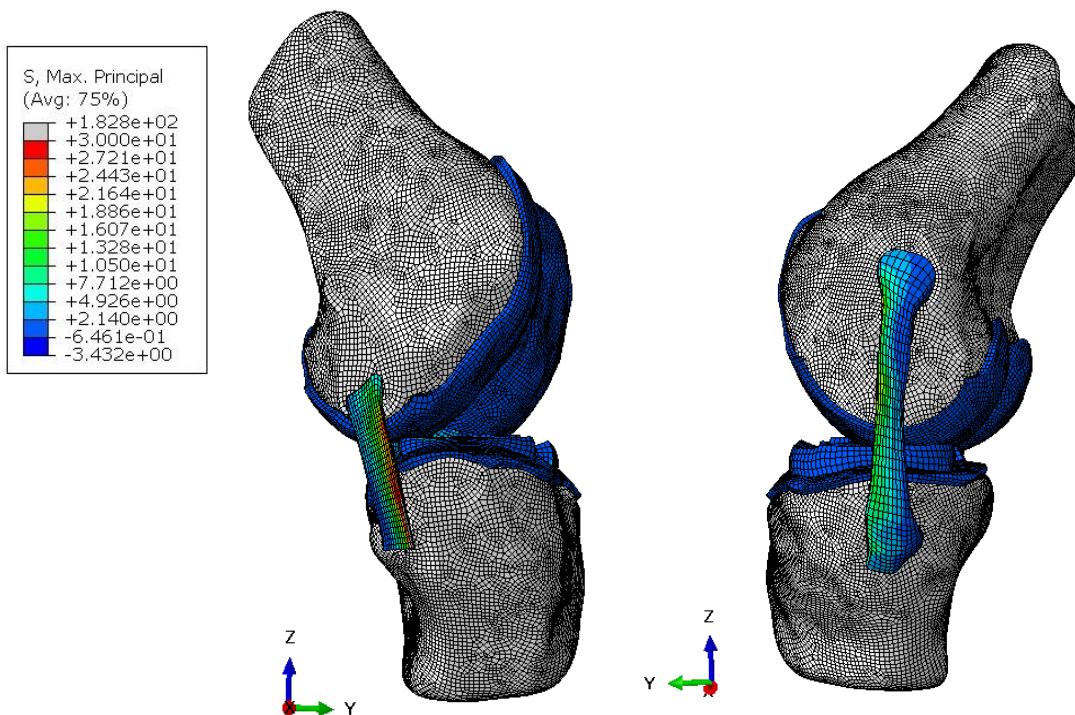


Figure 4.20 - ACL-deficient knee joint at 30° of flexion after the application of a 67 N posteriorly directed force on the femur using the HGO material model in the ligaments. (Left side) Lateral view. (Right side) Medial view.

When applying the posterior load to the ACL-deficient knee at 15 and 30° of flexion (Figures 4.16 and 4.20, respectively) we can observe a much larger displacement in comparison to the ACL-intact knee case presented earlier. The stresses developed in the collateral ligaments increased as expected, and their anterior region is more easily identified as the region of higher stresses.

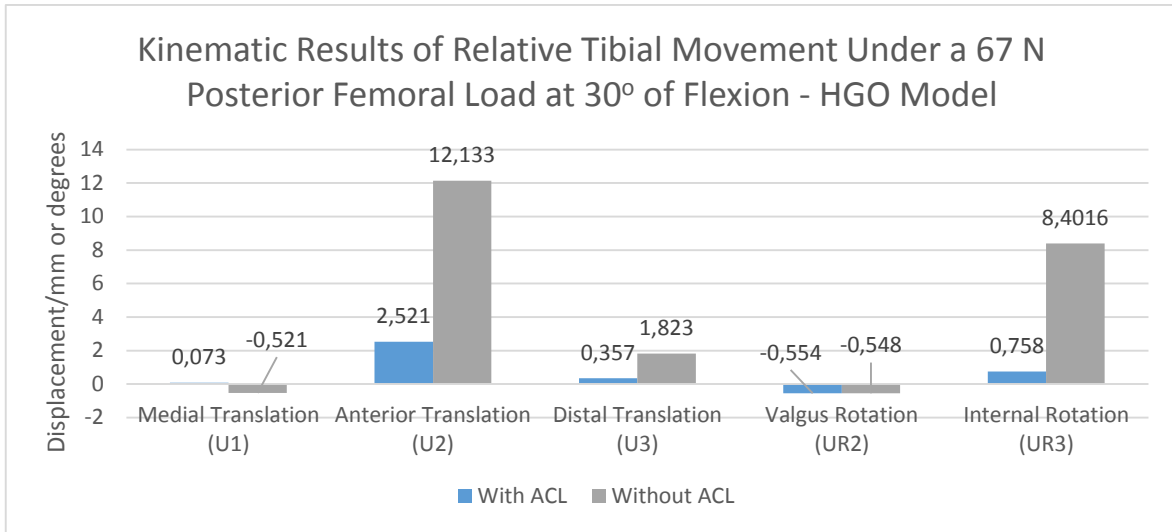


Figure 4.21 - Kinematic results of relative tibial movement under a 67 N posterior femoral load at 30° of flexion using the HGO model in the ligaments - comparison between the ACL-intact and ACL-deficient knees.

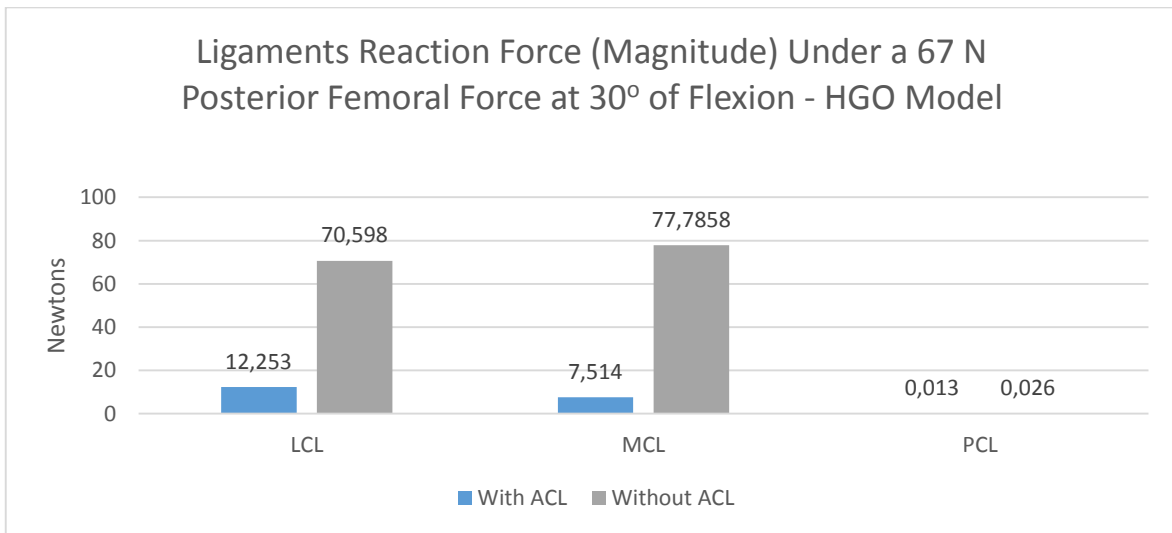


Figure 4.22 - Ligaments reaction force (magnitude) under a 67 N posterior femoral force at 30° of flexion using the HGO model in the ligaments - comparison between ACL-intact and ACL-deficient knees.

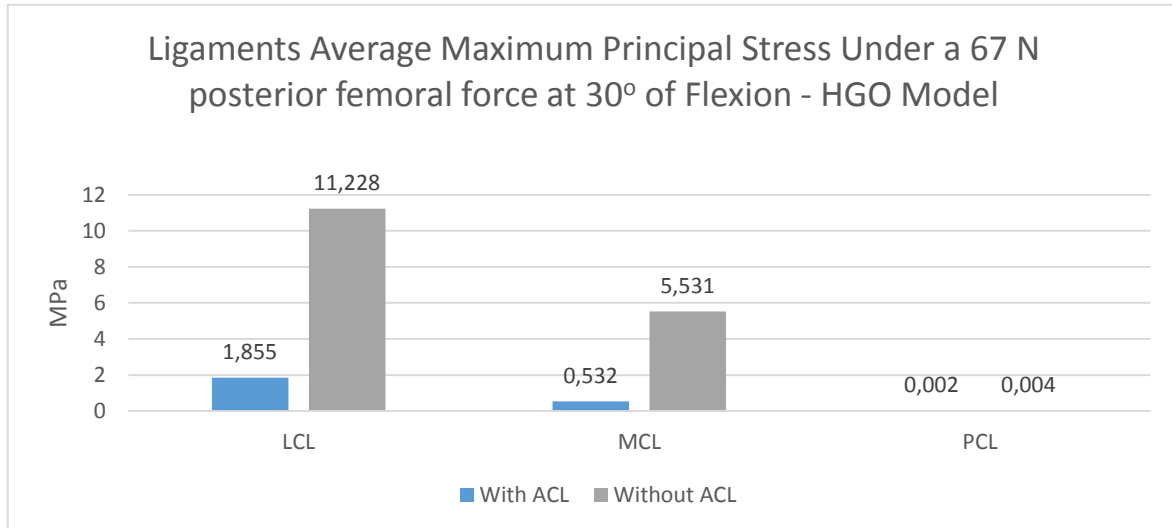


Figure 4.23 - Ligaments average maximum principal stress under a 67 N posterior femoral force at 30° of flexion using the HGO model in the ligaments - comparison between ACL-intact and ACL-deficient knees.

The plots above presented demonstrate the impact of the ACL in the kinematics and biomechanics of the tibiofemoral joint.

With the increase of the flexion angle, the kinematic results show the same growing trend in both anterior tibial translation and internal rotation seen in the first set of simulations with the ACL-intact knee, demonstrating the clear impact of the ACL in these DOFs.

Despite the decrease in distal translation with the increase of the flexion angle, the knee without the ACL always presents a higher value than the knee with the ACL, which also suggests the importance of the ACL in this proximal-distal direction.

Given that the experimental studies on cadaveric knees can apply the same 134 N anterior load on the tibia, the simulated results had to be compared with this data, taking into account the difference in the value of applied load.

For the 134 N anterior load, Kanamori et al. [71] obtained an anterior tibial displacement of 13.3 ± 1.4 , 17.3 ± 1.8 and 18.9 ± 2.3 mm in the ACL-deficient knee at 0, 15 and 30° of flexion, respectively. Similar results were acquired by Yagi et al. [72] with approximately 12.5 and 19 mm for 0 and 30° of flexion, respectively.

In terms of the *in situ* forces, Kanamori et al. verified that after the ACL transection the *in situ* forces of the MCL increase significantly from less than 20 N in the ACL-intact knee case to 36 ± 27 and 41 ± 16 at 0 and 30° of flexion, respectively.

Since the value of the applied force in the FE simulation was only half of the value applied in the experimental studies mentioned, it seems that the FE model overpredicts the anterior tibial displacement when the ACL is removed, as well as the *in situ* forces in the MCL. This fact, associated with the underprediction of movement for the same DOF when the ACL is present, suggests a revision of the ligament properties. For example, if the stiffness of the collateral ligaments was increased while the stiffness of the ACL was decreased, the FE simulation should produce a higher anterior tibial movement when the ACL is present and a lower value of the same quantity when the ACL is removed.

The stress-strain properties of the ligaments can greatly vary with the strain rate at which the uniaxial tension tests are performed, as we can attest in [73]. Therefore, one way to try to improve the results would be to do the curve fitting procedure to other experimental stress-strain curves with requirements described above.

Others reasons for the discrepancies found, would be the geometrical inaccuracies of the 3D model, in addition to the lack of some structures that should help maintain the integrity of the knee.

Despite the quantitative issues of the FE simulation results, it is clear that the absence of the ACL overloads the collateral ligaments at all the different angles of flexion. Even under this extra amount of loading, these ligaments cannot effectively compensate for the lack of the ACL, which produces significant changes in the kinematics of the knee. This can obviously have a negative impact on the knee health, due to the damage caused by wearing and excessive deformation of the other knee components, such as the collateral ligaments and the menisci.

5. Conclusion

In this work, the effect of an ACL rupture in the overall kinematics and biomechanics of the knee was studied by comparing the effect of a posterior force on ACL-intact and ACL-deficient knees.

Due to their non-linear stress-strain curve, the ligaments were modeled with two hyperelastic constitutive models: the Marlow and the HGO model. The Marlow model is a general first-invariant hyperelastic isotropic model, while the HGO model accounts for the characteristic anisotropy of ligaments collagen fibers. Both material models were fitted to the same experimental stress-strain curves obtained in uniaxial tension tests of the ACL, MCL and PCL.

During the realization of this work several hardships were encountered. Firstly, the choice of the solver: Abaqus/Standard or Abaqus/Explicit. Since the problem issued in this thesis produced (relatively) large displacements, which implies the activation of the NLGEOM option in Abaqus, the initial option was Abaqus/Explicit. Despite its virtues in handling the large displacement question, care must be taken when analysing the results produced by the explicit solver. If the balance between energies is not strictly maintained, the outcomes may not reflect the physics of the problem. This is particularly relevant in quasi static analysis which is the most frequent case in the literature for FE analysis of the knee in Abaqus/Explicit. Furthermore, the simulations using this solver were taking too much time, becoming impractical for the time span of a Master Thesis. Consequently, the model was migrated to Abaqus/Standard, a process that implied adjusting some definitions. For instance, the contacts had to be changed from *General Contact* in Explicit to *Surface-to-Surface* between each contact pair in Standard. Despite its advantages, Abaqus/Standard has the downside of not being very suited to handle large displacement problems. While this was not an issue when simulating the healthy knee, the large rigid body motions produced in the absence of the ACL raised convergence problems for high load values.

The meshing process of the complex 3D shapes with hexahedral elements also brought some difficulties that in the case of the ligaments, were surpassed only by recurring to the mesh provided by the Open Knee project.

Nevertheless, the biggest obstacle was definitely the estimation of the right parameters for the HGO model. The model is complex and understanding all the concepts related to its definition is indispensable to find the optimal parameters to simulate a biological tissue. It should be mentioned that only two studies have used this model in the knee ligaments [14,38]. From these, only [14] claims to have performed a fitting procedure for three different ligaments, and to have modelled the cruciate ligaments using two families of fibers. However, none of these studies presented any information regarding the value of the coefficients to use to model the knee ligaments. Without a good start point to begin with, many sets of parameters produced by the optimization routine created failed to recreate the kinematic behaviour of the knee. Even when a set of parameters produced reasonable results in a specific loading case, it did not necessarily mean that the same set would produce consistent results in another situation.

By comparing the kinematic outcomes of the FE simulations with both models, it is concluded that the HGO model presents more accurate results. This was expected since the HGO was designed to

capture the anisotropic properties of biologic tissues composed of collagen fiber bundles, such as the ligaments.

Using this model in the ligaments, the FE model is able to qualitatively (and mostly quantitatively) reproduce consistent kinematic results with experimental data in all degrees of freedom except for the valgus-varus rotation. These results confirm that the ACL provides the major constraint to anterior tibial motions and also plays an important role on restraining internal rotation of the tibia. These conclusions are also supported by the calculated force sustained by the four ligaments considered.

When the ACL is absent, the collateral ligaments are the first structures to be requested to sustain anterior-posterior forces, with obvious implications in their stress state. The MCL is the ligament that supports more load in this situation, supports the role attributed to the MCL as the secondary restraint to anterior tibial displacements.

To sum up, it is concluded that the ACL rupture induces several drastic kinematic changes which have a great impact on the overall biomechanics of the entire knee structure.

As usual in this type of simulations, there were some limitations in this study. The residual stresses present on the knee ligaments were not modeled since the Abaqus does not allow the prescription of pre-stresses in anisotropic hyperelastic models. However, when comparing a pre-stressed and a stress free ACL, Limbert et al.[41] found similar stress distributions in both cases, the difference being only the increased magnitude value of the pre-stressed one. The bones were not considered as deformable bodies, which could introduce some differences in the results produced. The ACL function was only tested by applying a posterior femoral load. The influence of the ACL in other types of movements was not tested.

Despite these limitations, the FE model developed in this thesis, based on the overall positive results produced, should provide a solid basis to develop further work in the biomechanical study of the knee. Some indications for future work are given in the next section.

5.1. Future Work

In the future, an obvious addition to the model would be the inclusion of the patellofemoral component.

The meniscal attachments to the tibia could also be more realistically modeled by defining the meniscal horns as a set of springs as in [23,29,38].

As for the knee ligaments modeling, it is known that the ligaments are not completely incompressible tissues. In a very recent study, Nolan et al. [74] demonstrated that the HGO model does not correctly characterizes the compressible anisotropic material behavior. In response to this fact, they proposed a modified anisotropic model based on the aforementioned model that is said to predict more accurately the anisotropic response to hydrostatic tensile loading. The employment of this new model would require an additional effort to implement the UMAT routine in Abaqus, but would also add an extra layer of realism to the ligaments material properties.

It would be interesting to verify the ACL role in more complex loading cases. A common test in experimental setups is the application of a 10 N m of valgus torque combined with a 5 Nm internal torque

to simulate the pivot shift test. The simulation of more dynamic situations like jumping or stair climbing together with a more detailed analysis of the other soft tissues of the knee such as the articular cartilage and the menisci would also provide great insights about the ACL-deficient knee functioning.

The open source nature of the Open Knee project promises new developments in the near future. With more accurate and detailed models, tested by different users in different loading scenarios, it would be certainly possible to develop more realistic FE models of the knee joint, with increased predicting capabilities.

6. References

- [1] Marieb, E., and Hoehn, K., 2013, *Human anatomy & physiology*, Pearson Education, Inc.
- [2] Hall, S., 2012, *Basic Biomechanics*, McGraw-Hill, New York, NY.
- [3] Kapandji, I. A., 1987, *The Physiology of the Joints: Lower Limb*, Churchill Livingstone.
- [4] Peña, E., Calvo, B., Martínez, M. a, and Doblaré, M., 2006, "A three-dimensional finite element analysis of the combined behavior of ligaments and menisci in the healthy human knee joint.," *J. Biomech.*, **39**(9), pp. 1686–1701.
- [5] Dargel, J., Gotter, M., Mader, K., Pennig, D., Koebke, J., and Schmidt-Wiethoff, R., 2007, "Biomechanics of the anterior cruciate ligament and implications for surgical reconstruction," *Strategies Trauma Limb Reconstr.*, **2**(1), pp. 1–12.
- [6] Kweon, C., Lederman, E. S., and Chhabra, A., 2013, "Anatomy and Biomechanics of the Cruciate Ligaments and Their Surgical Implications," *The Multiple Ligament Injured Knee: A Practical Guide to Management*, G.C. Fanelli, ed., Springer New York, New York, NY, pp. 17–27.
- [7] Siegel, L., Vandenakker-Albanese, C., and Siegel, D., 2012, "Anterior Cruciate Ligament Injuries: Anatomy, Physiology, Biomechanics, and Management.," *Clin. J. Sport Med. Off. J. Can. Acad. Sport Med.*, **22**(4), pp. 349–355.
- [8] Xie, F., Yang, L., Guo, L., Wang, Z., and Dai, G., 2009, "A Study on Construction Three-Dimensional Nonlinear Finite Element Model and Stress Distribution Analysis of Anterior Cruciate Ligament," *J. Biomech. Eng.*, **131**(12), pp. 121007–5.
- [9] Jones, C., and Grimshaw, P., 2011, "The biomechanics of the anterior cruciate ligament and its reconstruction," *Theoretical Biomechanics*, V. Klika, ed., InTech, pp. 361–384.
- [10] Woo, S. L.-Y., Abramowitch, S. D., Kilger, R., and Liang, R., 2006, "Biomechanics of knee ligaments: injury, healing, and repair.," *J. Biomech.*, **39**(1), pp. 1–20.
- [11] Frontera, W. R., Herring, S. A., Micheli, L. J., and Silver, J. K., 2007, *Clinical Sports Medicine, Medical Management and Rehabilitation*, Saunders Elsevier.
- [12] Zantop, T., Petersen, W., and Fu, F. H., 2005, "Anatomy of the Anterior Cruciate Ligament," *Oper. Tech. Orthop.*, **15**(1), pp. 20–28.
- [13] Song, Y., Debski, R. E., Musahl, V., Thomas, M., and Woo, S. L.-Y., 2004, "A three-dimensional finite element model of the human anterior cruciate ligament: a computational analysis with experimental validation," *J. Biomech.*, **37**(3), pp. 383–390.
- [14] Kiapour, A., Kiapour, A. M., Kaul, V., Quatman, C. E., Wordeman, S. C., Hewett, T. E., Demetropoulos, C. K., and Goel, V. K., 2014, "Finite Element Model of the Knee for Investigation of Injury Mechanisms: Development and Validation," *J. Biomech. Eng.*, **136**(1), p. 011002.
- [15] Herrera, A., Ibarz, E., Cegoñino, J., Lobo-Escolar, A., Puértolas, S., López, E., Mateo, J., and Gracia, L., 2012, "Applications of finite element simulation in orthopedic and trauma surgery.," *World J. Orthop.*, **3**(4), pp. 25–41.

- [16] Gardiner, J. C., and Weiss, J. a, 2003, "Subject-specific finite element analysis of the human medial collateral ligament during valgus knee loading.," *J. Orthop. Res.*, **21**(6), pp. 1098–1106.
- [17] Kluess, D., Wieding, J., and Souffrant, R., "x Finite Element Analysis in Orthopaedic Biomechanics," pp. 151–171.
- [18] Huiskes, R., and Blankevoort, L., 1990, "Anatomy and Biomechanics of the Anterior Cruciate Ligament: A Three-Dimensional Problem," *The Knee and the Cruciate Ligaments*, Springer Berlin Heidelberg, pp. 92–109.
- [19] Noronha, J., 1999, "Isometria na Reconstrução do Ligamento Cruzado Anterior," Instituto de Ciências Biomédicas Abel Salazar - Universidade do Porto.
- [20] Adouni, M., Shirazi-Adl, A., and Shirazi, R., 2012, "Computational biodynamics of human knee joint in gait: from muscle forces to cartilage stresses.," *J. Biomech.*, **45**(12), pp. 2149–2156.
- [21] Bendjaballah, M., Shirazi-Adl, A., and Zukor, D., 1997, "Finite element analysis of human knee joint in varus-valgus," *Clin. Biomech.*, **12**(3), pp. 139–148.
- [22] Dhafer, Y. Y., Kwon, T.-H., and Barry, M., 2010, "The effect of connective tissue material uncertainties on knee joint mechanics under isolated loading conditions.," *J. Biomech.*, **43**(16), pp. 3118–3125.
- [23] Hull, M. L., Donahue, T., Rashid, M., and Jacobs, C., 2002, "A Finite Element Model of the Human Knee Joint for the Study of Tibio-Femoral Contact," *J. Biomech. Eng.*, **124**(3), pp. 273–280.
- [24] Li, G., Gil, J., Kanamori, A., and Woo, S. L., 1999, "A validated three-dimensional computational model of a human knee joint.," *J. Biomech. Eng.*, **121**(6), pp. 657–662.
- [25] Park, H.-S., Ahn, C., Fung, D. T., Ren, Y., and Zhang, L.-Q., 2010, "A knee-specific finite element analysis of the human anterior cruciate ligament impingement against the femoral intercondylar notch.," *J. Biomech.*, **43**(10), pp. 2039–2042.
- [26] Ramaniraka, N. a, Saunier, P., Siegrist, O., and Pioletti, D. P., 2007, "Biomechanical evaluation of intra-articular and extra-articular procedures in anterior cruciate ligament reconstruction: a finite element analysis.," *Clin. Biomech. (Bristol, Avon)*, **22**(3), pp. 336–343.
- [27] Ramaniraka, N. a, Terrier, A., Theumann, N., and Siegrist, O., 2005, "Effects of the posterior cruciate ligament reconstruction on the biomechanics of the knee joint: a finite element analysis.," *Clin. Biomech. (Bristol, Avon)*, **20**(4), pp. 434–442.
- [28] Wan, C., Hao, Z., and Wen, S., 2013, "The Effect of the Variation in ACL Constitutive Model on Joint Kinematics and Biomechanics Under Different Loads: A Finite Element Study," *J. Biomech. Eng.*, **135**(4), p. 041002.
- [29] Yao, J., Snibbe, J., Maloney, M., and Lerner, A. L., 2006, "Stresses and Strains in the Medial Meniscus of an ACL Deficient Knee under Anterior Loading: A Finite Element Analysis with Image-Based Experimental Validation," *J. Biomech. Eng.*, **128**(1), p. 135.
- [30] Moglo, K. E., and Shirazi-Adl, a., 2003, "Biomechanics of passive knee joint in drawer: load transmission in intact and ACL-deficient joints," *Knee*, **10**(3), pp. 265–276.
- [31] Li, G., Suggs, J., and Gill, T., 2002, "The Effect of Anterior Cruciate Ligament Injury on Knee Joint Function under a Simulated Muscle Load: A Three-Dimensional Computational Simulation," *Ann. Biomed. Eng.*, **30**(5), pp. 713–720.

- [32] Ellis, B. J., Lujan, T. J., Dalton, M. S., and Weiss, J. A., 2006, "Medial Collateral Ligament Insertion Site and Contact Forces in the ACL-Deficient Knee," *J. Orthop. Res.*, (April), pp. 800–810.
- [33] Penrose, J. M. T., Holt, G. M., Beaugonin, M., and Hose, D. R., 2002, "Development of an accurate three-dimensional finite element knee model.," *Comput. Methods Biomech. Biomed. Engin.*, **5**(4), pp. 291–300.
- [34] Baldwin, M. a, Clary, C. W., Fitzpatrick, C. K., Deacy, J. S., Maletsky, L. P., and Rullkoetter, P. J., 2012, "Dynamic finite element knee simulation for evaluation of knee replacement mechanics.," *J. Biomech.*, **45**(3), pp. 474–483.
- [35] Halloran, J. P., Petrella, A. J., and Rullkoetter, P. J., 2005, "Explicit finite element modeling of total knee replacement mechanics.," *J. Biomech.*, **38**(2), pp. 323–331.
- [36] Godest, a C., Beaugonin, M., Haug, E., Taylor, M., and Gregson, P. J., 2002, "Simulation of a knee joint replacement during a gait cycle using explicit finite element analysis.," *J. Biomech.*, **35**(2), pp. 267–275.
- [37] Beillas, P., Papaioannou, G., Tashman, S., and Yang, K. H., 2004, "A new method to investigate in vivo knee behavior using a finite element model of the lower limb.," *J. Biomech.*, **37**(7), pp. 1019–1030.
- [38] Westermann, R. W., Wolf, B. R., and Elkins, J. M., 2013, "Effect of ACL reconstruction graft size on simulated Lachman testing: a finite element analysis.," *Iowa Orthop. J.*, **33**, pp. 70–77.
- [39] Peña, E., Martínez, M. a, Calvo, B., Palanca, D., and Doblaré, M., 2005, "A finite element simulation of the effect of graft stiffness and graft tensioning in ACL reconstruction.," *Clin. Biomech. (Bristol, Avon)*, **20**(6), pp. 636–644.
- [40] Pioletti, D., Rakotomanana, L., Benvenuti, J., and PF, L., 1998, "Finite Element Model of the Human Anterior Cruciate Ligament," *Comput. methods Biomech. Biomed. Eng.*
- [41] Limbert, G., Taylor, M., and Middleton, J., 2004, "Three-dimensional finite element modelling of the human ACL: simulation of passive knee flexion with a stressed and stress-free ACL.," *J. Biomech.*, **37**(11), pp. 1723–1731.
- [42] Suggs, J., Wang, C., and Li, G., 2003, "The effect of graft stiffness on knee joint biomechanics after ACL reconstruction--a 3D computational simulation.," *Clin. Biomech. (Bristol, Avon)*, **18**(1), pp. 35–43.
- [43] Kazemi, M., Dabiri, Y., and Li, L. P., 2013, "Recent advances in computational mechanics of the human knee joint.," *Comput. Math. Methods Med.*, pp. 1–27.
- [44] Parker, J. N., and Philip, P. M., eds., 2002, *The 2002 Official Patient's Sourcebook on Knee Ligament Injuries*, Tiffany LaRochelle, San Diego.
- [45] Tortora, G. J., and Derrickson, B., 2010, *Introduction to the Human Body*, John Wiley & Sons, Inc.
- [46] Drake, R. L., Vogl, A. W., and Mitchell, A. W. M., 2009, *Grays Anatomy for Students*, Churchill Livingstone.
- [47] Standring, S., ed., 2008, *Gray's Anatomy, The Anatomical Basis of Clinical Practice*, Churchill Livingstone.

- [48] Woo, S. L., Debski, R. E., Withrow, J. D., and Janaushek, M. A., 1999, "Biomechanics of Knee Ligaments," *Am. J. Sports Med.*, **27**(4), pp. 533–543.
- [49] Levangie, P., and Norkin, C., 2005, *Joint structure and function: a comprehensive analysis*, F. A. Davis Company, Philadelphia.
- [50] Tortora, G. J., and Derrickson, B., 2014, *Principles of Anatomy & Physiology*, Wiley.
- [51] Darrow, M., 2002, *The Knee Sourcebook*, McGraw-Hill.
- [52] Weiss, J. a., and Gardiner, J. C., 2001, "Computational Modeling of Ligament Mechanics," *Crit. Rev. Biomed. Eng.*, **29**(3), pp. 303–371.
- [53] Robi, K., Jakob, N., Matevz, K., and Matjaz, V., 2013, "The Physiology of Sports Injuries and Repair Processes," *Current Issues in Sports and Exercise Medicine*, M. Hamlin, ed., pp. 43–86.
- [54] Kjaer, M., Krogsgaard, M., Magnusson, P., Engebretsen, L., Roos, H., Takala, T., and Woo, S. L., eds., 2003, *Textbook of Sports Medicine, Basic Science and Clinical Aspects of Sports Injury and Physical Activity*, Blackwell Publishing.
- [55] Kutz, M., 2003, *Standard handbook of biomedical engineering and design*, McGraw-Hill.
- [56] Johnson, D. L., and Mair, S. D., 2006, *Clinical Sports Medicine*, Mosby Elsevier, Philadelphia.
- [57] Insall, J. N., and Scott, W. N., 2012, *Surgery of the Knee*, Churchill Livingstone, Philadelphia.
- [58] Erdemir, A., and Sibole, S., 2010, "Open Knee : A Three Dimensional Finite Element Representation of the Knee Joint, User's Guide, Version 1.0.0."
- [59] <https://simtk.org/home/openknee>, "Simtk.org: Open Knee: A ThreeDimensional Finite Element Representation of the Knee Joint."
- [60] Systemes, D., 2010, *Abaqus 6.10 Theory Manual*.
- [61] Marlow, R. S., 2003, "A General First-Invariant Hyperelastic Constitutive Model," *Constitutive Models for Rubber III*, pp. 157–160.
- [62] Gasser, T. C., Ogden, R. W., and Holzapfel, G. a, 2006, "Hyperelastic modelling of arterial layers with distributed collagen fibre orientations.," *J. R. Soc. Interface*, **3**(6), pp. 15–35.
- [63] Holzapfel, G. A., Gasser, T. C., and Ogden, R. A. Y. W., 2000, "A New Constitutive Framework for Arterial Wall Mechanics and a Comparative Study of Material Models," *J. Elast.*, **61**, pp. 1–48.
- [64] Holzapfel, G., and Gasser, T., 2001, "A viscoelastic model for fiber-reinforced composites at finite strains: Continuum basis, computational aspects and applications," *Comput. methods Appl. Mech. ...*, **190**, pp. 4379–4403.
- [65] Elkins, J. M., Stroud, N. J., Rudert, M. J., Tochigi, Y., Pedersen, D. R., Ellis, B. J., Callaghan, J. J., Weiss, J. A., and Brown, T. D., 2011, "The Capsule's Contribution to Total Hip Construct Stability – A Finite Element Analysis," *J. Orthop. Res.*, **29**(11), pp. 1642–1648.
- [66] Systemes, D., 2010, "Abaqus Keywords Reference Manual," **2**.
- [67] Quapp, K., and Weiss, J., 1998, "Material characterization of human medial collateral ligament," *ASME J. Biomech. Eng.*

- [68] Butler, D. L., Sheh, M. Y., Stouffer, D. C., Samaranayake, V. a, and Levy, M. S., 1990, "Surface strain variation in human patellar tendon and knee cruciate ligaments.," *J. Biomech. Eng.*, **112**(1), pp. 38–45.
- [69] Grood, E., and Suntay, W., 1983, "A joint coordinate system for the clinical description of three-dimensional motions: application to the knee," *J. Biomech. Eng.*, **105**, pp. 136–144.
- [70] Gabriel, M. T., Wong, E. K., Woo, S. L.-Y., Yagi, M., and Debski, R. E., 2004, "Distribution of in situ forces in the anterior cruciate ligament in response to rotatory loads.," *J. Orthop. Res.*, **22**(1), pp. 85–89.
- [71] Kanamori, A., Sakane, M., Zeminski, J., Rudy, T. W., and Woo, S. L.-Y., 2000, "In-situ force in the medial and lateral structures of intact and ACL-deficient knees," *J. Orthop. Sci.*, **5**(6), pp. 567–571.
- [72] Yagi, M., Wong, E. K., Kanamori, A., Debski, R. E., Fu, F. H., and Woo, S. L., 2002, "The American Journal of Sports Medicine Biomechanical Analysis of an Anatomic Anterior Cruciate Ligament Reconstruction," pp. 660–666.
- [73] Pioletti, D. P., Rakotomanana, L. R., and Leyvraz, P. F., 1999, "Strain rate effect on the mechanical behavior of the anterior cruciate ligament-bone complex.," *Med. Eng. Phys.*, **21**(2), pp. 95–100.
- [74] Nolan, D., Gower, A., Destrade, M., Ogden, R., and McGarry, J., 2014, "A robust anisotropic hyperelastic formulation for the modelling of soft tissue," *J. Med. Behav. Biomed. Mater.*, **39**, pp. 48–60.
- [75] Vaughan, C., Davis, B., and O'connor, J., 1999, *Dynamics of human gait*, Kiboho Publishers.
- [76] Bischoff, J., Siggelkow, E., and Sieber, D., 2008, "Advanced material modeling in a virtual biomechanical knee," *Abaqus Users Conf.*, pp. 1–15.

Appendix A – Optimization Code

HGO_optim_curvefit.m

```
function [] = HGO_optim_curvefit()
% This function connects MATLAB and Abaqus to calculate the optimal set of
% coefficients (C10,k1,k2 and kappa) for the Holzapfel-Gasser-Ogden (HGO)
% Model, provided experimental Stress-Strain (or, alternatively,
% Force-Strain) data.
%
% David Fernandes
% October, 2014

clear all; close all; clc;
decimal_places=1e4; % Constant that defines de number of decimal places used to
round the experimental data. The number of decimal places is given by the exponent
of the expression.

%----- Ligament Experimental Data -----
-----
strain_load=load('nom_strain_acl_mesfar.mat'); % Struct that loads the
experimental Strain data.
stress_load=load('nom_stress_acl_mesfar.mat'); % Struct that loads the
experimental Stress data.
exp_force=round((stress_load.nom_stress_acl_mesfar(1:28))*decimal_places)/decimal_
places; % Experimental Stress points rounded to the number of decimal places.
exp_strain=strain_load.nom_strain_acl_mesfar(1:28)*100; %Experimental Strain
points in percentage.
%-----

%-----%Experimental Data Manipulation-----
%Since the experimental data is not periodic, it is necessary to
%do some manipulation in order to compare it with the exact same points in
%Abaqus
max_stress=max(exp_stress);
time_points=exp_stress./max_stress;

time_points=round(time_points*1e3)/1e3;
j=2;
time_points_cut(1)=0;
exp_stress_cut(1)=0;
exp_strain_cut(1)=0;
for i=2:length(time_points)-1
    aux=time_points(i+1);
    if time_points(i)~=aux && time_points(i)~=0
        time_points_cut(j)=time_points(i);
        exp_strain_cut(j)=exp_strain(i);
```

```

        exp_stress_cut(j)=exp_stress(i);
        j=j+1;
    end
end

time_points_cut(length(time_points_cut)+1)=time_points(length(time_points));
exp_strain_cut(length(exp_strain_cut)+1)=exp_strain(length(exp_strain));
exp_stress_cut(length(exp_stress_cut)+1)=exp_stress(length(exp_stress));
time_points_cut=time_points_cut';
exp_strain_cut=exp_strain_cut';
exp_stress_cut=exp_stress_cut';

%csvwrite('time_points_cut.csv',time_points_cut) % Generates the file that will be
used in Abaqus/CAE to define the Time Points for the Output.

c0=[1 1 1 1/12]; % Initial approximation values for C10, k1, k2 and kappa,
respectively.
iter=0; % Iteration number. This value used to name the folders that will contain
the "Jobs" created by Abaqus in each simulation.
function [abq_strain]=abq_sim(c,exp_stress_cut)
    % abq_sim receives the vector of coefficients calculated by the
    % "lsqcurvefit" routine and returns the vector of strains calculated in
    % Abaqus for the points of the vector exp_stress_cut
    disp(['Iteration number = ' int2str(iter)]);
    disp(['Parameters used: C10 = ' num2str(c(1)) ' ; k1 = ' num2str(c(2)) ' ;
k2 = ' num2str(c(3)) ' ; kappa = ' num2str(c(4))]);
    start_time=fix(clock);

    [abq_load,abq_strain]=abq_values(c(1),c(2),c(3),c(4),iter); % The function
"abq_values" connects the MATLAB with Python
    %-----Plots and Report Info-----
    figure('Name',(sprintf('Data for Iteration= %d',
iter)));suptitle(sprintf('Data for Iteration= %d', iter));
    subplot(2,2,1);plot(exp_strain_cut,exp_stress_cut,'o');ylabel('Stress
(MPa)');xlabel('Strain (%)'); % Experimental Data
    subplot(2,2,2);plot(abq_strain,abq_load,'ro');ylabel('Stress ABQ
(MPa)');xlabel('Strain ABQ (%)'); % FE Simulation Data
    subplot(2,2,3);plot(exp_strain_cut,exp_stress_cut,'-
x',abq_strain,abq_load,'-ro');ylabel('Stress Both (MPa)');xlabel('Strain Both
(%)');legend('Experimental','FE Simulation','Location','NorthWest'); % Comparison
of the two data sets
    saveas(gcf,(sprintf('Job_%d.png', iter)));
    Rsquared=rsquare(exp_strain_cut,abq_strain);
    disp(['R Square value for Iteration number = ' int2str(iter) ' is '
num2str(Rsquared)]);
    disp(sprintf('\n'));

    fid = fopen('Info_iter.txt', 'at');

```

```

        fprintf(fid, 'Iteration number = %d \n', iter);
        fprintf(fid, 'Start time: %d-%d-%d : %d:%d:%d\n',
start_time(1),start_time(2),start_time(3),start_time(4),start_time(5),start_time(6
));
        fprintf(fid, 'Parameters used: C10 = %0.5f ; k1 = %0.5f ; k2 = %0.5f ;
kappa = %0.5f \n', c(1),c(2),c(3),c(4));
        fprintf(fid, 'RSquare value for Iteration number = %d is %0.5f \n', iter,
Rsquared);
        fprintf(fid, '\n');
        fprintf(fid, '\n');
        fclose(fid);
        iter=iter+1;
    end

%options=optimset('Display','iter-detailed','FinDiffRelStep',1e-
1,'FinDiffType','central');
options=optimset('Display','iter-detailed','FinDiffRelStep',1e-3);
[c,resnorm,residual,output]=lsqcurvefit(@abq_sim,c0,exp_stress_cut,exp_strain_cut,
[0.01,0.0001,0.0001,0.0001],[10,10000,10000,1/10],options)
end

```

abq_values.m

```
function [ abq_loads, abq_strains ] = abq_values( C10, k1, k2, kappa, iter )
% abq_values receives the HGO model constants and the iteration number as input
% and outputs two vectors, corresponding to the loads and
% strains calculated in the simulated uniaxial tension test for the given
% parameters.
%
% David Fernandes
% October, 2014

% Folder creation for each iteration of the optimization algorithm
parent_dir=pwd;
job_name=strcat('Job_',int2str(iter));
job_dir=strcat(parent_dir,'\ ',job_name);

% Creation of the file "Var_iter.py" that will contain the variables for
% each iteration
delete('Var_iter.py');
fid = fopen('Var_iter.py', 'w');
fprintf(fid, 'C10 = %0.5f\n',C10);
fprintf(fid, 'k1 = %0.5f\n',k1);
fprintf(fid, 'k2 = %0.5f\n',k2);
fprintf(fid, 'kappa = %0.5f\n',kappa);
fprintf(fid, 'iter = %d\n',iter);
fclose(fid);

mode='noGui';
system(['abaqus cae ',mode,'=main.py']); % Call of Abaqus/CAE executable in
"NoGui" mode to run the "Main_mod.py" file

% Reading of the report generated by Abaqus to create the load and strains
% vectors for the output.
report_name=strcat(job_dir,'\ ', 'rep_Job_',int2str(iter), '.csv');
report_data = importdata(report_name);
report_vars = fieldnames(report_data);
a=report_data.(report_vars{1});
abq_loads=a(:,2);
abq_strains=a(:,1)*100;
%specimen_length=39; % Length of the Test Specimen
%abq_strains=a(:,1)./specimen_length*100;
end
```

main.py

```
# File that executes the simulated FE uniaxial tension test in Abaqus with the HGO
# parameters given by the MATLAB function "abq_values.m"
# David Fernandes
# October, 2014

from part import *
from material import *
from section import *
from assembly import *
from step import *
from interaction import *
from load import *
from mesh import *
from job import *
from sketch import *
from visualization import *
from connectorBehavior import *
from Numeric import *
from abaqus import *
from abaqusConstants import *
from caeModules import *
import visualization
import os
import datetime
import shutil
from odbAccess import *

parent_dir=os.getcwd()
openMdb(
    pathName=parent_dir+'\unitary_cube.cae')
os.chdir(r"%s" % (parent_dir))

# Load variables and apply the changes to the Input file to use the new HGO parameters
execfile('Var_iter.py')
execfile("insert_parameter.py")

# Create directory for the Job
job_name='Job_'+str(iter)
job_dir=parent_dir+'\\'+job_name
if os.path.exists(job_dir):
    shutil.rmtree(job_dir)

os.makedirs(job_dir)
os.chdir(r"%s" % (job_dir))

# Write and Run a Job
mdb.Job(name=job_name, model='Model-1', description='', type=ANALYSIS,
```

```

    atTime=None, waitMinutes=0, waitHours=0, queue=None, memory=90,
    memoryUnits=PERCENTAGE, getMemoryFromAnalysis=True,
    explicitPrecision=SINGLE, nodalOutputPrecision=SINGLE, echoPrint=OFF,
    modelPrint=OFF, contactPrint=OFF, historyPrint=OFF, userSubroutine='',
    scratch='', multiprocessingMode=DEFAULT, numCpus=2, numDomains=2)
mdb.jobs[job_name].submit(consistencyChecking=OFF)
mdb.jobs[job_name].waitForCompletion()

# Create the report with the Load vs. Displacement data which is equivalent to
# Nominal Strain vs Nominal Stress since it is used a unitary cube for the FE simulation
o3 = session.openOdb(
    name=job_dir+'\\'+job_name+'.odb')
session.viewports['Viewport: 1'].setValues(displayedObject=o3)
odb = session.odbs[job_dir+'\\'+job_name+'.odb']
session.XYDataFromHistory(name='Displacement', odb=odb,
    outputVariableName='Spatial displacement: U1 at Node 4 in NSET NLOAD',
    steps=('Step-1', ), )
odb = session.odbs[job_dir+'\\'+job_name+'.odb']
session.XYDataFromHistory(name='Load', odb=odb,
    outputVariableName='Point loads: CF1 at Node 4 in NSET NLOAD', steps=(
    'Step-1', ), )
xy1 = session.xyDataObjects['Displacement']
xy2 = session.xyDataObjects['Load']
xy3 = combine(xy1, xy2)
xyp = session.XYPlot('XYPlot-1')
chartName = xyp.charts.keys()[0]
chart = xyp.charts[chartName]
c1 = session.Curve(xyData=xy3)
chart.setValues(curvesToPlot=(c1, ), )
session.viewports['Viewport: 1'].setValues(displayedObject=xyp)
xyp = session.xyPlots['XYPlot-1']
chartName = xyp.charts.keys()[0]
chart = xyp.charts[chartName]
x0 = chart.curves['_temp_1']
session.writeXYReport(fileName='rep_'+job_name+'.csv', appendMode=OFF, xyData=(x0,
    ))
mdb.save()
mdb.close()

```

insert_parameter.py

```
# Script that manipulates text in Abaqus Input (.inp) file by inserting or replacing Keywords.
# David Fernandes
# October, 2014

#-----Variables
ModelName='Model-1' # Abaqus Model Name
D=0

# Function that locates the Keywords of the Input file
def GetKeywordPosition(Model, blockPrefix):
    if blockPrefix == '':
        return len(mdb.models[Model].keywordBlock.sieBlocks)-1
    pos = 0
    foundCount = 0
    for block in mdb.models[Model].keywordBlock.sieBlocks:
        if string.lower(block[0:len(blockPrefix)])==string.lower(blockPrefix):
            return pos
        pos=pos+1
    return 0

mdb.models[ModelName].keywordBlock.synchVersions()
mdb.models[ModelName].keywordBlock.setValues(edited = 0)
mdb.models[ModelName].keywordBlock.synchVersions()
position = GetKeywordPosition(ModelName, '*Parts')
mdb.models[ModelName].keywordBlock.insert(position, """*Parameter
    Pi = 3.141592654
    gamma = 0*Pi/180
    theta1 = gamma
    c1 = cos(theta1)
    s1 = sin(theta1)
    theta2 = theta1-2*gamma
    c2 = cos(theta2)
    s2 = sin(theta2)""")

mdb.models[ModelName].keywordBlock.synchVersions()
mdb.models[ModelName].keywordBlock.setValues(edited = 1)
mdb.models[ModelName].keywordBlock.synchVersions()
position = GetKeywordPosition(ModelName, '*Material, name=acl_hgo')
mdb.models[ModelName].keywordBlock.replace(position, ""
*Material, name=acl_hgo
*Density
    1e-09,
*anisotropic hyperelastic,holzapfel, local directions=2
"""+ "%s,%s,%s,%s,%s" % (C10,D,k1,k2,kappa))

mdb.models[ModelName].keywordBlock.synchVersions()
```

```
mdb.models[ModelName].keywordBlock.setValues(edited = 1)
mdb.models[ModelName].keywordBlock.synchVersions()
position = GetKeywordPosition(ModelName, '*Orientation')
mdb.models[ModelName].keywordBlock.replace(position, ""*orientation,name=ori-
1,definition=offset to nodes, local directions=2
7,2,3
3,0.0
<c1>, <s1>, 0.0
<c2>, <s2>, 0.0""")
```